A Fault Detection and Diagnosis Strategy for VAV Air Distribution System

QIN Jianying

A thesis submitted in partial fulfillment of the requirements

for the Degree of Doctor of Philosophy

Department of Building Services Engineering

The Hong Kong Polytechnic University

December 2005

CERTIFICATE OF ORIGINALITY

The research described in this thesis is the original work except the sources quoted. It was carried out at the department of Building Services Engineering, the Hong Kong Polytechnic University under the supervision of Prof. Shengwei Wang and Prof. Francis Yik.

Qin Jianying

Department of Building Services Engineering

The Hong Kong Polytechnic University

Hong Kong, P.R. China

December 2005

ABSTRACT

Abstract of thesis entitled: A Fault Detection and Diagnosis Strategy for VAV Air Distribution System

Submitted by : Qin Jianying (0290)

For the degree of : Doctor of Philosophy

at The Hong Kong Polytechnic University in December, 2005

Variable air volume (VAV) systems and their control strategies become more and more complex in order to meet the increasing demands on indoor environment quality and energy conservation. Automatic monitoring and control of VAV systems are inevitable in modern buildings. Many supervisory VAV control strategies, such as supply air temperature reset, static pressure reset and advanced fresh air flow rate control, have been put into operation as well. Both components and sensors are playing essential roles in operation and control. Components and sensors in VAV air distribution systems often suffer from complete failure (hard fault) and partial failure (soft fault) easily, which result in energy waste, performance degradation or totally out of control. Therefore, fault detection and diagnosis (FDD) for VAV systems, especially for large-scale systems in which dozens of VAV boxes are involved, provides great benefits in improving system control and indoor environment quality, enhancing building energy efficiency, and prolonging components' life. However, studies on FDD for VAV systems are not sufficient and there is no applicable automatic commissioning tool for the whole VAV air distribution systems.

An automatic FDD strategy for VAV air distribution systems is developed in this study. A software package is developed on the basis of the FDD strategy for automatic commissioning. Prior to developing the FDD strategy, a site survey on the faults in practical VAV terminals was conducted. It was about a commercial building with 1251 VAV terminals in total. 20.9% VAV terminals were found ineffective and eleven root faults were identified in pressure-independent VAV systems. The FDD strategy therefore chooses these eleven root faults as the objects to be handled.

The FDD strategy is built up based on system knowledge, qualitative states and object-oriented SPC (statistical process control) models. Eight FDD schemes, organized at two steps, are set up to detect the eleven VAV root faults within the qualitative/quantitative FDD strategy. Ten faults, which would affect the system operation, are handled at Step 1 in parallel using the first seven schemes. The eleventh fault, which would not affect the basic system operation but would lead to imperfection under advanced supervisory control, is analyzed at Step 2 using the eighth scheme. The FDD strategy is tested and validated on typical VAV air-conditioning systems involving multiple faults both in simulation and in-situ tests.

Integrating quantitative models with qualitative knowledge helps to solve decision making problems more effectively and efficiently. Three schemes are developed simply from characteristic equations or based on qualitative states for simple fault detection like controller hard failure or damper stuck. However, other five schemes need further quantitative SPC models for fault detection or identification after the faulty patterns are recognized by characteristic equations or qualitative states.

The eighth scheme is developed for VAV terminal flow sensor bias detection and sensor reconstruction. PCA (Principal Component Analysis) models, at both system

level and terminal level, are built and employed in the scheme. Sensor biases are detected using both T^2 statistic and *SPE* (Square Prediction Error) and isolated using *SPE* contribution plot. As the reliability and sensitivity of fault isolation may be affected by the multiple sensor faults at the system level, terminal level PCA model is designed to further examine the suspicious terminals. The faulty sensor is reconstructed after it is isolated by the scheme and the fault detection process repeats using the latest reconstructed measurements until no further fault can be detected. Thus, the sensitivity and robustness of the scheme are enhanced significantly.

A software package is developed to implement the FDD strategy for automatic commissioning. With the data downloaded from the BMS, the pre-defined root faults could be detected and faulty sensor(s) could be reconstructed by the software. The main FDD report presents a list of major information of commissioning and a few other reports give other detailed information related to the characteristic parameters of the system concerned.

ACKNOWLEDGEMETNS

I would like to express my sincerest appreciation to Prof. Shengwei Wang, my supervisor, for his invaluable guidance, patience and encouragement during the course of this research. Also, I would like to thank Prof. Francis Yik, my co-supervisor, for his support and belief in my capability.

My special thanks go to all the participants of IEA (International Energy Agency) -ECBCS (Energy Conservation in Building and Community Systems) Annex 40 for the benefits received from the exchanges and communications with them within the framework of the research program.

I would like to thank my research mates, Ms. Xiao Fu, Mr. Xu Xinhua and Mr. Cui Jingtan, for their help and going forward side by side. The long load to accomplish this research is colorful because of their company.

Most importantly, I would like to express my deepest appreciation to my special friend, Jerry. His inspiration gave me the power to conquer all the difficulties with a smile. Finally, I would like to say a big ‘Thank you’ to all my family members. This thesis is to them.

LIST OF FIGURES

LIST OF TABLES

Page

NOMENCALTURE

ΔF	air flow variation
$\Delta time$	time
A	area
a	number of PCs
C	CO_2 concentration
$C2$	pollutant concentration
c_p	specific heat
CS	strength of CO_2 source
DP	differential pressure
E	variable expectation
$\boldsymbol{E}$	residual matrix
F	air flow rate
G	humidity
GS	strength of humidity source
H	damper position (0-1)
h	convection coefficient
I	identity matrix
LCL	lower control limit
M	mass of air
m	mass flow rate
P	pressure
$\boldsymbol{P}$	principal laoding matrix
PS	strength of pollutant source
q	weighting vector
Q	heat laod
R	reversal
R	heat resistance in Chapter 5
$\boldsymbol{R}$	Covariance matrix of X
RH	relative humidity
SPE	square prediction error
SPE_α	threshold of SPE

t	time
T	temperature
$\boldsymbol{T}$	score matrix
T^2	T^2 statistic
T^2_{α}	threshold of T^2
TF	total flow rate of the system
u	reconstruction error
UCL	upper control limit
V	volume
v	volume flow rate
X	variable matrix under normal operation condition, n sample of m variables
x_{new}	new normalized observation matrix
y	process variable
y_{new}	new observation matrix
z	reconstructed data
+	increase
++	greatly increase
-	decrease
--	greatly decrease

Greek

$\boldsymbol{V}$	matrix of eigenvectors of $\boldsymbol{R}$
$\boldsymbol{\Lambda}$	matrix of eigenvalues of $\boldsymbol{R}$
α	weighting factor
δ	threshold of the slope
μ	control signal to terminal damper
ξ	fault direction vector
σ	standard deviation
η	the contribution to the total variance

Subscripts

amb	ambient

delt	preset period
design	design
E	variable expectation
exf	exfiltration
F	air flow rate
fan	fan
fh	outdoor air
fut	furniture
i	the *i*th variable
inf	infiltration
k	the *k*th variable
load	indoor cooling load
leak	leakage
max	maximum
min	minimum
new	new samples
trans	the solar gain transmitted through the window
trn	return air
s	supply air
sa	sol-air
set	set-point
st	static
th	threshold
wi	wall inside
win	window
α	the level of significance

Superscripts

^	estimated output on the score space
~	estimated output on the residual space
–	estimated output on EWMA

A FAULT DETECTION AND DIAGNOSIS STRATEGY FOR VAV AIR DISTRIBUTION SYSTEM

Table of Contents

CHAPTER 1 INTRODUCTION

1.1 Background

Variable-air-volume (VAV) air-conditioning system, which was deemed more economical than other alternative systems, has been widely adopted in the building engineering to maintain the cooling and heating demands. However, in complex VAV systems, faults at system level, sub-system level, component level, control and sensor level would not only reduce the economic benefits of the system but also lead to occupant discomfort. Though the benefits for fault detection and system improvement are difficult to quantify, the potential saving out of faulty and non-optimal operation of HVAC system alone in commercial buildings were estimated to be 20-30% (Hyvarinen and Karaki 1996).

Research on fault detection and diagnosis (FDD) techniques for HVAC systems and equipment became very active and intensive in recent years. Various faults have been attacked at different levels. Some collaborative IEA (International Energy Agency) research programs on HVAC FDD had been completed, such as Annex 25 (Hyvarinen and Karaki 1996), Annex 34 (Dexter and Pakanen 2001) and Annex 40 (Visier et al. 2005). Furthermore, the IEA team has set up another research program (Annex 47) on commissioning of existing and low energy building HVAC systems for improved energy performance.

Commissioning is the process of ensuring that systems are designed, installed, functionally tested and capable of being operated and maintained to perform in

conformity with design intent and to keep buildings in optimal condition (Annex 40). It is considered a process not an action and described in a much broader way than in the UK (CIBSE 1996). Continuous commissioning is a successive commissioning process at operation and maintenance levels to resolve operating problems, improve comfort, optimize energy use, and recommend retrofits if necessary. Commissioning and continuous commissioning tools play a more and more important role in modern HVAC systems.

1.2 Motivation

VAV systems and their control strategies become more and more complex to meet the increasing demands on indoor environment quality (IEQ) and energy conservation. Automatic monitoring and control of VAV systems are necessary in modern buildings. Many supervisory VAV control strategies, such as supply air temperature reset, static pressure reset and advanced fresh air flow rate control, have been put into operation as well. Both components and sensors are playing essential roles in operation and control. However, both components and sensors in VAV air distribution systems suffer from complete failure (hard fault) and partial failure (soft fault) easily, which result in energy waste, performance degradation or totally out of control. Therefore, FDD in VAV systems is of great interest.

Although many studies have been carried out on the FDD of VAV subsystems, little has been done on cases involving sensor faults and sensor validation in VAV air distribution systems. The more and more complex control strategies in VAV systems increase risks of performance degradation resulting from both component faults and

sensor faults. It is essential to guarantee healthy components and sensors in VAV air distribution systems for efficient operation.

In VAV systems, the most significant technical problem perceived is the interaction among VAV units equipped with a control loop, where information exchange takes place between several control strategies (Yoshida and Kumar 1999). Such interaction must be carefully analyzed and measured for achieving optimal control and therefore, in development of any FDD techniques. On the whole, the commissioning and continuous commissioning tool developed from FDD strategy for entire VAV air distribution system with the component faults, sensor faults and interactions concerned is desirable.

Building management systems (BMSs) are widely employed in modern buildings. The huge amount of data available on BMS central stations and outstations provide rich information for monitoring, optimization and FDD of HVAC systems. Also, BMS provides essential and rich information for VAV system fault detection and diagnosis, which offer the hardware basis for the development of FDD strategy and therefore the automatic commissioning tool application.

1.3 Literature Review

1.3.1 FDD Research in HVAC Field

Faults typically found in HVAC systems are due to improper design, application, or operation of the systems (Linder and Dorgan 1997). FDD in HVAC systems has been considered from different angles, such as viewing building as a whole system, viewing from subsystems (e.g. water-side and air-side) and viewing from individual components. For whole building diagnostics, House and Kelly (1999), and Claridge et

al. (1999) applied systematic methods with top-down and bottom-up approaches to detect and locate the causes of the degradation of building performance, such as poor IEQ and energy waste after a period of operation. At the building system level diagnosis, reference models can be categorized into physical models and data driven models. Physical models are based on the first principles, such as EnergyPlus model (Crawley et al. 2000). Statistical models, such as benchmarking (Piette et al. 2001), and black-box models, such as artificial neural networks (Kalogirou et al. 1997), are some data driven model applications for the whole building diagnosis.

Water-side Systems

Chillers are the most important components in HVAC water-side subsystems. Chiller performance degrades naturally and different kinds of faults (system/component faults and sensor faults) may occur in the course of operation, which might result in a great waste of energy. Comstock and Braun (1999) conducted a survey on chiller faults. The main thirteen soft faults of chillers were selected, such as refrigerant overcharge, non-condensable gas (e.g. air) in the refrigerant, defective expansion valve and refrigerant leak/undercharge. It was estimated that approximately 60% of those faults could be detected using measurements of the thermodynamic states of chillers. According to their survey, the listed faults accounted for about 42% of the service requirements and about 26% of the repair costs.

Gordon and Ng (1995) developed a simple thermodynamic model to capture the universal aspects of chiller behavior. The model predicts chiller performance over many different operating conditions by using just a few measurements. It was tested with reciprocating, centrifugal and absorption chillers. Stylianou and Nikanpour (1996) used this model as part of their FDD approach applied to a reciprocating chiller. This

model was used solely for fault detection (not diagnosis) during steady-state operation of the chiller. Stylianou (1997) added a statistical evaluation of the model residuals in order to improve the diagnostic classifier later. Bailey (1998) trained an artificial neural network (ANN) using normal and fault data from a screw chiller in order to provide direct classification of normal and faulty performance. The ANN model used a large number of inputs to predict the output classes.

Rossi and Braun (1997) presented an FDD method for packaged air conditioners using nine temperature measurements and one humidity measurement to detect and diagnose five faults: refrigerant leakage, liquid line restriction, leaky compressor valves, fouled condenser coil, and dirty evaporator filter. A steady-state model was used to predict temperatures in a normally operating unit in order to generate innovations or residuals for both the fault detection and diagnostic classifiers. The magnitudes of the residuals are statistically evaluated to perform fault detection and compared with a set of rules based on directional changes to perform fault diagnosis.

Breuker and Braun (1998a) analyzed a database of service records about rooftop air conditioner from an HVAC service company. The faults were analyzed in terms of both frequency of occurrence and total cost involved. Transient tests were carried out on a three-ton packaged rooftop unit in a laboratory over a range of conditions and fault levels. Eleven measurements were taken in order to characterize the fault impacts. A set of rules for the FDD was derived from the test data. Moreover, Breuker and Braun (1998b) did extensive experimental evaluations of the FDD performance using the test data. The data without faults were used to train the models for normal operation and determine statistical thresholds for fault detection, while the transient data with faults were used to evaluate FDD performance. Good performance was

achieved in detecting and diagnosing five faults using a “low-cost” design with only six temperatures (2 input and 4 output) and linear models.

McIntosh et al. (2000) further developed the detailed mechanistic chiller model which was originally set up by Braun (1988). Within the model, the characteristic quantities (CQs) that are most sensitive to faults are identified for their use in fault detection and diagnosis.

Other equipment in chilling systems was studied as well as chillers. Ahn et al. (2001) applied a model-based method for the detection and diagnosis of faults in the cooling tower circuit of a central chilling system. Faults that occur in the cooling water temperature sensor, the cooling tower pump, and the cooling tower fan are considered. The faults are detected through deviation in the values of CQs. The CQs chosen to represent the performance are the conductance-area product of the tower, the approach, the effectiveness, and fan power.

FDD technique was also extended to predictive maintenance. Rossi and Braun (1996) evaluated the maximum cost saving associated with using optimal service scheduling for the cleaning of heat exchangers in packaged air-conditioning equipment and developed a near optimal scheduling technique for practical use. It demonstrated that there is a significant opportunity for cost saving associated with optimal scheduling of condenser and evaporator maintenance by comparing it with results for regular service intervals and service dictated only by violation of the constraints. Savings of between 5% and 15% of costs were found to be possible through optimal maintenance scheduling.

Sensors often suffer from drifting, fixed bias, accuracy degradation and complete failure (constant output). Sensor biases happen unnoticeably at a slow rate but

progressively worsen over a period. Wang and Wang (1999, 2001 and 2002) developed a law-based sensor FDD&E strategy, which took all the commonly used temperature and flow rate sensors in chilling plant into account at the same time. The unbalance residuals of the energy conservation and mass conservation equations in steady state were used as an index to detect sensor biases. Wang and Cui (2005) proposed a strategy for sensor FDD in centrifugal chiller systems, which was evaluated by validation tests

Air-side Systems

VAV systems serve as the air-side systems widely. A survey was conducted to sort out the top ten faults of VAV air handling system by collecting information from professionals (Yoshida 1996): (1) poor air quality, (2) water leakage, (3) room air temperature deviation due to excessive heat generation, (4) room air temperature deviation due to inadequate air-flow rate, (5) too much or less air volume of VAV unit, (6) excessive pressure difference across an air filter, (7) abnormal noise or vibration, (8) room air temperature deviation due to inadequate positions of diffusers, (9) false opening signal to a VAV unit control, (10) room air temperature deviation due to insufficient water flow rate. Further investigation revealed that mechanical faults (such as coil and damper malfunction) were common.

Previous FDD studies of air-side systems focused on the major equipment, such as air handling units (AHUs), fans and local feed water pumps. Lee et al. (1997) generally described 11 faults of the system from fan failure to sensor failure and the use of a two-stage artificial neural network for fault diagnosis in a simulated AHU. The stage one neural network was trained to identify the subsystem in which a fault occurred. The stage two neural network was trained to diagnose the specific cause of a

fault at subsystem level. Regression equations for the supply and mixed air temperatures were obtained from simulation data and were used to compute input parameters to the neural networks. Results demonstrated that the recovered estimate of the supply air temperature could be used in a feed-back control loop to bring the supply air temperature back to the set-point value.

Dexter et al. (Dexter and Benouatets 1996, Ngo and Dexter 1999, Dexter and Ngo 2001, Liu and Dexter 2001) concentrated on coil heat exchange process of AHUs and analyzed 5 faulty modes: fouled coil, valve leak, valve stuck closed, valve stuck midway and valve stuck open. They designed a robust fuzzy model for AHU fault diagnosis accounting the temperature sensor error. The model-based approach was assessed by applying the fault diagnosis scheme to remotely commission the AHUs in a commercial building. The scheme was robust since no false alarms were generated. A multi-step fuzzy model-based approach further developed the robust diagnosis scheme. A computer simulation study demonstrated that a more precise diagnosis could be obtained using this new scheme. Experimental results presented that the proposed scheme did not generate any false alarms. A supervisory control scheme that adapted to water-side and air-side fouling using fuzzy models was evaluated as successful.

House et al. (1999, 2001) considered several faulty cases of an AHU including stuck cooling coil valve, fouled cooling coil, leaky heating coil valve, supply fan degradation, return fan controller failure, mixing box linkage failure and went further to VAV box damper stuck. Five classifiers, i.e. ANN classifier, nearest neighbour classifier, nearest prototype classifier, rule-based classifier and Bayes classifier, were tested for detecting and diagnosing seven faults of a simulated AHU system. An

expert rule set with 28 simple rules for fault detection in AHUs was used to identify some obvious faults. Field trials of the expert rule set successfully identified two occurrences of faults with mixing box dampers. The first was a stuck damper and the second was a manual override of a control signal that was not returned to automatic operation. However, they pointed out that the effort devoted to developing diagnostic capabilities for VAV boxes had been limited in comparison to AHUs and other types of HVAC equipment (House et al. 2003).

Norford et al. (Shaw et al. 2002, Norford et al. 2002) investigated both abrupt and degradation faults on the air mixing section (stuck-closed damper, leaky damper), filter coil section (leaky cooling coil valve, reduced coil capacity) and fan section (drifting pressure sensor, unstable fan controller, slipping fan belt) of three real AHUs and demonstrated two methods for fault detection and diagnosis. These two methods are physical model-based method and grey box method. The physical model predicted the temperature of the air or static pressure at the outlet of the component. A fault can be detected in terms of degradation in the expected system performance. The grey box method used models derived from the system characteristics that related electrical load to certain variables. A fault could be described as a change in the expected system energy consumption. Both physical model method and grey-box model method detected nearly all of the faults in the two matched AHUs. However, physical model approach relied on the sensor typically installed in VAV system and grey-box model approach could not detect a fault that affects performance but has no effect on the electrical load.

Researchers began to focus their interest on subsystems in recent years. Katipamula et al. (Brambley et al. 1998, Katipamula et al. 1999) noticed that a failure

of the economizer may go completely unnoticed. She and her partners designed the Outdoor-Air/Economizer (OAE) Diagnostician to monitor the performance of AHUs and automatically detect problems with economizer operation or ventilation problems for systems without economizers using decision tree method. A decision tree structure was installed on seven AHUs in two commercial buildings for out-door air ventilation and economizer diagnosis. The findings clearly demonstrated the potential of automated diagnosis technology to detect about 20 different basic operation problems.

Dodier et al. (1998) particularly studied on fan-powered mixing box for both damper failure and power failure. The probabilistic inference methods were adopted in Real-Time Diagnostic System (RTDS). The results of applying the RTDS to HVAC laboratory data were presented. The tests indicated that application of this inference system to the diagnosis of mixing box failures yielded encouraging results.

Wang and Chen (2001) paid particular attention to the air flow sensor failure of sensor-based demand control ventilation systems. It was testified by the simulation test that fault-tolerant control for outdoor ventilation air flow rate based on neural network was applicable. Furthermore, Wang and Xiao (2004a, 2004b) developed a strategy based on the principal component analysis (PCA) method to detect and diagnose the sensor faults in AHUs. Sensor faults were detected using the Q statistic (squared prediction error, SPE). They were isolated using the Q statistic and Q contribution plot supplemented by simple expert rules. The fault isolation ability of the PCA method was improved using the multiple models. Simulation tests and measurements from the BMS of a building were used to verify the strategy. The robustness of the PCA based strategy in detecting/diagnosing sensor faults was examined.

As overall system reliable control counts on proper works of every component, researchers began to particularly throw light on VAV terminals and valves. McGhee et al. (1997) listed typical failures in valves and actuators and classified faults in process valves and actuators. ANN method applied to valve process diagnosis was validated by both experimentation and simulation tests. Wang and Jiang (2004) developed a recurrent celebellar model articulation controller (RCMAC) to learn the normal characteristics of the valve. Two characteristic variables were defined as the degradation index and waveform index for analyzing the residual errors. The strategy to identify the type and the severity of the degradation was evaluated by the simulation tests.

Seem et al. (1999) looked into VAV terminal on-line control recently. Two indices were calculated from BMS driven data for VAV box on-line monitoring and fault detection. One index provided an indication of how well the controller maintain the process output while the other provided the indication of mechanical components (actuators, dampers) operating status. Schein and House (2003) developed VPACC (VAV box performance assessment control charts) using a small number of control charts to assess the performance of VAV boxes. VPACC was tested using emulation, laboratory, and field data sets with encouraging results.

Yoshida et al. (1996, 1999, 2001) intensively worked on VAV damper failure and tested his approach on both sudden and consecutive faults. Both ARX model and extended Kalman Filter were tested to detect an abrupt fault of VAV damper stuck and malfunction of AHU control loop. It was shown that faults that were difficult to detect by a simple limit checking method could be detected in both cases. By making

artificial faults in the tested system, it was verified that the ARX method is robust and can even detect different faults including damper stuck at half open position.

A few studies were conducted on VAV system control stability. Zhang and Nelson (1992) used a numerical model to simulate a space controlled by a VAV system. The effects of building system components, including envelop heat transmission, thermal mass of building enclosure, non-temperature-related heat gains, cooling system capacity, and time delay of thermal effect, were all examined using this model. However, this simple model does not address the problems associated with system interactions, nor those associated with VAV air distribution. The unstable operation caused by interaction among the components and the non-linear nature of the components was analyzed by Li and Levermore (2000) based on a simple VAV test rig. The stability regions for the VAV test rig system were established through two new approaches. The boundary lines of the stability regions were simply given in terms of the proportional gain and the integral gain of the fan PI controller.

Control of VAV air distribution systems counts on the proper design and control of all components. Dean and Ratzenberger (1985) presented a mathematical description of all the components in the feedback loop that determine the operation of a variable volume terminal unit. It was concluded that there were three principal differences between the “poor” design and the “good” design: duct pressures, terminal unit sizes, and type of actuator used. House et al. (2003) discussed the relationship between controls and diagnostics for air distribution systems. New findings from a diagnostic method that enabled operational characteristics of individual HVAC components to be extracted from high-frequency measurements of whole building power were presented. Some research challenges were also addressed.

A controller performance index developed by Desborough and Harris (1992) was proposed as a fault detection technique for the online monitoring of feedback control systems. Fasolo and Seborg (1995) pointed out that the advantage of this approach was that the performance index can distinguish between process variability due to external sources and variability due to a significant change in the feedback loop.

The most significant technical problem perceived in VAV systems is interaction among VAV units equipped with a control loop. In most cases, faults and their symptoms are nested, i.e., one fault may have many symptoms and one symptom may be associated with many faults. Han et al. (1999) presented an overall model-based FDD system to attack the problem on many levels of abstraction: from the signal level, controller programming level, system component level, all the way up to the information and knowledge processing level. However, detailed fault analysis in VAV air distribution system was not included. There is no applicable commissioning and continuous commissioning tool for VAV air distribution system when component faults, system interaction, controllers and sensor faults are of concern.

1.3.2 Comparison of FDD Methods

There are many different methods developed for the FDD of HVAC systems. But there is unlikely to be a ‘best’ solution to every problem because engineering designs always involve trade-offs between competing priorities. The FDD methods were roughly divided into two categories as model-based and model-free but many mathematical thoughts could be used by both. Model-free FDD methods do not utilize explicit mathematical model of the target system (Figure 1.1), and model-based FDD methods employ the system models (Figure 1.2). Generally speaking, a good FDD system should have better sensitivity, faster detection speed and less false alarms.

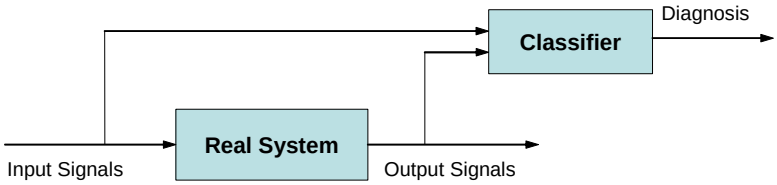

Figure 1.1 Schematic diagram of a typical model-free FDD method

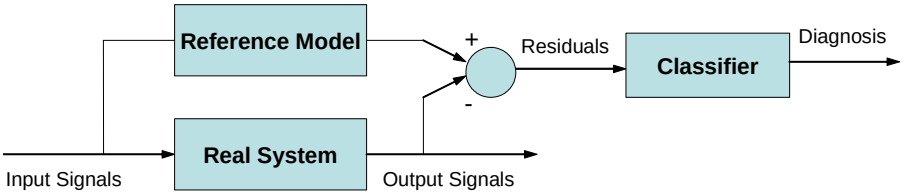

Figure 1.2 Schematic diagram of a typical model-based FDD method

Except knowledge-based FDD methods, most model-free methods aim at one instrument each time, such as physical redundancy method. Physical redundancy approach can often be effective in achieving sensor FDD, but its cost, space, and complexity of installing redundant sensors make it unattractive in engineering practice. Limit checking method has been proved to be effective in univariate quality control (Haves 1999). However, fault measurements that are within the limits but do not follow the normal correlation among variables are undetectable using this approach. At the same time, it is difficult to find a variable to evaluate the whole system performance in modern large-scale engineering systems. For some simple engineering systems, it is easy to detect and diagnose faults by mapping symptoms to fault originals, i.e. using experience knowledge. It is challenging to apply knowledge-based approach to large-scale and distributed systems, such as HVAC systems, because the fault-symptom knowledge is seldom completed, not all rules are applicable due to changing operation condition, and it also requires high skills to develop an expert system.

Model-based FDD method can hardly avoid the complexity of setting up models, no matter first principle models, data-driven models (black box models) including ANN, ARX, state space equations, PCA etc., or semi-physical models (grey box models) are used. Usually, first principle models can obtain the best final results of FDD, i.e. finding the fault position, because each variable in the model has direct physical meaning. However, dynamic physical models are always differential equations, plenty of approximation are made in order to solve them, which decreases the accuracy of physical models. On the other hand, model parameters, which depict the physical characteristics, are seldom enough because either the design data or the manufacturer's data are usually incomplete. Data-driven models can avoid the complexity of setting up physical models, but they meet great challenge to obtain good final results due to their non-physical nature. At the same time, training model needs a lot of fault-free data with high quality and high mathematic techniques. Once a model is built up, how to use it in each control mode needs consideration because the training data are in relative short span compared with total operation period. Semi-physical models partly compromise the final solvability of physical models and data-driven models. The demand on model training technique is also very high.

More and more advanced techniques in mathematics, statistics, signal process, linear/nonlinear theory, system identification, patter recognition, etc, have been introduced to FDD applications in engineering systems. In order to solve the problem, sometimes various techniques and methods are used in parallel.

1.4 Aim and Objectives

FDD for VAV systems, especially for large-sized systems in which dozens of VAV boxes are involved, could provide great help in improving system control and

indoor air quality, enhancing building energy efficiency, and prolonging components' life. Automatic commissioning tool developed from the FDD strategy could ensure the healthy condition of the systems without delay. However, past studies on FDD for VAV systems are not sufficient though research efforts in this field are growing recently. No applicable automatic commissioning tools for VAV systems had been developed with comprehensive faults and the interaction among the faults considered.

This thesis aims at multiple fault detection and diagnosis of VAV air distribution systems, with objectives listed as follows:

1. Develop a FDD strategy of acceptable robustness and computational efficiency for multiple VAV faults of typical pressure independent VAV air distribution systems. Various faults and system interactions are to be considered. Methodology and computation algorithms are developed.
2. Develop a commissioning and continuous commissioning application tool on the basis of the FDD strategy.

This thesis assesses and evaluates the performance of the developed FDD strategy using both simulation and in-situ data. The automatic commissioning tool developed from the FDD strategy is validated using both simulation data and real BMS database with in-situ validation as well.

1.5 Organization of This Thesis

This chapter described the background of FDD and commissioning in the HVAC field. The motivation to develop a commissioning and continuous commissioning tool for typical VAV air distribution systems was described through emphasizing the importance of the proper design and control of all components/sensors/controllers in

the systems. Literature of FDD in HVAC field was critically reviewed. The objective of developing a FDD strategy for VAV air distribution system multiple faults was presented.

Chapter 2 introduces the typical control of VAV zones. A high-rise commercial building served by pressured-independent VAV air-conditioning systems was investigated. VAV terminal faults were observed during the terminal re-commissioning exercise. Root causes for VAV air distribution system typical faults are summarized.

Chapter 3 briefs the statistical process control (SPC) techniques. The overall architecture for a VAV FDD strategy is presented, which integrates qualitative reasoning and quantitative models. The strategy consists of eight FDD schemes to attack the eleven root faults concerned at two steps. The hard faults are analyzed at the first step and the soft fault is dealt with at the second step.

Chapter 4 presents the outline of Principal Component Analysis (PCA) method, which is chosen to deal with the soft fault, VAV terminal flow sensor biases, at the second step. PCA models at system level and terminal level are set up serially. Both T^2 statistic and *SPE* are used for fault detection. Contribution plot is applied for fault isolation. Sensor reconstruction is conducted after fault identification. Iteration process is adopted using the recovered measurements to enhance the robustness and accuracy of the PCA-based FDD scheme for multiple sensor fault detection and isolation.

Chapter 5 describes two test facilities. The first one is a simulated system on TRNSYS platform. A typical VAV system is simulated to generate the test data. The

first principle models of VAV equipment, components, controllers and sensors are presented. The realistic system network model is developed to simulate the real air distribution system. The second one is real systems.

Chapter 6 presents the test results for FDD strategy validation. The FDD schemes and their interaction on component faults and sensor hard faults at the first step of the strategy are evaluated. Both simulation tests and in-situ tests were carried out to test the FDD ability of the schemes. Multiple faults are introduced to verify the interaction among the schemes in parallel.

Chapter 7 presents the validation results of the PCA-based flow sensor FDD scheme using both simulation tests and site data retrieved from a real building BMS. Multiple sensor faults could be detected by sensor data recovery and iteration process of the scheme. The robustness and sensitivity analysis of the PCA-based FDD method is conducted.

Chapter 8 presents the software package developed from the FDD strategy to implement the commissioning and continuous commissioning automatically. The software package is applied with the input data read in from the database. The software package is validated using both the simulation data files and real building database.

Chapter 9 summaries the work reported in this thesis, and gives recommendations for future application and research works in the related areas.

CHAPTER 2 SITE STUDY – FAULTS OF VAV TERMINALS AND THEIR ROOT CAUSES

Site investigation on all VAV terminals in a large-scale modern commercial building revealed that 20.9% of the total terminals in the building were ineffective, which indicates VAV terminal faults are common. This chapter presents the site study on all VAV terminals in this high-rise commercial building in detail.

Section 2.1 introduces the typical control loops for VAV zone temperature control. Section 2.2 briefly describes the building and its VAV air-conditioning system. The observed VAV terminals faults are presented in detail. Section 2.3 concludes the root causes of the observed faults and Section 2.4 summarizes this chapter.

2.1 Typical VAV Zone Control

VAV air conditioning systems are highly dynamic and nonlinear due to the interaction between various zone air temperature control loops and the static pressure control loop. There are two typical VAV terminal control loops, namely pressure-dependent and pressure-independent, to stabilize the zone air temperature with the effects of system dynamics and nonlinearity.

Pressure-dependent VAV terminal control damper’s position in response to the room temperature (Figure 2.1) and flow may increases and decreases as the main duct

pressure varies. The block diagram of pressure-dependent VAV zone air temperature control is shown in Figure 2.2.

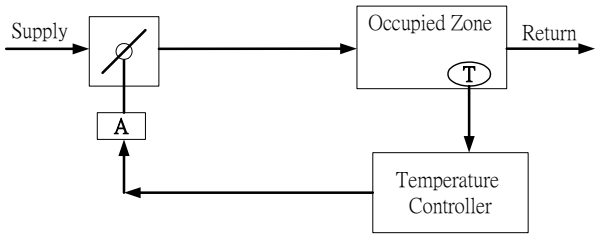

Figure 2.1 Schematic of pressure-dependent VAV terminal

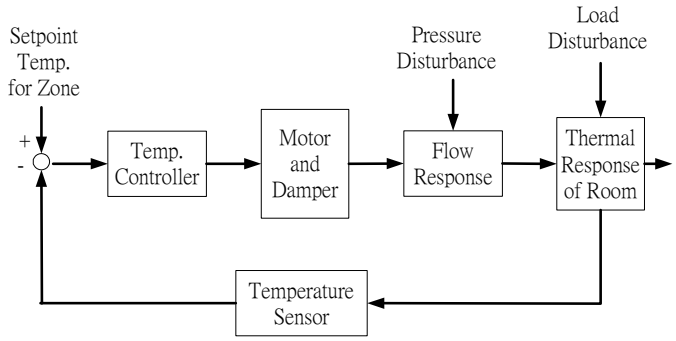

Figure 2.2 Block diagram of pressure-dependent VAV zone air temperature control

Pressure-independent VAV terminal measures actual supply air flow rate and control flow in response to room temperature (Figure 2.3). The block diagram of pressure-independent VAV zone air temperature control is shown in Figure 2.4. The terminals can be field- or factory-adjusted for maximum and minimum air settings. They could operate at inlet static pressure as low as 50 Pa.

Cascade control is the basis for the pressure-independent controllers. Basic cascade control has two loops (Figure 2.4). The inner loop is called the secondary loop; the outer loop is called the primary loop. The reason for this terminology is that the outer loop deals with the primary measured signal. It is also possible to have a cascade

control with a number of measured signals, up to a certain limit. By dealing with the faster and slow processes (loops) in the control systems separately, the controller compromises the response speed and control stability and achieve quicker response and more stable control than that can be achieved by using the process variable to modulate the control signal directly.

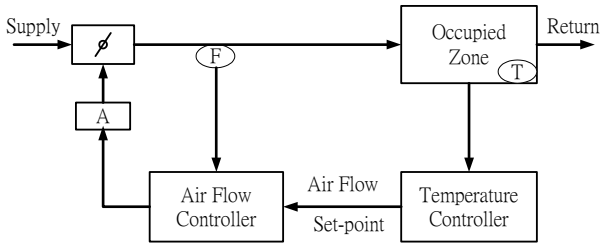

Figure 2.3 Schematic of pressure-independent VAV terminal

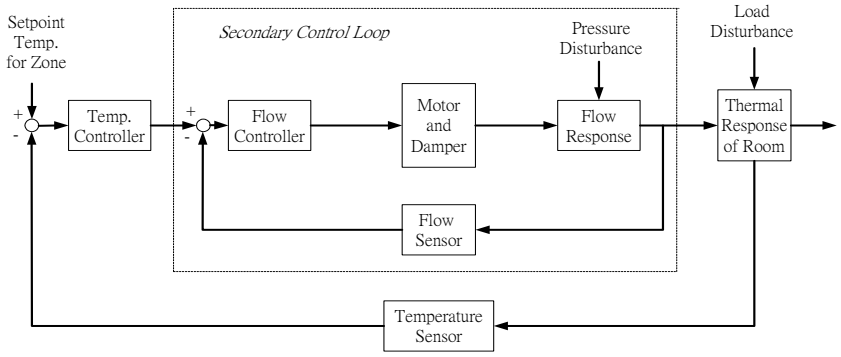

Figure 2.4 Block diagram of pressure-independent VAV zone air temperature control

The pressure independent flow controller with cascade control works precisely due to better control stability and faster response in load changes. It is achieved by employing two control loops separating the flow set-point reset based on the deviation of the measured air temperature in the occupied space from its set-point and flow control based on the deviation of the measured VAV air flow rate from its set-point. That allows the effect of fluctuations in the pressure supply as the results of

disturbances from other parts of the systems on the space temperature control is eliminated as the inner loop response quickly to these fluctuations before they affect the space temperature control.

A detailed stability study on practical VAV zone air temperature control loop compared the performance of typical pressure dependent and pressure independent VAV zone flow controllers (Hung et al. 1999). With steady static pressure, both pressure dependent and pressure independent flow controllers provided stable zone air temperature control, with slightly superior performance given by the latter. However, with large fluctuating static pressure, the performance of zone air temperature response by pressure independent control was excellent while that by pressure dependent control resulted in zone air temperature swings. The pressure independent flow controller is thus widely used in large complex VAV air conditioning systems.

2.2 VAV Terminal Faults Observed from Site Investigation

2.2.1 Building and System Description

The site study, along with the VAV system re-commissioning involving all VAV terminals was carried out in a commercial building (Figure 2.5). The building, located in Hong Kong Island, was completed in 1995. The AHUs and VAV systems provide ventilation, cooling or heating, as needed, throughout the year. The strategy of outdoor air demand-control was achieved in this building by the carbon dioxide sensors installed in the main return air ducts at each floor. The building configuration is listed in Table 2.1.

Figure 2.5 Commercial building

Table 2.1 Configuration of the building

Total Gross Floor Area:	Over 55,000 m^2
Number of Storeys:	39
Typical Floor Area:	~ 1,500 m^2
Number of VAV Terminals at Each Floor:	35 ~ 43
Total number of VAV Terminals:	1,251

All the VAV terminals are pressure-independent under cascade control. Four variables are involved in the terminal control loop: i). zone temperature, ii). zone temperature set-point, iii) required air flow rate (or air flow set-point), iv). measured air flow rate.

The building employs a fully automated BMS which performs the environmental control of the indoor spaces. The BMS schematic diagram is shown in Figure 2.6.

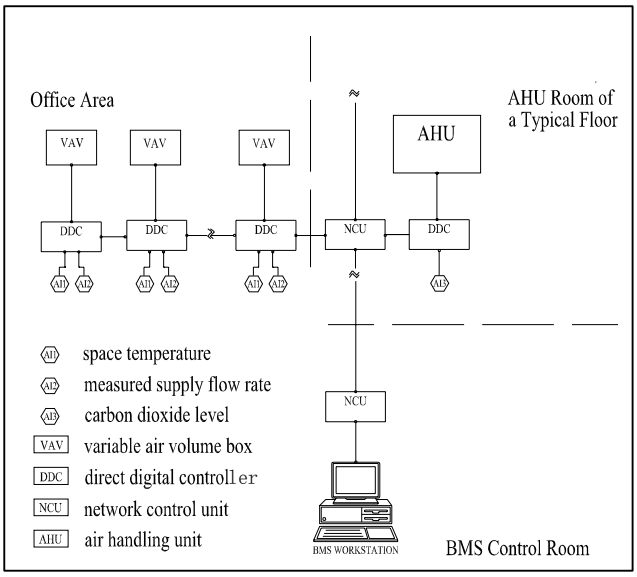

Figure 2.6 BMS schematic diagram of the building

All data of VAV terminals could be collected through the direct digital controller (DDC) of the terminals and temporarily stored in Network Control Unit (NCU). When the storage space of NCU is full, all data would be transferred to the hard-disk of BMS workstation.

2.2.2 VAV Terminal Faults Observed

The VAV terminal re-commissioning exercise was carried out in August 2002. The procedure of the re-commissioning was designed as follows:

1. Logged the system variables and the four measurements for the VAV terminals. Due to the limitation of BMS hardware, the four variables for the VAV terminals of three floors were logged at 5-minute intervals for three days simultaneously.

2. Set the criteria to screen the ‘suspected’ VAV terminals. The measured variables deviated more than ±10% from the set-point would be deemed as ‘suspected’.
3. Created a form for the technicians to check the ‘suspected’ VAV terminals on site. The associated symptoms of the ‘suspected’ terminals should be recorded in the form.

Table 2.2 Summary of VAV terminal faults/symptoms

No.	Faults and Symptoms	No.	Percentage
1	Temperature sensor hard error	66	25.3%
2	DDC error	46	17.6%
3	Diffuser damper closed as requested by tenants	41	15.7%
4	Design flow too large	28	10.7%
5	VAV boxes dismantled by tenant	14	5.4%
6	Damper actuator failure	10	3.8%
7	Part of diffuser being wrapped by adhesive tape	9	3.5%
8	Temperature set point too low	7	2.7%
9	Abnormal space temperature requested by tenants	5	1.9%
10	Temperature sensor located too close to VAV diffuser outlet	4	1.5%
11	Too many people in a room	1	0.4%
12	VAV box not accessible (cause unknown)	30	11.5%

The re-commissioning and investigation of each VAV terminal was based on the trend data of three days. By investigating the operation of the VAV terminals, it was found that very often the measured VAV airflow could not approach the flow set-point and the space temperature could not approach the set point. General screening got 261 ‘suspected’ VAV terminals out of 1251, which means that 20.9% of the total terminals

in the building were probably problematic. All the 261 ‘suspected’ VAV terminals were further examined and verified by the technicians over fourteen days. Such detailed checking found twelve faults/symptoms among the ‘suspected’ VAV terminals identified as listed in Table 2.2.

Around 46% of the suspected VAV terminals were found faulty due to temperature sensor error, VAV DDC error or damper actuator failure. Part of the terminals (19%) were found faulty due to illegal operation on site, such as diffuser dampers closed or diffusers wrapped by adhesive tape, while the cause(s) of 11.5% faulty terminals could not be identified as they were not accessible.

The consequences of faults could be classified into four categories related to: poor environment, waste of energy, unreachable design value, and physical damage. The observations of this survey match with the conclusion of the survey on AHU system faults conducted by Yoshida et al. (1996), which covered a wider range of faults from design faults to user-level faults in AHU and VAV systems. Concerning VAV terminals, their survey revealed that zone air temperature error and local DDC error were common, which was in line with our investigation results.

2.3 Root Causes of the Observed Faults

In most cases, faults and their symptoms are mixed up. One fault may have different symptoms and one symptom may be associated with a few faults. The above 12 faults/symptoms discovered in the site study could actually be either causes or symptoms. If investigating each case carefully, we found that the causes could be divided into two categories: mechanical failures (damper failure; diffuser wrapped,

VAV terminal under/over capacity) and sensor/controller failures (temperature/flow sensor failure; PI controller failure). Detailed site investigation found that there were many different causes related to various faults in VAV terminal. However, for the convenience and efficiency of commissioning and fault diagnosis, it is desirable to classify the causes of faults into a few general categories. Based on the actual VAV physical systems and the causes of the faults discovered on the terminals investigated, eleven root faults are summarized for the pressure independent VAV air distribution systems as listed below (Faults of AHU are not included in this study):

- Fault 1: Poor tuning of static pressure control loop
- Fault 2: Zone temperature sensor reading frozen
- Fault 3: VAV controller hard failure
- Fault 4: VAV terminal under/over capacity
- Fault 5: VAV damper stuck
- Fault 6: VAV flow sensor reading frozen
- Fault 7: VAV flow sensor reading deviation to minimum/maximum
- Fault 8: Poor tuning of VAV controllers
- Fault 9: VAV damper sticking
- Fault 10: VAV damper hysteresis
- Fault 11: VAV flow sensor bias

The static pressure sensor is regarded as fault free in this study since the sensor fault was analyzed by the researchers previously (Wang and Xiao 2004a, 2004b). Zone temperature sensor bias would not be detected by the system characteristics and might be offset by adjusting the zone temperature setting. Thus this fault is not

included. The same serial numbers of faults are used in the following chapters of FDD study.

2.4 Summary

This chapter describes typical zone control loops of VAV systems. Both pressure-dependent and pressure-independent control loops are introduced. Pressure-independent control gives superior performance especially under fluctuating static pressure.

The detailed site study on all VAV terminals of a local commercial building was conducted. Four variables of each terminal were logged by the BMS. They are zone temperature, zone temperature set-point, air flow set-point and the measured air flow rate. Checking on the data trend screened 261 ‘suspected’ VAV terminals, which was 20.9% of the total terminals. Further site investigation on the ‘suspected’ terminal summarized 12 symptoms and causes.

To set up the FDD strategy and then commissioning tool for the typical VAV air distribution system, it is desirable to classify the causes of faults into a few general categories. Eleven root faults are summarized according to actual physical systems and the fault causes discovered in VAV terminal investigation.

CHAPTER 3 FDD STRATEGY FOR MULTIPLE VAV FAULTS

The full scale site survey summarized eleven root faults in the VAV air distribution system in Chapter 2. On this basis, a FDD strategy is developed using hybrid approach to deal with multiple VAV faults as an automatic commissioning tool. Qualitative reasoning and quantitative models are adopted in the strategy to deal with the faults. PCA (Principal Component Analysis) method is used for VAV terminal flow sensor bias detection and reconstruction.

In the FDD strategy, the eleven root faults are detected by eight FDD schemes constructed within the overall architecture of qualitative/quantitative reasoning. The hard faults are designed to be analyzed at the first step in parallel and the sensor soft fault is designed to be analyzed at the second step in the strategy. Statistical quality control (SPC) techniques are adopted in a few FDD schemes to build up the object-oriented SPC models to analyze the specified fault(s).

Section 3.1 briefly introduces the SPC techniques used in the FDD strategy. Section 3.2 briefs the qualitative/quantitative FDD methods. Section 3.3 depicts the FDD strategy for multiple faults in VAV systems. Section 3.4 details the eight FDD schemes for eleven root faults detection. Section 3.5 summarizes this chapter.

3.1 A Brief of Statistical Process Control (SPC) Techniques

As SPC models are widely used in the FDD strategy developed in this thesis, the SPC techniques are briefly introduced here below.

The SPC generally uses certain statistical methods designed to detect changes in a process over a time. The objective of the SPC is to monitor the performance of a process over time in order to verify that the process is remaining in a 'state of statistical control', which exists if certain process or product variables remain close to their desired values.

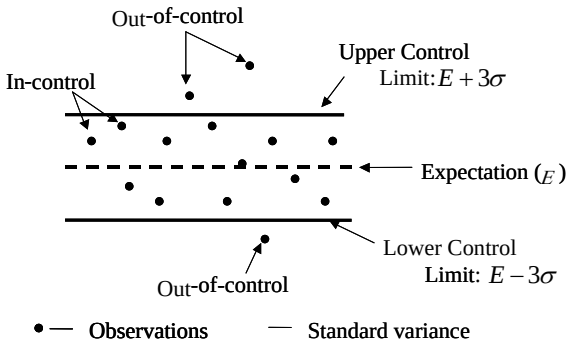

Figure 3.1 Illustration of Shewhart chart

The development of the SPC research and application involves two major stages, i.e. the univariate process control and the multivariate process control. In some earlier manufacture processes, one or several uncorrelated quality characteristics are assumed to have stable expectations, and used to define the quality of the product. Traditional univariate statistical control charts, such as the Shewhart chart (so-called the 'three-sigma' principle) as shown in Figure 3.1, are widely used to monitor those independent characteristics, and therefore monitor the process and product quality.

The normal distribution is the most important distribution in the application of statistics. Under normal distribution, 99.73% of the population values fall within the 'three-sigma' control limits defined by the expectation plus and minus three standard deviation ($E \pm 3\sigma$).

Two very effective alternatives to the Shewhart control chart may be used when small shifts are of interest: the cumulative sum (CUSUM) control chart, and the exponentially weighted moving average (EWMA) control chart.

The CUSUM chart directly incorporates all the information in the sequence of sample values by plotting the cumulative sums of the deviations of the sample values from a target value, *E*, as shown in Equation 3.1.

$$CUSUM_k = \sum_{i=1}^{k}(y_i - E) = (y_k - E) + \sum_{i=1}^{k-1}(y_i - E) = (y_k - E) + CUSUM_{k-1} \qquad (3.1)$$

The process remains in control if the CUSUM defined is a random walk with mean zero. However, if the mean shifts upwards, then a positive drift will develop in the CUSUM. Conversely, if the mean shifts downwards, a negative drift in CUSUM will develop.

To present CUSUMs, the tabular CUSUM is widely used. The tabular CUSUM works by accumulating derivations from *E* that are above target with one statistic C^+ and accumulating derivations from *E* that are below target with another statistic C^-. The statistics C^+ and C^- are called one-sided upper and lower CUSUMs, respectively. They are calculated as follows, where the starting values are $C_0^+ = C_0^- = 0$:

$$C_k^+ = \max\left[0, y_k - (E + K) + C_{k-1}^+\right] \qquad (3.2)$$

$$C_k^- = \max\left[0, (E - K) - y_k + C_{k-1}^-\right] \qquad (3.3)$$

In Equations 3.2 and 3.3, *K* is usually called the reference value. It is often chosen about half of the process standard deviation, i.e. 0.5σ. If either C_k^+ or C_k^- exceed the decision interval *H*, the process is considered to be out of control. A reasonable value

for *H* is five times the process standard deviation, i.e. 5σ. It is noted that the CUSUM and Shewhart charts are equivalent if the CUSUM parameters *K* and *H* are selected as *K=3* and *H=0*.

The EWMA control chart is also a good alternative to the Shewhart control chart when we are interested in detecting small shifts. The EWMA is typically used with individual observations. It is defined as Equation 3.4.

$$\bar{y}_k = \alpha \cdot \bar{y}_{k-1} + (1-\alpha) \cdot y_k \tag{3.4}$$

The sensitivity is determined by the weighting factors α. A high value provides secure output but reduce the tool's capability to detect when the system is in transient state. Montgomery (2001) describes the use of EWMA control charts and claims that the weighting factor between 75% and 95% works well in practice.

Since the EWMA can be viewed as a weighted average of all past and current observations, it is very insensitive to the normality assumption. It is therefore an ideal control chart to use with individual observations. The control limits for the EWMA control chart are as follows:

$$UCL = E + 3\sigma\sqrt{\frac{1-\alpha}{1+\alpha}\left(1-\alpha^{2k}\right)} \tag{3.5}$$

$$LCL = E - 3\sigma\sqrt{\frac{1-\alpha}{1+\alpha}\left(1-\alpha^{2k}\right)} \tag{3.6}$$

However, for a multivariate process, individual variable in-control hardly means the process is in control. This can be easily illustrated by a two-dimensional process, in which two variables (*x, y*) are considered. Suppose that, when the process is in a state of statistical control where only common disturbance, such as noises, is present. *x* and *y* are correlated as illustrated in the joint plot of *x* vs. *y* in Figure 3.2. The ellipse

represents the control limits for the in-control process at some confidence level. The individual Shewhart charts with their upper (*UCL*) and lower (*LCL*) limits are also shown in Figure 3.2 respectively. The dash square surrounded by the individual Shewhart control limits is no longer suitable for monitoring this two-dimensional process, because observations shown as empty dots in Figure 3.2 in the square are out of the control ellipse, which means they are out of control.

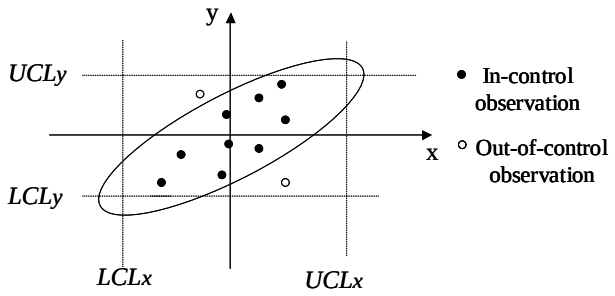

Figure 3.2 Control monitoring of two correlated variables
illustrating the natural defect of univariate control charts

Statistics are often used as the performance indexes in multivariate process monitoring. The Hotelling's T^2 statistic and the *Q-statistic* are the most popular statistics used in multivariate process monitoring. Many techniques have been used to develop multivariate monitoring statistics, such as the Principle Component Analysis (PCA), the Fisher Discriminant Analysis (FDA), the Partial Least Square (PLS) and the Canonical Variate Analysis (CVA) (Russell 2000).

3.2 Qualitative/Quantitative FDD Methods

3.2.1 A Brief of Qualitative Reasoning

Our knowledge of the world is finite and incomplete but we function quite well in the world in spite of never fully understand it (Kuipers 1994). People cope with the demands of the physical world, usually quite successfully, with the incomplete knowledge. Part of the answer is that people can build and use qualitative descriptions of mechanisms in the physical world. A qualitative description is one that captures distinctions that make an important, qualitative difference, and ignores others. A number of researchers in artificial intelligence are working to apply qualitative descriptions of the physical world to problem solving at both commonsense and expert levels.

Qualitative reasoning is developed based on qualitative descriptions to provide a theoretical framework for expertise reasoning about the physical system. The basic idea of qualitative reasoning is to obtain system structure, i.e., components and connections among them for physical system, describing it either by qualitative equations or by causal constraints, then to solve these equations or analyze these constraints. Causal reasoning is an effective and natural approach of qualitative reasoning when documenting and analysing behavior for complex systems, which traces the cause back along the directed graphs. Direct graphs are the traditional graphs representing the influences on the system. In the graph, the nodes correspond to the state variables of the system, and the branches represent the immediate influences between the nodes. Positive and negative influences, respectively, are distinguished by signs '+' and '-' given to the branches.

Qualitative structure is defined as a tuple (*P, C, L, I*) (Wang and Chen, 1995), where $P = \{f_i : i = 1,..., n\}$ is set of parameters, $C = \{C_i(f_1,..., f_n, df_1,..., df_n) : i = 1,..., k\}$ is the constraints on *P*, $df_1,\ldots df_n$ are

differential of $f_1,\ldots,f_n$ respectively, $L = \{l_j : j = 1,...,m\}$ is the set of landmark points, and $I = \{IQ(f_i) : i = 1,...,n\}$ is set of incremental qualitative values. Qualitative state is defined as Equation 3.7.

$$QS(f_i, t) = (QVal, QDir) \tag{3.7}$$

where qualitative value
$$QVal = \begin{cases} l_j,\ f_i(t) = l_j \\ (l_j, l_{j+1}), l_j < f_i(t) < l_{j+1} \end{cases} \tag{3.8}$$

and qualitative direction
$$QDir = \begin{cases} inc, \dfrac{df_i(t)}{dt} > \delta \\ std, \left|\dfrac{df_i(t)}{dt}\right| \le \delta \\ dec, \dfrac{df_i(t)}{dt} < -\delta \end{cases} \tag{3.9}$$

Parameters are the variables describing the physical system. In order for qualitative reasoning to be possible, we must restrict variables to correspond to reasonable functions. First, a reasonable function must be continuously differentiable. Second, it should be convenient to consider each varaible, including time, to range over the extended real number line, which includes the endpoints -∞ and +∞. Third, we need to avoid functions of time whose qualitative properties change infinitely often in a finite interval.

Constraints along with their corresponding values specify the qualitative relationships of the system. Differential equations describe the direction of change for each variable. The moving slope estimation is employed, which estimates the slope of the linearly regressed line of the parameter and a sufficiently large slope indicates the presence of increasing or decreasing (Equation 3.9).

Landmark values are the “natural joints” that break a continuous set of values into qualitatively distinct regions. A landmark value is a symbolic name for a particular real number, whose numerical value may or may not be known. It serves as a precise boundary for a qualitative region. The qualitative properties of a landmark value in the set depend primarily on its ordinal relations with the landmarks.

Qualitative state is dynamic. As the system changes with time, the qualitative state (Equation 3.7) descibes the sequences of the change. In order to predict a behavior of the system, we need to know the transitions from one qualitative state to another. In addition to qualitative magnitude, the direction of change of each variable is also described in Equation 3.7. Thus, for each variable, Equation 3.7 describes its qualitative state in terms of its magnitude and its direction of change: increasing, decreasing, or steady.

Qualitative reasoning derives parameter values even with incomplete and imprecise knowledge about the model. It derives behavior from the description of a model and does not rely, necessarily, on heuristic knowledge. Generally speaking, it is a methodology for evaluating the behavior of conceptual structural designs where limited information about the structure is available.

Qualitative reasoning tends to emulate human being’s thinking by giving explanations for observed behavior. This explanation is based on expertise, which is represented as system structure. The structure model can be qualitative or quantitative. After qualitative simulation gives result at qualitative level, the numerical models may be set up for solving quantitative sub-problems. Integration of qualitative simulation and causaility analysis with conventional quantitative models helps solve problems especially under complex circumstances.

3.2.2 Critical Review on Qualitative/Quantitative FDD Methods

As explained previously in Chapter 2, faults and their symptoms are mixed up in VAV air distribution systems. There are many different causes related to the same fault and many different faults related to the same cause. Conventional decision analysis based on quantitative models suffers from the lack of ability to handle qualitative knowledge especially under complex circumstances (Wang and Chen, 1995) like the mentioned VAV air distribution system. Integrating quantitative models with qualitative knowledge helps to solve decision making problems more effectively and efficiently.

Yu and Lee (1991) developed a framework for integrating quantitative process knowledge into the qualitative model. Once quantitative process information was available, it could be incorporated into the simplest qualitative process model called the signed directed graph (SDG), which describes the cause and effect relationships among process variables. A chemical reactor example illustrated the design and performance of the qualitative/quantitative model-based diagnostic system. This approach could be extended to the multiple-fault situations in a straightforward manner.

A few qualitative models were used for AHU fault detection in VAV air-conditioning systems (Glass et al. 1995, Fornera et al. 1995). The qualitative models were used to describe the steady-state operation of a controlled central AHU. The fault detector based solely on qualitative observable features could obtain the same results as the quantitative simulators achieved. However, qualitative knowledge means two things, inaccuracy and causality. Inaccuracy is resulted from uncertain data, factors

expressed qualitatively. Causality arises when people use interrelationships to reason. Thus the application of pure qualitative models for FDD in HVAC field was limited.

The quantitative approach relies mainly on physical laws and requires advanced knowledge about the structure of the system and the values of the parameters. Ghiaus (1999) developed a bond graph model of a direct-expansion, mechanical vapor-compression air conditioning system. He then proposed a method for recursively solving the qualitative system of equations derived from the bond graph. The bond graph model could be presented by both quantitative representation, in which parameters had numerical values, and qualitative approach, in which they were classified qualitatively. Fault diagnosis was initiated by a fault detection mechanism which also classified the quantitative measurements into qualitative values. However, the fault detection was not presented in the paper.

Zhou et al. (1994) constructed an Intelligent System for Operation Planning (ISOP) in HVAC processes using important expertise, qualitative reasoning and quantitative computation. It provided a real-time integrated operation planning method offering better energy conservation, comfort and indoor air quality than other methods being used. An integrated intelligent system framework was introduced to integrate qualitative reasoning and quantitative computation in HVAC field (Figure 3.3).

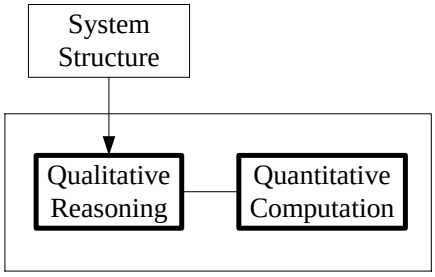

Figure 3.3 Framework of an ISOP

Intergration of qualitative reasoning and quantitative computation in fault diagnosis is recently used in some fields like *Artificial Intelligence*. However, the application of qualitative/quantitative reasoning in HVAC FDD has not been well developed. An overall architecture integrating qualitative reasoning and quantitative models is developed for VAV fault detection and diagnosis (VAV FDD) is developed in this study.

3.3 FDD Strategy for Multiple Faults in VAV Systems

3.3.1 VAV Air-Conditioning System and Its Qualitative Description

Air handling processes in VAV air-conditioning systems are typical multivariate control processes, in which many physical variables (such as temperature, flow rate and pressure) and positions of control devices (such as dampers and valves) are measured and controlled. Complex but advanced local and supervisory control strategies are probably employed to improve the IEQ and energy efficiency.

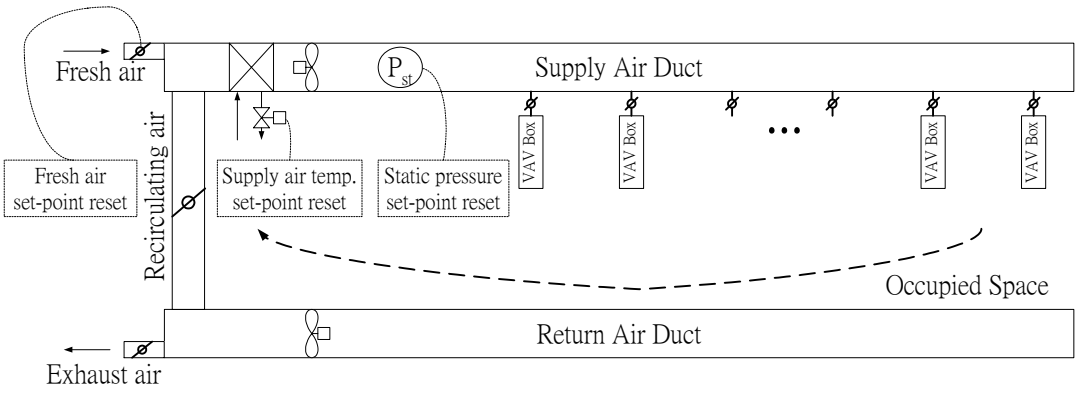

Figure 3.4 Schematic of a typical VAV air-conditioning system

Figure 3.4 demonstrated the schematic of a typical VAV air-conditioning system. Two fans are equipped as VAV supply fan and return fan, respectively. Both fans could be variable blade angle type, or centrifugal type equipped with inlet guide vanes or variable frequency drivers to adjust the air flow rates. The supply air fan is controlled to maintain the set static pressure and the the return air fan is controlled to adjust the exfiltration flow rate in order to maintian possitive pressure in the building. The chilled water flow rates of the cooling coils are moderated to control the coil outlet air temperature. The VAV terminals could be pressure-dependent type or pressure-independent type. Pressure-independent type is normally adopted in modern buildings due to its advantages in control as explained in Chapter 2. Fresh air flow rate is controlled by adjusting the fresh air damper, the exhaust air damper and the recirculating air damper (the three damper are interlocked.).

Typical but advanced control strategies are implemented to provide adequate outdoor air ventilation, suitable supply air temperature and static pressure for minimizing energy use. PID controllers are widely employed to control the supply air temperature, supply air static pressure, outdoor airflow rate, and return fan speed. Some optimal control strategies could be used to reset the set-points of the local PID control loops of supply air temperature and supply static pressure to save energy. The split-range sequencing control strategy is commonly accepted as an optimal control strategy for outdoor airflow control (Wang and Xu 2002), which combines the demand controlled ventilation (DCV) control and enthalpy-based economizer control. In order to guarantee the validity of PID controllers and optimal control strategies, accurate sensor measurements are required.

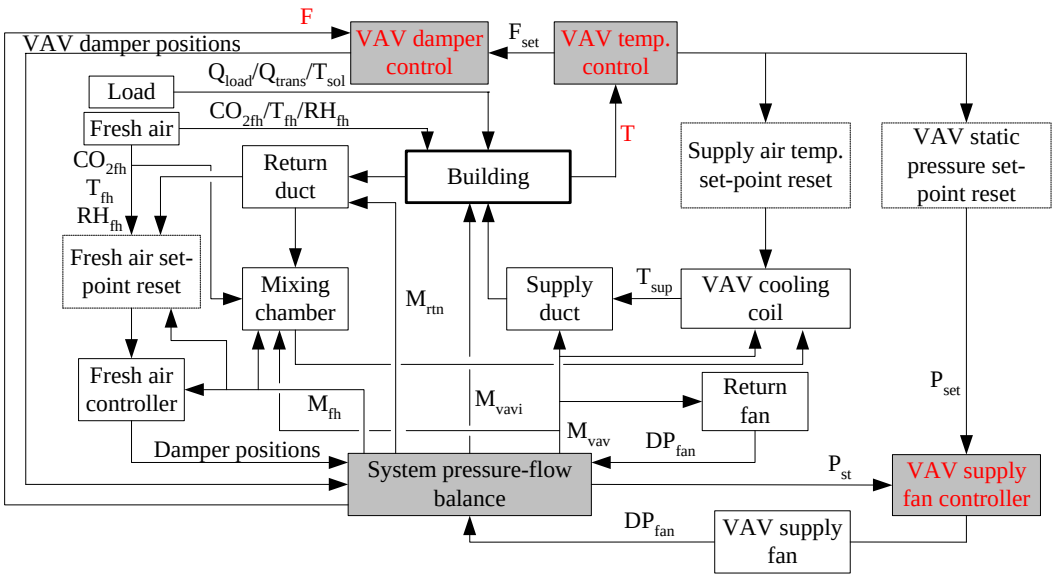

Figure 3.5 Illustration of conceptual model of VAV system

The physical knowledge about the VAV system structure, i.e. component and connections among them, helps to set up the conceptual model for VAV system qualitaitve description. The conceptual model describes the physical processes. It also presents how they relate to each other and which processes dominate the system. It cpatures the main distinctions which make an important, qualitative difference in VAV air distribution system, and ignores others.

Figure 3.5 illustrated the conceptual model. The process of 'system pressure-flow balance' is the main process in the model. As described in Chapter 2, eleven root faults were predefined in typical VAV air distribution systems. To analyze those faults, VAV supply fan controller, VAV temperature and damper control process within the system pressure-flow balance main process are the essential parts, which are marked red in Figure 3.5. Furthermore, the measurements of zone temperature and the VAV flow rate affect the system control, which are marked red as well.

3.3.2 Overall Architecture of VAV FDD

An overall architecure integrating system structure, qualitative reasoning and quantitative models is developed for VAV air distribution system FDD as shown in Figure 3.6. The architecture consists of two levels of frames. The first level presents the physical knowledge about the system structure. On the second level, the qualitative/quantitative reasoning is conducted.

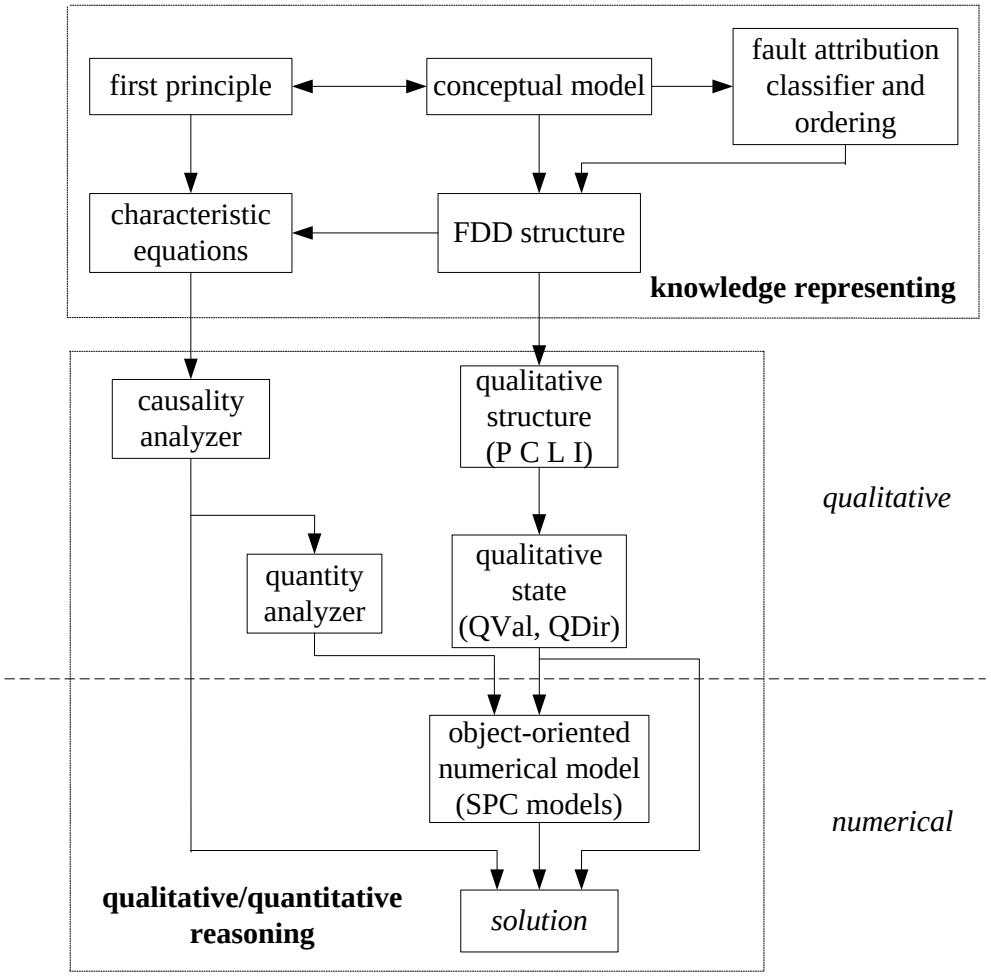

Figure 3.6 Overall architecture of VAV FDD

Knowledge representation on the first level is the base. It presents faults and its related domain knowledge consisted of three parts: frames, parameters and rules. A conceptual model is developed from the physical knowledge in first principle models. It describes the physical processes that are part of FDD environment. It also explains

how they relate to each other and which processes dominate the system. It defines the general physical framework within which the process details can be worked out and associated numerical relations can be developed. Based on the conceptual model, the predefined faults are classified then ordered and the FDD structure is set up. From the FDD structure, we can obtain the qualitative structures (*P, C, L, I*) of the faults.

Qualitative physics is a research topic in artificial intelligence, and provides theories on how to conduct qualitative reasoning on the behavior of natural or man-made systems whose behavior is governed by the laws of physics. Qualitative reasoning uses physical information such as relative magnitudes, and the directions of change in variable values, as opposed to precise values to understand the initial problems qualitatively. However, there is an inherent limitation of the qualitative reasoning since only qualitative terms are employed in the model. It can provide more possible fault interpretations in addition to the true one. Therefore, the numerical sub-models are integrated into the architecture to solve quantitative sub-problems after recognizing the limitation of qualitative reasoning.

Causality analyzer analyzes the cause and effect relationships among variables and factors, which are qualitatively derived from the characteristic equations of processes. Quantity analyzer involving numerical models is further applied if causality analyzer cannot identify the fault. The solution to faults would be finally worked out after fault detection.

The purpose of this architecture is to provide a structure for qualitative/quantitative reasoning on VAV air distribution system FDD by integrating physical knowledge, qualitative reasoning and quantitative models.

3.3.3 FDD Strategy for Multiple VAV Faults

The FDD strategy for multiple VAV faults forms within the above-mentioned FDD architecture. The conceptual model about the physical process relationships in typical VAV system is illustrated in Figure 3.5. When the faults of VAV air distribution system are of concern, the network pressure-flow balance is the dominant process of the system. The static pressure control process, the VAV temperature and flow control process are essential parts to balance the system.

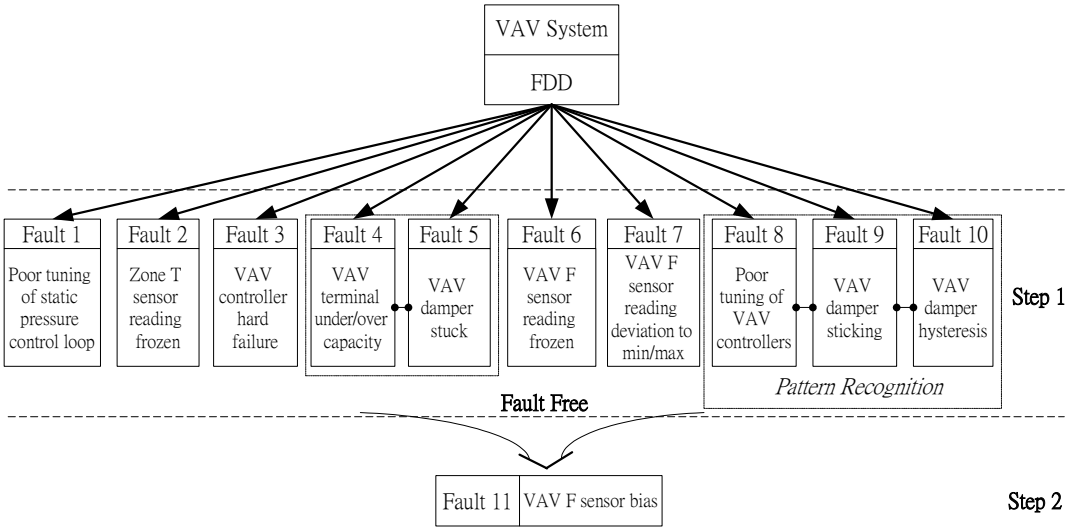

Figure 3.7 VAV fault grouping and ordering

Eleven root faults summarized in Chapter 2 are studied within the overall architecture to develop the FDD strategy. Fault classifying and ordering play an important role in describing system FDD structure. The eleven faults are classified into eight groups, while Fault 4 and 5 are treated together in one group and Fault 8, 9 and 10 are treated together in another group. The eight groups of faults are dealt with by eight relevant FDD schemes. Fault 1-10 are hard faults, which would affect the normal operation of the system. They are treated in parallel by Scheme 1-7 at Step 1. Fault 11 is flow sensor soft fault. It would not affect the normal control process if the readings are within the normal range as it can be compensated by resetting the air flow

set-point. This fault is analyzed by Scheme 8 at Step 2 when it is confirmed that the system is hard fault free at Step 1. VAV faults grouping and ordering are shown in Figure 3.7. The schemes for the eight-group faults are illustrated in Figure 3.8.

Considering the interaction amongst the faults, the first seven FDD schemes and their relevant FDD results are studied simultaneously at Step 1. As the hard faults (Fault 1-10) are dealt in parallel, the ability of the FDD schemes designed for the specific fault(s) could be interfered by other faults. Therefore, all the ten faults are studied carefully to determine their effects on each FDD scheme. The fault(s) could only be detected by the relevant schemes while the other associated schemes give the indication of fault free as illustrated in Figure 3.8.

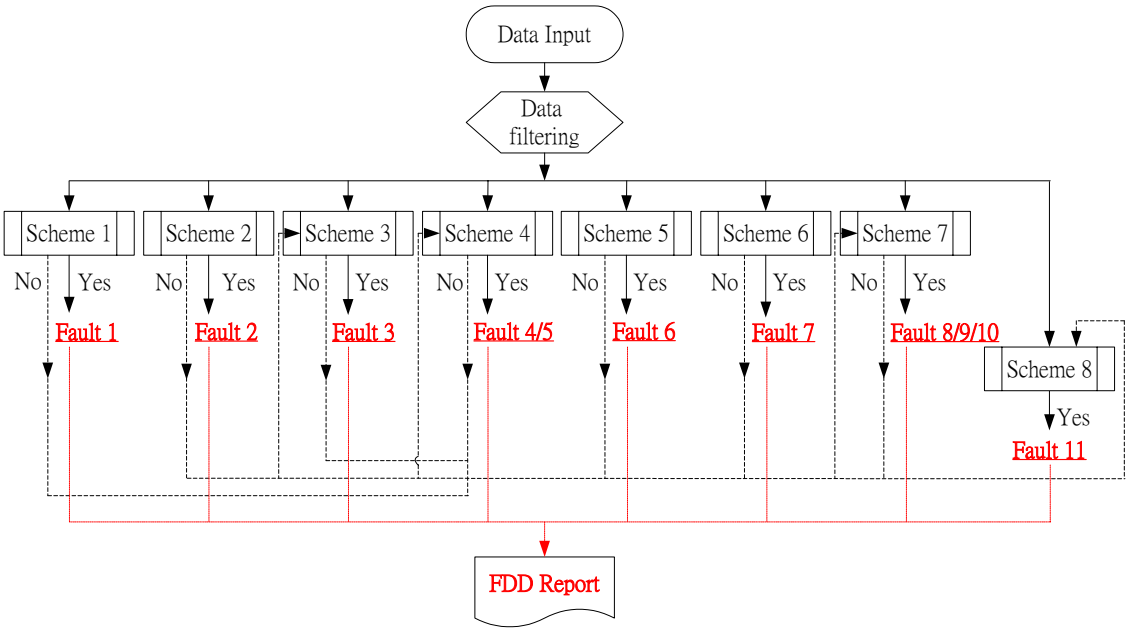

Figure 3.8 FDD process of the FDD strategy

FDD Scheme 1 for Fault 1 is independent as other faults would not affect the characteristic equations employed in Scheme 1. Similarly, Scheme 2 for Fault 2, Scheme 5 for Fault 6 and Scheme 6 for Fault 7 are independent as the schemes' FDD ability for the specific faults would not be affected by the existence of other faults.

Faults to be detected under these schemes could be identified within the individual schemes.

However, as for Scheme 3 (for Fault 3) and Scheme 4 (for Fault 4/5), the fault detection ability is affected by the existence of Fault 2 as zone temperature is an important parameter in the both schemes to detect the relevant faults. Single Fault 2 could give the same results as Fault 3 gives under Scheme 3 and Fault 4/5 gives under Scheme 4. Fault 3 and Fault 4/5 could only be detected by Scheme3 and Scheme 4 respectively when it is confirmed that the sub-system (VAV terminal) is free of Fault 2. In other words, the existence of Fault 2 affects the fault detection results of Scheme 3 and Scheme 4.

Under Scheme 7, other faults could result in the same symptoms under this scheme. The symptom of flow control sluggish response could be due to Fault 4&6, Fault 4&7, Fault 5, Fault 8 or Fault 10. The symptom of temperature control sluggish response could be due to Fault 2, Fault 3, Fault 4, Fault 5, Fault 7 or Fault 8. Flow oscillation could be due to Fault 1, Fault 8, Fault 9 or Fault 10. Flow set-point oscillation could be due to Fault 6 or Fault 8. Therefore Scheme 7 only works under the condition that the sub-system (VAV terminal) is free of Fault 1-7.

Within the overall architecture of FDD strategy, qualitative reasoning described by qualitative state or simplified by causality analyzer begins to detect the fault(s) on the second level. Object-oriented numerical models based on statistical process control techniques are set up to finally identify the fault(s) if pure qualitative reasoning is not accurate enough to affirm the fault(s) under some schemes. The FDD schemes designed for different groups of faults are detailed in the following section.

3.4 Schemes of FDD Strategy

The VAV terminal damper openness is an important basis to build up the qualitative/quantitative models in the FDD schemes. However, in normal pressure independent VAV systems, the signal of damper openness is not available. Position algorithm controllers are commonly used for VAV damper control. The control signal to damper (μ) typically represents the position of an actuator and therefore the openness of the VAV damper (Kamimura et al. 1994). Thus, μ is used to represent the damper openness in the FDD strategy developed in this study.

To eliminate the effects of system dynamics and ensure the reliability of the measurements used, the measurements usually go through a filter before they are used for fault detection and diagnosis. The filter is constructed on the basis of EWMA techniques for the calculation of qualitative states as shown in Equation 3.4. A factor of 90% is used for most cases in this study. Reversal counting is used to describe the state of oscillation in some FDD schemes. To increase the sensitivity, we choose the factor of 50% for the reversal counts in case of oscillation.

The illustration of reversal counts is shown in a univariate statistical control chart (Figure 3.9), where σ is the standard deviation of the noise inherent in the process variable. The reversal counting starts when the process variable exceeds the Shewhart control limit from the in-control range ($R=1$) and one more reversal is counted ($R=R+1$) once the variable exceeds the threshold at the opposite direction. In most circumstances, the maximum tolerable number of reversals is set to be four (Salsbury 1999).

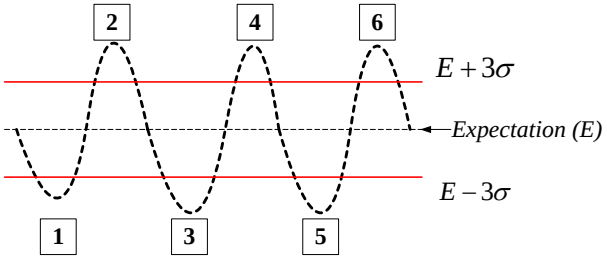

Figure 3.9 Illustration of reversal counts

Besides, the sensor reading frozen could be completely frozen at a fixed value (Case 1) or floating within a certain range (Case 2) as shown in Figure 3.10. The sensor frozen of Case 2 is further confirmed by the CUSUM control method besides the readings are within Shewhart control limits. In both applications of statistical control for reversal counting and sensor frozen detection, the control limits should be determined carefully.

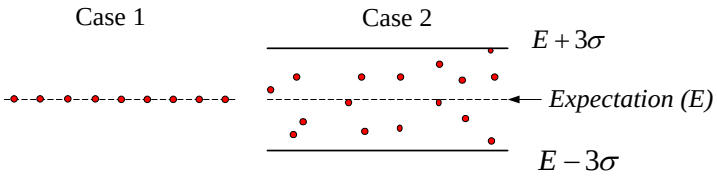

Figure 3.10 Illustration of sensor reading frozen

3.4.1 Scheme 1 – Poor Tuning of Static Pressure Control Loop

Controller failure would lead to three types of unsatisfactory control performance (Salsbury 1999). They are unresponsive control process, sluggish response and oscillatory behavior. The controlled process is said to be unresponsive when the controlled variable does not change in response to changes in the set-point. The behavior is usually said to be sluggish if the set-point is subjected to a step change and the time taken for the controlled variable to approach the new steady-state value is

significantly longer than an open loop response. Oscillatory behavior occurs when the controlled variable alternately overshoots and undershoots its steady-state value.

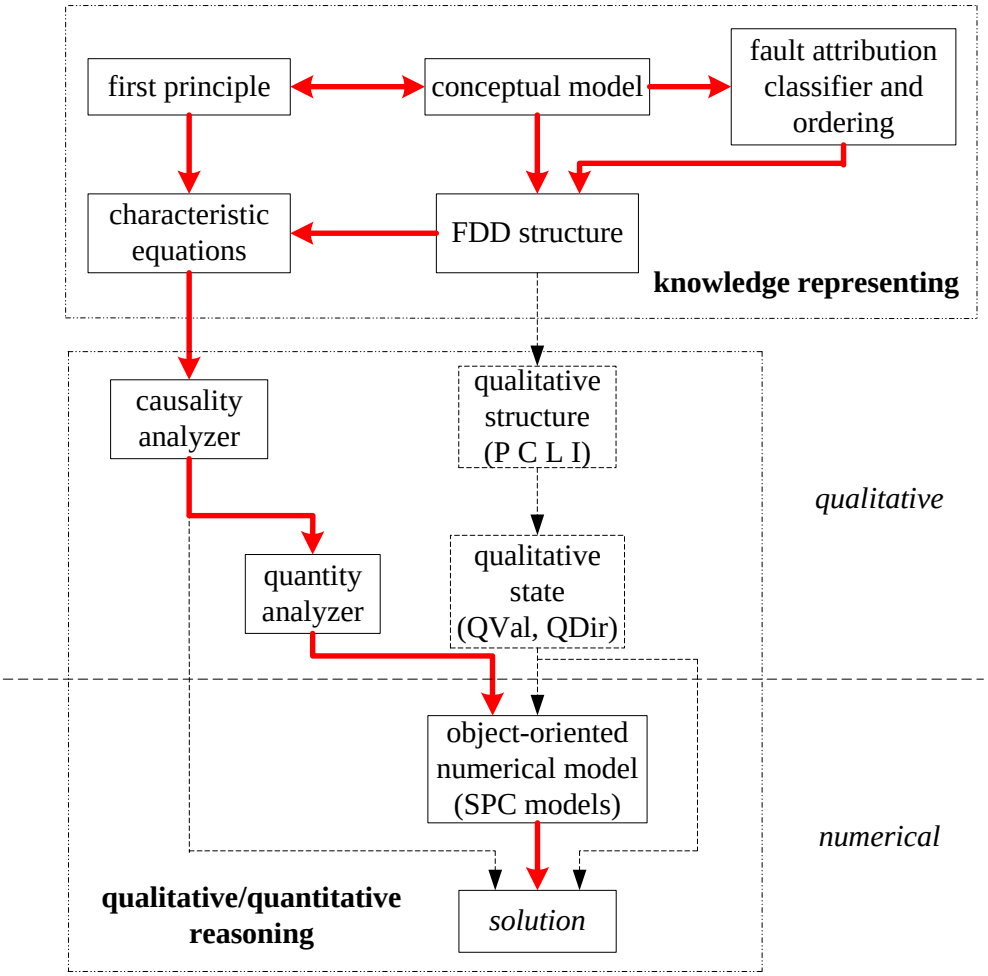

Figure 3.11 Qualitative/quantitative reasoning process of Scheme 1 & 7

As the VAV system supply fan characteristics and its control are not the focal points of this study, the static pressure controller failure is studied focusing on excessive oscillation. Static pressure oscillation would cause unstable control of the whole VAV air distribution system and VAV damper premature wear/tear. As the fault could not be diagnosed by causality analyzer qualitatively, quantity analyzer supported by the object-oriented SPC model is therefore adopted. Figure 3.11 shows

the process of qualitative/quantitative reasoning of this scheme (Scheme 1) for Fault 1 within the overall architecture.

Fault 1 is detected by the SPC model for counting excessive consecutive reversals of the static pressure around its set-point over a preset period (t_{delt}) as shown in Equation 3.10. Before reversal counting, the flow set-point is filtered on the basis of EWMA ($\alpha = 50\%$) as recommended previously.

$$R_{P,st} \geq 20 \Big| \quad \Delta time < t_{delt} \tag{3.10}$$

The SPC model for reversal counting is built up according to the above-mentioned method based on a univariate statistical control chart. Oscillation is detected when the counted number of the pressure reversal within the preset period (t_{delt}) is over a certain limit (20). For common VAV systems, $3\sigma_P$ for static pressure was set at 10 Pa and the preset period (t_{delt}) could be set as 10 minutes.

Free of Fault 1 ensures the stable static pressure of the whole VAV air distribution system. Most of FDD schemes for individual terminal faults are implemented based on healthy system static pressure control.

3.4.2 Scheme 2 – Zone Temperature Sensor Reading Frozen

When the zone temperature sensor readings are frozen, the zone temperature could not be measured correctly and the VAV subsystem would be totally out of control eventually. Without resetting the zone temperature set-point, the flow set-point calculated by the controller would be fixed within certain range. For instance, the flow set-point is usually fixed at the maximum or minimum if the fixed temperature reading is not equal to the temperature set-point.

The process of qualitative/quantitative reasoning for fault detection under Scheme 2 is shown in Figure 3.12. The scheme for Fault 2 is presented as qualitative state in Equation 3.13 while the parameters and the landmark points of the qualitative structure are defined in Equation 3.11 and 3.12 respectively. However, this qualitative state does not affirm the fault of temperature sensor reading frozen yet. SPC models based on the above-mentioned CUSUM control method are constructed for both temperature and flow set-point. Fault 2 is detected if both temperature and flow set-point are with their CUSUM control as well over a preset period (t_{delt}) as shown in Equation 3.14.

$$P = \{T, F_{set}\} \tag{3.11}$$

$$L = \{T_E - 3\sigma_T, T_E + 3\sigma_T, F_{set,E} - 3\sigma_F, F_{set,E} + 3\sigma_F\} \tag{3.12}$$

$$QVal = \begin{cases} (T_E - 3\sigma_T, T_E + 3\sigma_T), T \\ (F_{set,E} - 3\sigma_F, F_{set,E} + 3\sigma_F), F_{set} \end{cases} \tag{3.13}$$

$$\left.\begin{array}{l} (T_E - 3\sigma_T < T < T_E + 3\sigma_T) \\ AND(C_T^+ < 5\sigma_T) \\ AND(C_T^- < 5\sigma_T) \\ AND(F_{set,E} - 3\sigma_F < F_{set} < F_{set,E} + 3\sigma_F) \\ AND(C_{F,set}^+ < 5\sigma_F) \\ AND(C_{F,set}^- < 5\sigma_F) \end{array}\right| \quad \Delta time > t_{delt} \tag{3.14}$$

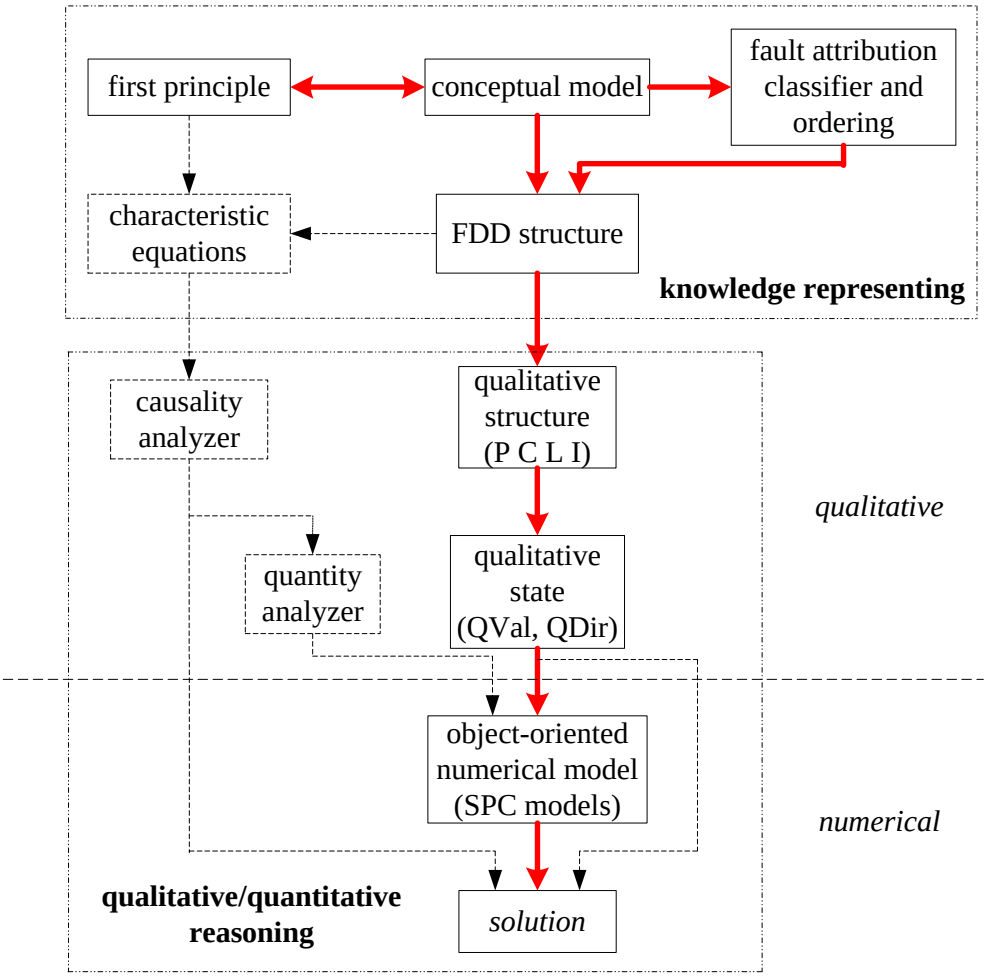

Figure 3.12 Qualitative/quantitative reasoning process of Scheme 2, 5 & 8

In Equation 3.12, 3.13 and 3.14, the variable expectation (E) could be estimated as the sample mean. For common VAV terminals, $3\sigma_T$ for temperature was set at 0.3°C and $3\sigma_F$ for flow was set at 10 l/s. As the cooling load of a zone is seldom kept unchanged for half a day in practice, the preset period (t_{delt}) was set as 5 hours.

The space temperature changes significantly during morning pull-down period after switch on the system. The violation of temperature frozen limits indicates fault free.

3.4.3 Scheme 3 – VAV Controller Hard Failure

VAV controller hard failure would provide wrong control signals, then improper control of VAV dampers. It prevents the subsystem from providing appropriate air flow rate into the zone. The zone temperature would therefore deviate from its set-point. The qualitative/quantitative reasoning process of the scheme (Scheme 3) is shown in Figure 3.13. Fault 3 of VAV controller hard failure is detected by the following charateristic equations (Equation 3.15-3.18), where temperature is filtered through EWMA ($\alpha = 90\%$) and the preset period was set as 30 minutes.

$$\left.\begin{array}{l}(\bar{T} - T_{set} < -T_{th}) \\ AND(F_{set} = F_{\min}) \\ AND(\mu = \mu_{\max}) \\ AND(F > F_{\min})\end{array}\right| \Delta time > t_{delt} \tag{3.15}$$

$$\left.\begin{array}{l}(\bar{T} - T_{set} > T_{th}) \\ AND(F_{set} = F_{\max}) \\ AND(\mu = \mu_{\min}) \\ AND(F < F_{\max})\end{array}\right| \Delta time > t_{delt} \tag{3.16}$$

$$\left.\begin{array}{l}(\bar{T} - T_{set} < -T_{th}) \\ AND(F_{set} = F_{\max}) \\ AND(\mu = \mu_{\max})\end{array}\right| \Delta time > t_{delt} \tag{3.17}$$

$$\left.\begin{array}{l}(\bar{T} - T_{set} > T_{th}) \\ AND(F_{set} = F_{\min}) \\ AND(\mu = \mu_{\min})\end{array}\right| \Delta time > t_{delt} \tag{3.18}$$

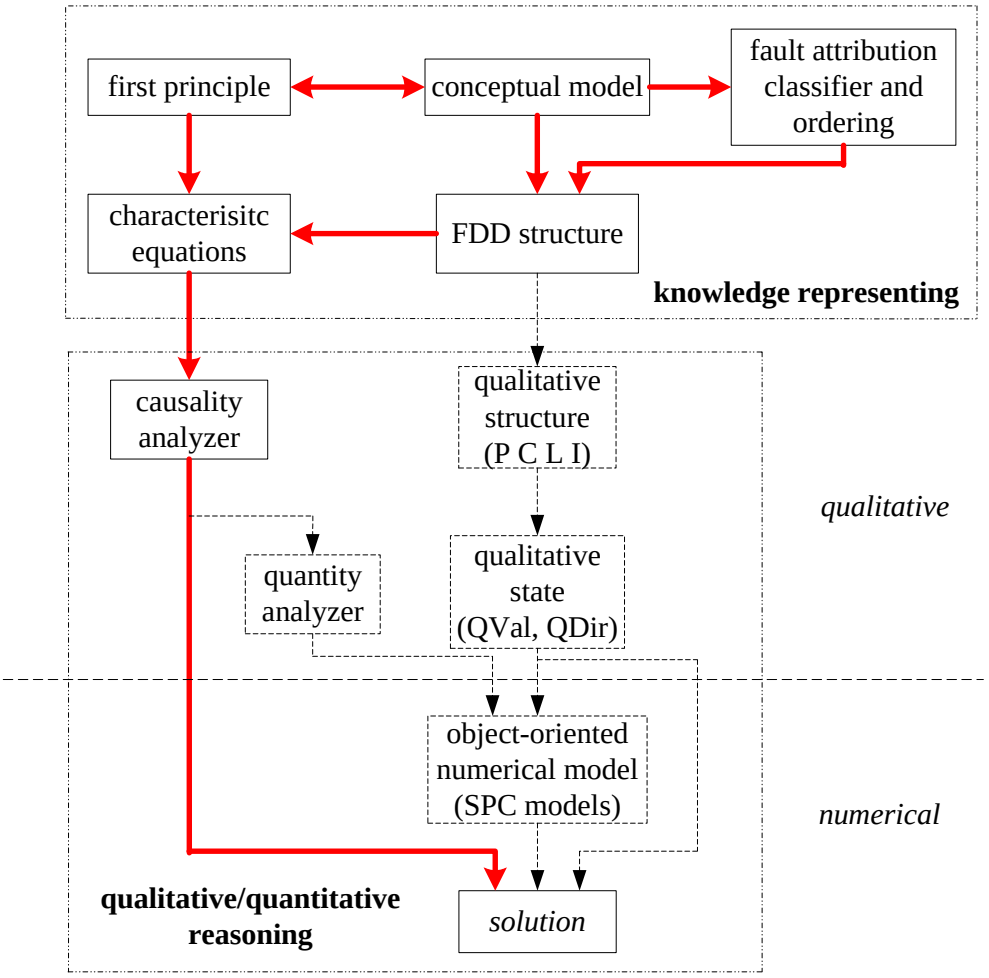

Figure 3.13 Qualitative/quantitative reasoning process of Scheme 3 & 6

3.4.4 Scheme 4 – VAV Terminal under/over Capacity and/or VAV Damper Stuck

VAV terminal under/over size (Fault 4) or damper stuck (Fault 5) would prevent the subsystem from providing appropriate air flow rate into the zone, therefore the zone temperature cannot meet its set-point. A scheme (Scheme 4) based on qualitative reasoning is designed to detect Fault 4 and/or Fault 5 and its process is shown in Figure 3.14.

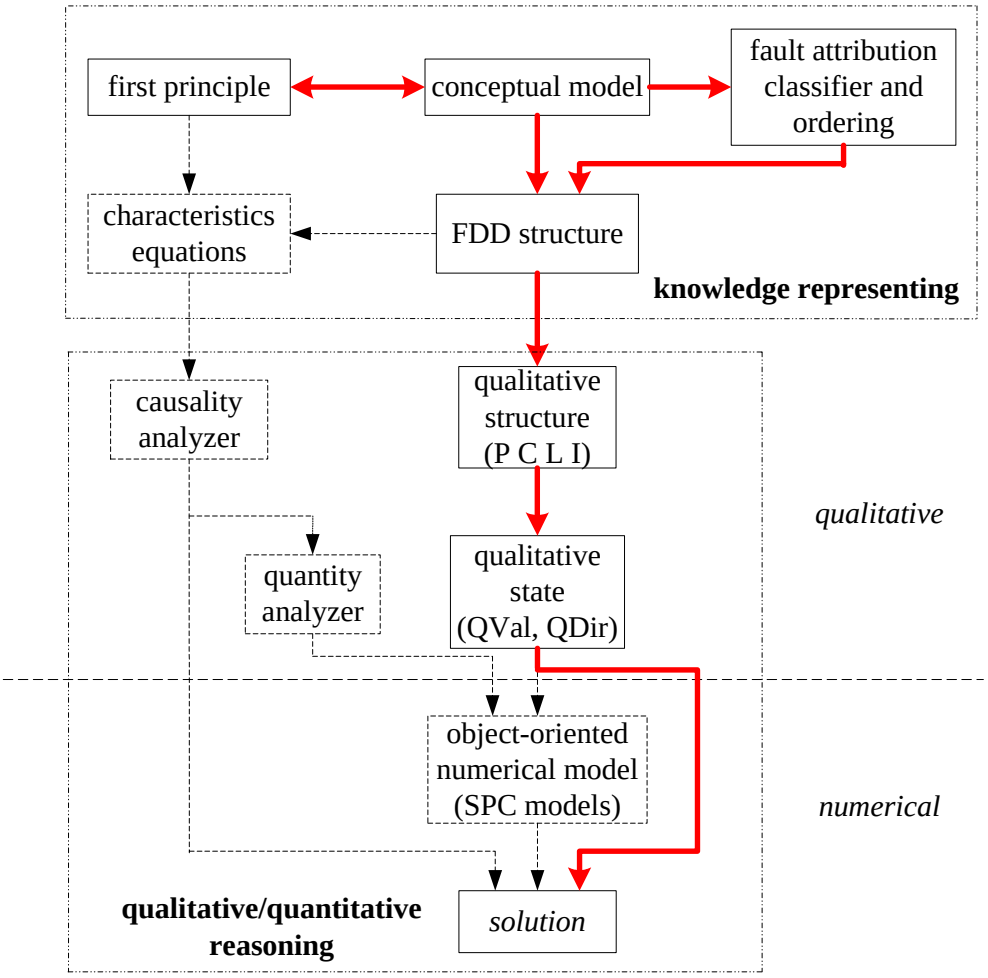

Figure 3.14 Qualitative/quantitative reasoning process of Scheme 4

The parameters and the landmark points of the qualitative structure are defined in Equation 3.19 and 3.20 respectively. The qualitative state for Fault 4/5 is expressed in Equation 3.21 and 3.22 presenting the deficiency of the temperature control loop and flow control loop as well as no variation of the measured flow rate over a preset period. Before the zone temperature measured and the flow measured are used to present the qualitative state, they go through a filter of EWMA ($\alpha = 90\%$). The permissive temperature error (T_{th}) was set at 1.5^{o}C and the preset period (t_{delt}) was set as 30 minutes.

$$P = \left\{ \overline{T} - T_{set}, \mu, \Delta\overline{F} / F_{design} \right\} \tag{3.19}$$

$$L = \left\{ -T_{th}, T_{th}, \mu_{\max}, \mu_{\min}, 0, 0.05 \right\} \tag{3.20}$$

$$QVal_1 = \begin{cases} (-\infty, -T_{th}), \overline{T} - T_{set} \\ \mu_{\min}, \mu \\ (0, 0.05), \Delta\overline{F} / F_{design} \end{cases} \tag{3.21}$$

$$QVal_2 = \begin{cases} (T_{th}, \infty), \overline{T} - T_{set} \\ \mu_{\max}, \mu \\ (0, 0.05), \Delta\overline{F} / F_{design} \end{cases} \tag{3.22}$$

Fault 4 and 5 cannot be differentiated by the automatic strategy and it does not cause much inconvenience in application as the fault is already focused. The hardware failure of damper stuck (mechanically stuck or actuator failure) and terminal under/over capacity are recommended to be identified manually by adjusting the zone temperature set-point (Figure 3.15) since both faults need manual rectification eventually.

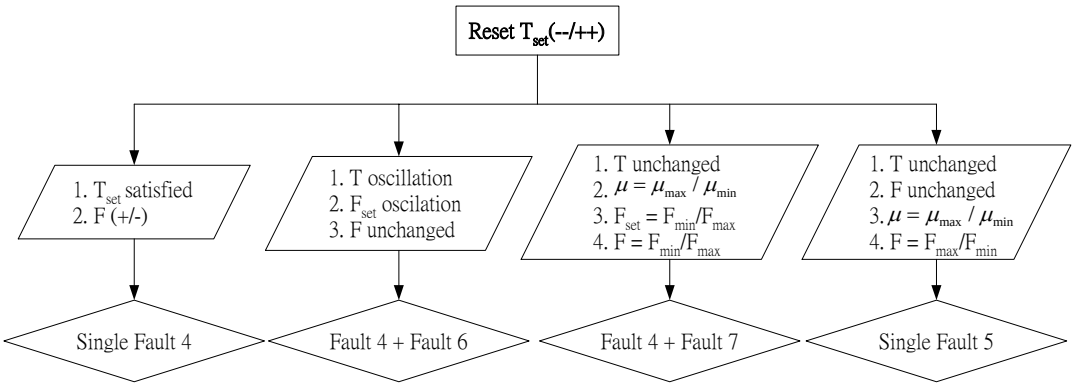

Figure 3.15 Manual identification process of Fault 4/5/6/7

As shown in Figure 3.15, if the measured temperature is less than the set-point, the temperature setting is suggested to a value lower than the measured one, and vice versa. Single Fault 4 would be ascertained when the measured flow changes to satisfy the space temperature set-point. Both Fault 4 and Fault 6 could be detected if the reading of measured flow is frozen and both the measured temperature and flow set-point are oscillating (The details of Fault 6 detection would be introduced in Section 3.3.5.). Both Fault 4 and Fault 7 could be detected if frozen flow reading reaches its minimum/maximum limit and the damper control signal μ does not match with the relevant flow set-point (The details of Fault 7 detection would be introduced in Section 3.3.6.). Single Fault 5 could be judged if both the measured temperature and the measured flow are unchanged with the matched flow set-point and damper control signal μ.

In addition, the site survey results indicate that most cases of 'terminal box under capacity' are due to illegal local adjustments, i.e. diffuser dampers closed or diffusers wrapped with adhesive tapes, which also require maintenance works on site. Moreover, the improper location of zone temperature sensor is common after renovation. The fault of terminal under capacity may relate to this fault, which should be confirmed on site as well. Besides, the alteration of set-points to out of range values or significant temperature sensor bias would lead to the same symptoms. Those faults should be isolated from Fault 4 by further site investigation.

3.4.5 Scheme 5 – VAV Flow Sensor Reading Frozen

If the reading of a terminal flow sensor is frozen but within the normal range ($F_{min}<F<F_{max}$), the zone control loops would oscillate due to the deceiving flow readings received. The zone temperature oscillates around the set-point within a small

range, which usually will not be sensed by occupants but the terminal damper oscillation could cause the actuator to wear out prematurely.

To detect this fault, the scheme (Scheme 5) is developed along the same process of qualitative/quantitative reasoning shown in Figure 3.12. The qualitative state of the flow reading frozen is shown in Equation 3.23-3.25.

$$P = \{F\} \tag{3.23}$$

$$L = \{F_E - 3\sigma_F, F_E + 3\sigma_F\} \tag{3.24}$$

$$QVal = (F_E - 3\sigma_F, F_E + 3\sigma_F), F \tag{3.25}$$

As the qualitative state does not provide sufficient information for fault detection, the SPC models for flow reading frozen and flow set-point reversal counting are further constructed. The SPC model to confirm the flow reading frozen is constructed based on the CUSUM control method adopted in Scheme 2 and the SPC model for flow set-point reversal counting is built up according to the above-mentioned univariate statistical control chart.

Before reversal counting, the flow set-point is filtered on the basis of EWMA ($\alpha = 50\%$) as recommended previously. Fault 6 is detected when the counted number of the flow set-point reversal ($R_{F,set}$) around the flow reading within a preset period (t_{delt}) is over certain limit while the flow reading is detected frozen using the CUSUM SPC model (Equation 3.26).

$$\left.\begin{array}{l}(R_{\bar{F},set} \geq 5) \\ AND(F_E - 3\sigma_F < F < F_E + 3\sigma_F) \\ AND(C_F^+ < 5\sigma_F) \\ AND(C_F^- < 5\sigma_F)\end{array}\right| \; \Delta time < t_{delt} \tag{3.26}$$

For common VAV systems, the threshold of $3\sigma_F$ was set as 10 l/s and the maximum tolerable number of reversals is set to be four, which means five or more reversals indicate fault. The preset period was set as 30 minutes. The flow reading expectation (F_E) could be estimated as the sample mean.

3.4.6 Scheme 6 – VAV Flow Sensor Reading Deviation to Minimum/Maximum

The cascade control of VAV terminal would be totally ruined when the flow sensor reading deviates to the minimum/maximum flow of the terminal. The symptoms are that both the flow set-point and the flow measured are at the minimum while the zone temperature is relatively low, or on the contrary, both the flow set-point and the flow measured are at the maximum while the zone temperature is relatively high. As the VAV subsystem consists of components and control loops, this fault might mix with other faults. Technical staff may focus on mechanical faults, such as terminal under/over capacity, for this case and neglect the flow sensor problem.

Within the cascade control loops, when the secondary control loop receives the deceiving minimum/maximum flow readings from the sensor, the flow controller compares the flow reading with the flow set-point and operates the damper in the opposite direction so that the space temperature deviates from the set-point.

The process of the scheme (Scheme 6) is also shown in Figure 3.13. Fault 7 is detected by the characteristic equations as shown in Equation 3.27 and Equation 3.28, which are based on checking the deficiency of the temperature control loop and flow control loop over the preset period. The zone temperature measured goes through a filter of EWMA ($\alpha = 90\%$) before it is applied to the equations. The permissive temperature error (T_{th}) was set as 1.5^{o}C and the preset period (t_{delt}) was set as 30 minutes.

$$\left.\begin{array}{l}(\overline{T} - T_{set} < -T_{th}) \\ AND(\mu = \mu_{\max}) \\ AND(F \le F_{\min}) \\ AND(F_{set} = F_{\min})\end{array}\right| \Delta time > t_{delt} \tag{3.27}$$

$$\left.\begin{array}{l}(\overline{T} - T_{set} > T_{th}) \\ AND(\mu = \mu_{\min}) \\ AND(F \ge F_{\max}) \\ AND(F_{set} = F_{\max})\end{array}\right| \Delta time > t_{delt} \tag{3.28}$$

3.4.7 Scheme 7 – Poor Tuning of VAV Controllers, VAV Damper Sticking and Hysteresis

Canadian team within the framework of IEA Annex 34 (Choiniere and Beaudoin 2000) adopted the performance indices method and demonstrated their application to detect and diagnose four main faults of the VAV controllers: instability of flow set point, instability of output (the measured flow), temperature set-point not satisfied and airflow set-point not satisfied. Nevertheless, the root causes for the four main faults could be unresponsive control process, sluggish response and oscillatory behavior but were not identified. Moreover, damper sticking or hysteresis would cause the above-mentioned faults as well (Astrom and Hagglund 1995). A sticky damper results mainly from the increment of the static friction, which hinders the opening of the damper and causes damper oscillation. Hysteresis results mainly from slack in the actuator linkage mechanism, which gives rise to the deficiency of flow control (sluggish response and oscillation). Further rules should be added to perform a diagnosis.

To sort out the root causes, the air flow rate control is analyzed first. The reason is that the faulty response may be misjudged as other faults if the air flow set-point is not

reached because of faulty flow controller, sticking or hysteresis. The process of the scheme (Scheme 7) is shown in Figure 3.11.

The sluggish response can be identified if the flow set-point is not satisfied within the preset period (t_{delt}) as shown in the characteristic equation (Equation 3.29). Similarly, the air flow measured would be filtered by EWMA ($\alpha = 90\%$) before applied to the equation. For common VAV systems, the preset period was chosen as 2 minutes and the threshold of air flow rate control (F_{th}) was chosen as 10 l/s.

$$\left|\overline{F} - F_{set}\right| > F_{th}\left| \quad \Delta time > t_{delt} \right. \tag{3.29}$$

Oscillation could be caused by both the primary and secondary control loops due to the nature of cascade control, thus the oscillation of both control loops should be analyzed simultaneously. The oscillation in temperature control loop is certified by the SPC model counting the excessive flow set-point reversals ($R_{\overline{F},set} \geq 15$) within the preset period (30 minutes). However, the oscillation in flow control loop could only be detected by the SPC model counting the excessive flow reversals ($R_{\overline{F}} \geq 20$) around the flow set-point within the preset period (30 minutes) under the condition that no excessive flow set-point oscillation is detected. The reversals are counted using the same method employed previously and the variables are filtered by EWMA ($\alpha = 50\%$) before counting.

The temperature controller (the primary control loop) faults can be analyzed afterwards if no fault is detected for the flow control. The fault of sluggish response is detected by the characteristic equation (Equation 3.30) as the zone temperature set-point is not satisfied within the preset period (30 minutes). The temperature is filtered

through EWMA ($\alpha = 90\%$) and the temperature control threshold (T_{th}) was chosen as 1.5°C.

$$\left| \overline{T} - T_{set} \right| > T_{th} \left| \quad \Delta time > t_{delt} \right. \tag{3.30}$$

Damper sticking or hysteresis would cause oscillation or sluggish response like the faulty flow controller may cause. To distinguish the mechanical faults from the poor flow controller setting, pattern recognition indices are adopted to characterize the different response patterns. Previous researches (Seem 1997, 1998) employed two dimensionless parameters (oscillation ratio and the close-loop response time) to characterize the close-loop response pattern. In this study, two pattern recognition indices are designed to characterize the pattern of sluggish response and the pattern of oscillation respectively.

The pattern of sluggish response caused by the mechanical reason of hysteresis can be distinguishable from the poor flow controller tuning using the pattern recognition index designed as the CUSUM of the air flow rate ($\overline{F}$), where the air flow rate is filtered through EWMA ($\alpha = 90\%$). After the disturbance, the sluggish response caused by hysteresis is identified by the in-control index (Equation 3.31) within the preset period (t_{delt}). The air flow rate before the disturbance was taken as the expectation value for the $C_{\overline{F}}^{+}$ and $C_{\overline{F}}^{-}$ calculation and the preset period was set according to VAV terminal characteristics.

$$\left. \begin{array}{l} (C_{\overline{F}}^{+} < 5\sigma_F) \\ AND (C_{\overline{F}}^{-} < 5\sigma_F) \end{array} \right| \quad \Delta time < t_{delt} \tag{3.31}$$

The pattern of oscillation caused by mechanical reasons of sticking and hysteresis is distinguished by the pattern recognition index designed as ($\overline{F}_k - \overline{F}_{k-1}$). Oscillation

caused by mechanical reasons is identified by the dominated points (more than 50%) of the recognition index within the control limits (Equation 3.32) for a preset period (t_{delt}), which was chosen as 10 minutes for common VAV systems.

$$-Average(ABS(\overline{F}_k - \overline{F}_{k-1})) < \overline{F}_k - \overline{F}_{k-1} < Average(ABS(\overline{F}_k - \overline{F}_{k-1})) \quad (3.32)$$

3.4.8 Scheme 8 – VAV Terminal Flow Sensor Bias

VAV terminal flow sensor bias would not affect the normal control process if the readings are within the range as it can be compensated by resetting the air flow set-point. However, sensor drift, bias, and precision degradation would lead the bias to a certain level, which makes the reading reach the minimum/maximum flow of the VAV terminal (Fault 7) and ruins the control process. Early soft fault detection and data recovery of VAV terminal flow sensors are important but have not been studied by the researchers yet.

The process of the scheme (FDD Scheme 8) for flow sensor bias is also demonstrated in Figure 3.12. To detect this fault, object-oriented SPC models are constructed on condition that the qualitative state conforms to Equation 3.33-3.35, which indicate the flow sensor readings are within the normal range of VAV terminals.

$$P = \{F_i : i = 1,...,n\} \quad (3.33)$$

$$L = \{F_{\min(i)}, F_{\max(i)} : i = 1,...,n\} \quad (3.34)$$

$$QVal = (F_{\min(i)}, F_{\max(i)}), F_i \quad (3.35)$$

As the network characteristics are related to dozens of process variables in the system, a multivariate SPC technique, PCA, is selected as the suitable technique for

sensor fault detection and data reconstruction. PCA is a dimension reduction technique. It produces a lower dimensional representation in a way that preserves the correlation structure between the process variables, and is optimal in terms of capturing the variability in the data. The details of PCA models for VAV terminal flow sensor bias detection and data reconstruction are described in the next chapter.

3.5 Summary

This chapter describes an overall achitecture integrating system structure, qualitative reasoning and quantitative models for VAV FDD. Qualitative/quantitative reasoning is adopted to establish the FDD schemes to build up the FDD strategy.

With the qualitative description of typical VAV system, the FDD structure is set up. The eleven root faults summarized in Chapter 2 are grouped and then analyzed by eight FDD schemes at two steps. The hard faults (Fault 1-10) are analyzed by the first seven schemes (Scheme 1-7) simultaneously at Step 1 of the strategy. The soft fault (Fault 11) is analyzed under Scheme 8 at Step 2 of the strategy. The details of the FDD schemes and their relationships are also described.

CHAPTER 4 PCA-BASED FLOW SENSOR FDD SCHEME

Sensor failure and bias are harmful to the process control of air-conditioning systems resulting in poor control of indoor environment and waste of energy. It can be observed that the study on sensor faults in air-conditioning system is very limited compared with the efforts paid on studying the component faults, although the IEA Annex 34 strongly pointed out the impacts of unreliable measurements on the control optimization and even component fault detection and diagnosis (Dexter and Pakanen 2001).

Section 4.1 briefly introduces PCA method and the reasons of selecting the PCA method in this scheme. Section 4.2 explains how to determine the number of principal components based on best reconstruction. Two statistics, Hotelling T^2 and *SPE*, are introduced in Section 4.3. Both are used to detect sensor faults. Section 4.4 builds up the PCA models at system level and terminal level. Section 4.5 outlines the structure of PCA-based flow sensor FDD scheme. Section 4.6 summarizes this chapter.

4.1 A Brief on PCA Method

PCA is a multivariate analysis technique, which is also a dimension reduction technique. It produces a lower dimensional representation in a way that preserves the correlation structure between the process variables, and is optimal in terms of capturing the variability in the data (Russell et al. 2000).

The PCA method is one of the popular SPC methods. It uses pure mathematic models (also know as data-driven models), which are unlike physical models since not much internal information on the system itself is demanded. Although the PCA-based FDD method also requires training data under normal operation conditions, they are different from the FDD methods based on the conventional data-driven models, such as the neural model and the state space model as the PCA-based FDD method deals with the correlations among process variables in a more straightforward way.

Conventional model-based FDD methods always describe the correlations using various models and then evaluate the changes of the correlations (i.e. the residual between model prediction and actual measurement). However, the PCA-based FDD method considers that the training data cover the correlations and statistics are used to validate those correlations directly. The difficulties in building or training many complex physical or mathematical models and analyzing the residuals of different models are avoided, which is particularly the case while many sensors are validated simultaneously. Therefore, the PCA method is chosen for VAV flow sensor FDD scheme.

4.1.1 Normalization of Measurements

To effectively extract the information in the data relevant to process monitoring, it is necessary to pre-treat the data. The pretreatment procedures consist of three tasks: removing variables, removing outliers, and auto-scaling.

There are process variables that have no information relevant to monitoring the process, and these variables should be removed before further analysis. The PCA model is constructed with the relevant variables left. Outliers in the training set should be removed to improve the model precision. Obvious outliers can be removed by

plotting and visually inspecting the data for outlying points. More rigorous methods based on statistical thresholds can be employed for removing outliers, and a method using T^2 statistic is applied in the validation tests.

Process data need to be scaled to avoid particular variables dominating the process monitoring method. For example, when performing an un-scaled dimensionality reduction procedure on temperature measurements varying between 20^{o}C and 24^{o}C and the air flow measurements varying between 200l/s and 300l/s, the air flow measurements would dominate even though the air flow may be no more important than the temperature for monitoring the process.

Given a PCA training model (matrix) of n observations (rows) and m process variables (columns) constructed from n samples of normal data, the normalized training matrix (X_{nxm}) could be obtained by auto-scaling the process variables. It consists of two steps. The first step is to subtract each variable by its sample mean because the objective is to capture the variation of the data from the mean. The second step is to divide each variable of the mean-centered data by its standard deviation. Thus each column of X_{nxm} has zero mean and unit variance, which ensures that process variables with high variances do not dominate. When autoscaling is applied to new process data, the mean to be subtracted and the standard deviation to be divided are taken from the training set.

4.1.2 A Brief on PCA

The sample covariance matrix $\boldsymbol{R}$ of the PCA training set (X_{nxm}) could be calculated as Equation 4.1. An eigenvalue decomposition of the covariance matrix $\boldsymbol{R}$ should be as Equation 4.2, where the weights on each variable are given by the loading matrix $\boldsymbol{V}_{mxm}$.

$$R = X^T X / (n-1) \tag{4.1}$$

$$R = V \Lambda V^T \tag{4.2}$$

$\boldsymbol{\Lambda}$ is the diagonal matrix whose diagonal elements are the characteristic values or eigenvalues of decreasing magnitude ($\lambda_1 \geqslant \lambda_2 \geqslant \ldots \geqslant \lambda_m \geqslant 0$), as shown in Equation 4.3.

$$\Lambda = \begin{bmatrix} \lambda_1 & & & \\ & \lambda_2 & & \\ & & \cdots & \\ & & & \lambda_m \end{bmatrix}_{m \times m} \tag{4.3}$$

The training sample variance of the *ith* loading vector in matrix $\boldsymbol{V}$ is λ_i, and the total system variance is the trace of the covariance matrix $\boldsymbol{R}$, $tr(\boldsymbol{R})$. There is: $tr(R) = \sum_{j=1}^{m} \lambda_j$, i.e. the sum of the eigenvalues is equal to the trace of the covariance matrix ($\boldsymbol{R}$). Therefore, the percent variance captured by the l loading vectors is as shown in Equation 4.4, which is known as the cumulative percent variance (*CPV*).

$$CPV(l) = \frac{\sum_{j=1}^{l} \lambda_j}{\sum_{j=1}^{m} \lambda_j} \times 100\% = \frac{\sum_{j=1}^{l} \lambda_j}{tr(R)} \times 100\% \tag{4.4}$$

In order to optimally capture the variations of the data while minimizing the effect of random noise corrupting the PCA representation, the loading vectors in matrix $\boldsymbol{V}$ corresponding to the a largest eigenvalues are typically retained as principal loading matrix ($\boldsymbol{P}_{mxa}$) (Figure 4.1). It is commonly accepted that the portion of the PCA space (PC subspace) corresponding to the larger eigenvalues describes most of the systematic or state variations occurring in the process, and the portion of the PCA

space (residual subspace) corresponding to the smaller eigenvalues ($\tilde{P}_{mx(m-a)}$) describes the random noise.

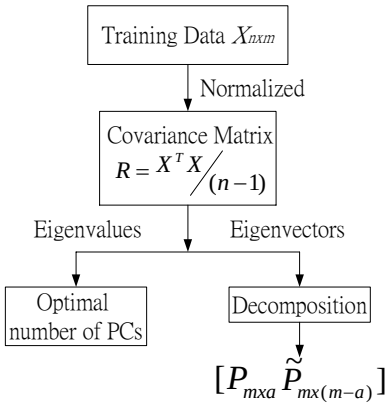

Figure 4.1 Flow chart of PCA decomposition

Several techniques exist for determining the optimum number (*a*) of principal loading vectors, which is also called determining the number of principal components (PCs), but there appears to be no dominant techniques. The screen test technique is often used to determine the number of PCs, which assumes the eigenvalues form a linear profile. The number of PCs is determined by locating the eigenvalue where the profile is no longer linear. However, the identification of this break can be ambiguous when several breaks from linearity occur in the profile. It was found that eigenvalue profile is strongly irregular in VAV applications. That makes the screen test method not applicable in this study. Experiences show that variance of reconstruction error (VRE) can be used as the index to determine the number of principal components in a PCA model for best reconstruction (Qin and Dunia 2000) and therefore solve the problem. The VRE method is employed in this study and will be explained in detail in the next section.

After determining the number of PCs, *a*, the principal loading matrix P_{mxa} is confirmed. The projections of the new observations in X_{new} into the lower dimensional

space are contained in the score matrix $\boldsymbol{T}$ as shown in Equation 4.5. The projection of $\boldsymbol{T}$ back into the PC subspace (PCS) is calculated as Equation 4.6. The difference between X_{new} and $\hat{X}_{new}$ is the residual matrix E as shown in Equation 4.7 and in Figure 4.2.

$$T = X_{new}P \tag{4.5}$$

$$\hat{X}_{new} = TP^T \tag{4.6}$$

$$E = X_{new} - \hat{X}_{new} \tag{4.7}$$

The residual matrix $\boldsymbol{E}$ captures the variations in the residual subspace (RS) spanned by the loading vectors associated with the m-a smallest eigenvalues ($\tilde{P}_{mx(m-a)}$).

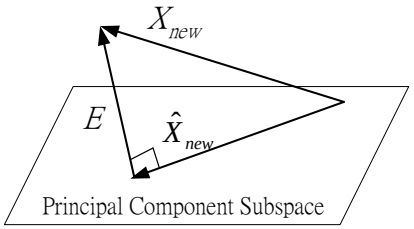

Figure 4.2 Geometric interpretation of the new sample projection

In the application of the PCA method, only those eigenvectors, P_{mxa}, in $\boldsymbol{V}$, which are associated with the first a largest eigenvalues, are retained in PCA models, as they capture most variance of a process. Therefore, only a PCs, normally much less than the number of the original variables (m), need to be analyzed. Fault detection, identification and diagnosis of the new observations could be carried out based on the lower dimensional PCs.

4.1.3 Critical Review on Applications of PCA Method

The PCA method has been widely used for statistical process control in many fields. It is used to monitor the performance of a process over time in order to verify that the process is 'in control'. The state of 'out of control' could be due to abnormal process or sensor error(s). Tong and Crowe (1994) proposed a new class of test statistics based on PCA for detection and identification of gross errors. It was compared to the other statistics like univariate, maximum power and chi-square tests. The results showed that the PCA statistics was capable of detecting gross errors of small magnitudes and had substantial power to correctly identify the variables in error, when the other statistics failed.

Even though there has been a recent interest in the use of PCA for sensor fault detection and identification, few identification schemes for faulty sensors have considered the possibility of an abnormal operation condition of the plant. Dunia, R. et al. (1996) used the PCA for sensor fault identification via reconstruction. A sensor validity index (SVI) was proposed for sensor fault identification. This validity index can distinguish abnormal operational conditions from a single sensor fault, which was verified by the application to a boiler process.

To distinguish between failed sensors and process upsets, Doymaz et al. (2001) proposed a novel approach based on PCA statistics. In this study, the importance of using the T^2 and the *SPE* (squared prediction error) together for fault detection and identification was emphasized. Correlation coefficient criterion was utilized to infer about the state of the correlation structure between one sensor and its closest neighbor for distinguishing between sensor failures and process upsets. The strategy was verified on an industrial liquid-fed ceramic melter.

Recently, Wang and Xiao (2004a and 2004b) applied the PCA method in AHU sensor FDD. Two PCA models were built based on the heat balance and pressure-flow balance of the air-handling process, aiming at reducing the effects of the system non-linearity and enhancing the robustness of the strategy in different control modes. The fault isolation ability of the method was improved using the multiple models. The robustness of the PCA-based strategy in detecting/diagnosing AHU sensor faults was verified by both simulation tests and site data from the BMS of a building. The PCA method was successfully applied for sensor FDD in HVAC field.

4.2 Determining Number of Principal Components – VRE Method

Sensitivity of a PCA-based FDD method needs to be viewed from two sides. It is not preferable for a method to be too sensitive or too insensitive. If a method is too sensitive, fault alarms due to normal disturbances or measurement noises and disturbance will be frequently raised. However, if it is too insensitive, some slight faults may be undetectable. There is a compromise between sensitivity and reliability of an FDD method.

The sensitivity of the PCA-based FDD method is also closely relative to the quality of the training data. There must be sufficient training data to capture the correlations. However, training data must not spread in too large range when the operation condition is concerned. The PCA method aims at capturing as much as possible normal variation in the process from the training data. If the operation conditions vary too much, the sensitivity of the PCA may be decreased because the

variations caused by the sensor faults are not significant compared with modeling error. These effects will be demonstrated in the validation tests.

Besides the quality of training data, two other factors affect the sensitivity of a PCA model: one is the number of retained PCs and the other is the confidence level of the threshold. The more PCs are retained, the more information on the correlations among the variables is retained. However, retaining more PCs also means more unimportant and unstable correlations retained in the model, and heavier computation burden in modeling. Optimization of the number can be used to determine how much information to be retained in the PCA models. Method proposed by Qin and Dunia (2000) is applicable to get the optimal number of the retained PCs. Similarly, the larger the confidence level of the threshold is, the more sensitive the PCA model is and vice versa. 95% is an acceptable level for most engineering practice.

4.2.1 The Variance of Reconstruction Error (VRE)

Most existing approaches to determining the number of PCs based on monotonic indices are subjective because there may be a rather constant decrement in the index and there can be more than one location which satisfies the criterion.

The method proposed by Qin and Dunia (2000) to determine the number of PCs is based on the best reconstruction of variables. The VRE is used as an index to determine the number of PCs.

The criterion of VRE method used in this study for determining the number of PCs is based on the fact that, when the PCA model is used to recover the missing measurements or reconstruct the faulty sensors, the reconstruction error is a function

of the number of PCs. Previous studies guaranteed that there is a minimum of VRE index corresponding to the best reconstruction.

The VRE can be decomposed into a portion in the PCS and a portion in the RS. The portion in the RS is shown to decrease monotonically with the number of PCs and that in the PCS in general increase with the number of PCs. The VRE always has a minimum which points to the optimal number of PCs (Figure 4.3).

The VRE calculation uses normal data only and does not require actual faults to occur. It is applicable to other purpose than fault reconstruction, although it is derived from fault reconstruction.

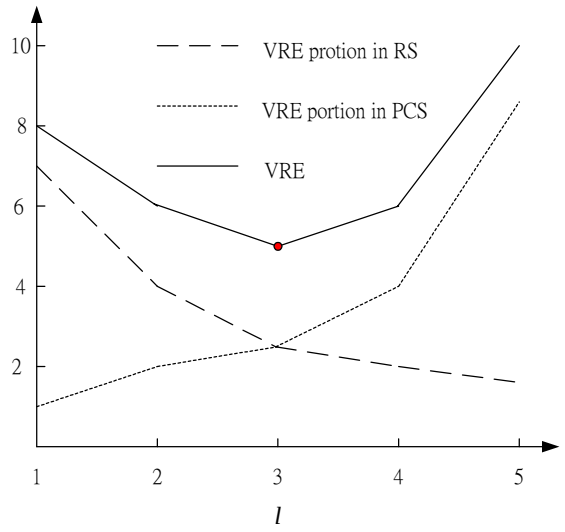

Figure 4.3 Illustration of VRE index

4.2.2 Number of Principal Components for Best Reconstruction

The reconstruction error for the *i*th variable (u_i) is represented by the sum of the error in the RS ($\tilde{u}_i$) and the PCS ($\hat{u}_i$) in Equation 4.8. The VRE is the sum of all sensor reconstruction errors. When the weighting indices of the sensors are of concern, the VRE can be calculated as Equation 4.9, where q is a weighting vector. Such a

vector allows one to adjust the model depending on how critical each sensor fault is to process operation. As $q^T\tilde{u}$ is gradually decreasing and $q^T\hat{u}$ is increasing when the number of PCs, *a*, gets large, *a* is finalized providing the minimum for $q^T u$ as shown in Equation 4.10.

$$u_i = \tilde{u}_i + \hat{u}_i \tag{4.8}$$

$$q^T u = q^T\tilde{u} + q^T\hat{u} \tag{4.9}$$

$$\min_a q^T u = \min_a\left(q^T\tilde{u} + q^T\hat{u}\right) \tag{4.10}$$

The error on the residual space ($\tilde{u}_i$) and the score space ($\hat{u}_i$) are calculated according to Equation 4.11 and 4.12:

$$\tilde{u}_i = u_i\left\|\tilde{\xi}_i\right\|^2 = \tilde{\xi}_i^{0T}\tilde{R}\tilde{\xi}_i^0 \tag{4.11}$$

$$\hat{u}_i = \tilde{u}_i\frac{\left\|\hat{\xi}_i\right\|^2}{\left\|\tilde{\xi}_i\right\|^2} \tag{4.12}$$

where, ξ_i is the *i*th column of the identity matrix as the direction of a process fault shown in Equation 4.13. For example, $\xi_1 = [1...0...0]^T$ presents the first sensor is faulty among all sensors. $\hat{\xi}_i$, $\tilde{\xi}_i$ and $\tilde{\xi}_i^0$ are calculated as illustrated by Equation 4.14 – 4.16. $\tilde{R}$ is the un-modeled portion of the covariance matrix ***R*** (Equation 4.17).

$$\xi_i = [0...1...0]^T \tag{4.13}$$

$$\hat{\xi}_i = PP^T\xi_i \tag{4.14}$$

$$\tilde{\xi}_i = (I - PP^T)\xi_i \tag{4.15}$$

$$\tilde{\xi}_i^0 = \frac{\tilde{\xi}_i}{\left\|\tilde{\xi}_i\right\|} \tag{4.16}$$

$$\tilde{R} = (I - PP^T)R(I - PP^T) \tag{4.17}$$

As the sensor reconstruction error is deduced from the covariance matrix $\boldsymbol{R}$ and sensor identity matrix ξ (Equation 4.11&4.12), no sensor reconstruction is actually needed to calculate the VRE. The number of PCs could be determined directly from the PCA training set.

4.3 PCA-based Fault Detection, Diagnosis and Sensor Reconstruction

4.3.1 Statistic I: Hotelling T^2 and Its Threshold

The Hotelling T^2 is the earliest multivariate statistic, which is a quantity indicating the overall conformance of an individual sample vector to its mean or an established standard or reference. It is simply the locus on the ellipse-like confidence region in the multidimensional space. A two-dimensional example is shown in Figure 4.4.

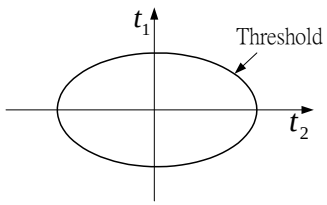

Figure 4.4 t scores and T^2 statistic with 2 PCs

The T^2 statistic assumes that the observation at one time instant is statistically independent to the observations at other time instances. This can be a bad assumption for short sampling interval in most engineering processes. However, if there are

enough data in the training set to capture the normal process variations, the T^2 can be an effective tool for process monitoring even if there are deviations from the normality or statistical independence assumption (Russell et al. 2000).

The original form of the T^2 is shown in Equation 4.18. Because the new observation, x, is normalized to zero mean and unit standard in PCA method, the T^2 defined in PCA method can be written as Equation 4.19.

$$T^2 = (x - \bar{x})' R^{-1} (x - \bar{x}) \tag{4.18}$$

$$T^2 = x^T R^{-1} x \tag{4.19}$$

Substituting Equation 4.2 into Equation 4.19 yields:

$$T^2 = x^T (V \Lambda V^T)^{-1} x = x^T V \Lambda^{-1} V^T x \tag{4.20}$$

When the number of observation variables is large and the amount of data available is relatively small, the T^2 tends to be an inaccurate representation of the in-control process behavior, especially in the loading vector directions corresponding to the smaller eigenvalues. Inaccuracies in these smaller eigenvalues have a huge effect on the calculated T^2 because they are inverted in Equation 4.20. Therefore, the loading vectors associated only with the larger eigenvalues should be retained in calculating the T^2 statistic.

If only a principal loading vectors, as normal in PCA method, instead of all of them are used, the T^2 is:

$$T^2 = x^T P \Lambda_a^{-1} P^T x \tag{4.21}$$

where Λ_a is the diagonal matrix whose diagonal elements are corresponding eigenvalues of $\boldsymbol{P}$.

Assuming the observations are randomly sampled from a multivariate normal distributed process, an upper control limit on the T^2 is given by:

$$T_a^2 = \frac{a(m-1)(m+1)}{m(m-a)} F_\alpha(a, m-a) \tag{4.22}$$

where $F_\alpha(a,m-a)$ is the upper 100α % critical point of the F-distribution with a and $m-a$ degrees of freedom. A new multivariate sample that produces a T^2 statistic greater than the upper control limit will indicate the process is out of control.

Fault detection and isolation based on the information captured by the T^2 is somewhat insensitive to changes in the sensor arrays or to small process upsets because T^2 is based on the linear combination of all variables. A fault in one of the sensors, or small process upsets may not be amplified sufficiently to trigger the alarm and give an indication to out-of-control signal.

4.3.2 Statistic II: *SPE* and Its Threshold

The *Q* statistic, also known as the *SPE*, is a squared 2-norm measuring the deviation of the observations to the lower dimensional PCA presentation. The *SPE* is more sensitive to sensor changes compared with the T^2 as the error of any type will be propagated to all scores.

The *SPE* is defined as the squared sum of the residual in the PCA method as shown in Equation 4.23, where the residual is actually the difference between model estimation and measurement.

$$SPE = \left\|E\right\|^2 = \left\|X - \hat{X}\right\|^2 = \left\|X(I - PP^T)\right\|^2 \tag{4.23}$$

The *SPE* represents the sum of squares of the distance of the new observation, *x*, from the principal component subspace that the PCA model defines. Since *SPE* does not

directly measure the variations along each loading vector but measures the total sum of variations in the residual space, the *SPE* does not suffer from an over-sensitivity to inaccuracies in the smaller eigenvalues.

Previous research works proved that the quantity c in Equation 4.24 is approximately normally distributed with zero mean and unit variance. SPE_α denotes the upper limit for the *SPE* under normal condition. The parameters in Equation 4.24 are defined as shown in Equations 4.25 to 4.28 (Jackson 1991).

$$c = \theta_1 \frac{\left[\left(\frac{SPE_\alpha}{\theta_1} \right)^h - \frac{\theta_2 h_0 (h_0 - 1)}{\theta_1^2} - 1 \right]}{\sqrt{2\theta_2 h_0^2}} \tag{4.24}$$

$$\theta_1 = \sum_{i=a+1}^{m} \lambda_i \tag{4.25}$$

$$\theta_2 = \sum_{i=a+1}^{m} \lambda_i^2 \tag{4.26}$$

$$\theta_3 = \sum_{i=a+1}^{m} \lambda_i^3 \tag{4.27}$$

$$h_0 = 1 - \frac{2\theta_1 \theta_3}{3\theta_2^2} \tag{4.28}$$

λ are the eigenvalues of the covariance matrix sorted in descending order, a is the number of principal components, and m is the number of variables. The upper limit SPE_α for the *SPE* can be derived according to Equation 4.24, as shown in Equation 4.29.

$$SPE_\alpha = \theta_1 \left[\frac{c_\alpha \sqrt{\theta_2 h_0^2}}{\theta_1} + \frac{\theta_2 h_0 (h_0 - 1)}{\theta_1^2} + 1 \right]^{1/h_0} \tag{4.29}$$

c_α is the normal deviate cutting off an area of α under the upper tail of the distribution if h_0 is positive and under the lower tail if h_0 is negative. A new multivariate sample that produces a *SPE* greater than the upper control limit will indicate sensor error(s).

4.3.3 Fault Detection with Both T^2 and *SPE*

T^2 is the quantity indicating the overall conformance of an individual observation vector to its mean or an established standard. *SPE*, the squared sum of the residual, is the deviation of the observations to the lower dimensional PCA representation, which measures the random variations of the process. The thresholds ($T_\alpha^{\,2}, SPE_\alpha$) represent the normal dynamics and measurement noises of the system that cannot be modeled.

The level of significance, α, specifies the degree of tradeoff between the false alarm rate and the missed detection rate. α for HVAC measures can be set to 0.05 or 0.025. The thresholds of T^2 and *SPE* could be calculated after α is selected.

In well-instrumented process settings, there may be many sensors at various locations measuring the same or different quantities, such as flow rates, temperatures, pressures, etc. Due to process characteristics, these variables should be cross-correlated with each other. When a process upset occurs, its aftereffect will be detected by a group of sensors rather than only by one of them. The threshold of T^2 is likely to be exceeded. However, if a sensor (for measuring only) malfunction is the case, then this will only appear in the individual sensor response. The threshold of *SPE* is likely to be exceeded while T^2 could be within the normal range. Nevertheless, if the malfunction sensor is measuring a manipulated variable, which is called manipulating sensor in this study, in the system, the information conveyed to a

feedback controller will be inaccurate. As a result, sensor malfunctioning may manifest itself in more than one sensor.

Process upsets and sensor failures can be identified by applying both T^2 statistic and *SPE* with PCA model. When no fault exists, T^2 and *SPE* are less than the thresholds. On the contrary, when faults exist, the correlation among the measurements of variables will be destroyed, higher value(s) of T^2 and/or *SPE* is detected (Doymaz et al. 2001). T^2 and *SPE* along with their appropriate thresholds detect different types of faults. The advantage of both statistics can be utilized by employing the two measures together to isolate the sensor fault from the process upsets (Figure 4.5). The VAV terminal FDD scheme is developed by using both statistics.

For sensor fault detection, T^2 is somewhat insensitive to changes in the sensor arrays. However, the *SPE* measure is more sensitive to such changes compared to T^2. When a disturbance occurs, it is most likely to manifest itself in the *SPE* by violating the upper control limit rather than that of the T^2. Significant changes in the process or in the sensor characteristics can trigger both alarms. Nevertheless, there might be process upsets undetected by the *SPE* due to the extrapolating feature of the model. In such cases, T^2 will capture these changes, but no violation in the *SPE* will be observed (Doymaz et al. 2001).

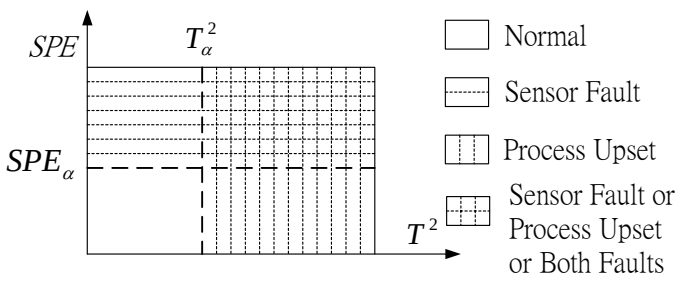

Figure 4.5 Fault diagnosis using *SPE*-T^2 plot

In this approach of isolating the disturbances (sensor failures and/or process upsets), it is possible to capture multiple sensor malfunctions. If a sensor failure and a process upset occur simultaneously, the method is capable to distinguish between these two disturbances.

4.3.4 Fault Isolation Using Contribution Plot

Once sensor fault has been detected, the faulty sensor should be identified. Normally, univariate statistical techniques are employed for fault isolation. As the univariate statistical techniques do not account for correlations among the process variables, they can leave out variables that are responsible for the fault or can give alarms for so many variables that the engineer has little guidance on the main variables of concern.

Considering correlations among the variables, researchers have developed a number of fault identification methods: *(i).* backward elimination for sensor identification (BESI) (Doymaz 2001), *(ii).* sensor validity index (SVI) proposed to determine the status of individual sensor (Dunia 1996) particularly for sensor malfunction, *(iii).* multiple faults identification to construct separate PCA models for each process unit (Wang and Xiao a 2004, Wang and Xiao b 2004, Russel 2000), *(iv).* to introduce new models for each combination of faults, which is a straightforward approach for diagnosing multiple faults, *(v).* correlation coefficient (CC), which is used as the criterion for multiple faults identification (Doymaz 2001).

The drawbacks of the first approach are computationally expensive, almost impossible to incorporate it within a nonlinear PCA framework, and the *SPE* space may not reveal all process upsets. The second approach concentrates on the identification of a single faulty sensor only. The third approach will not unequivocally

diagnose the cause and technology is still needed to further identify the cause, although it can narrow down the cause of abnormal process operations. The disadvantage of fourth approach is that the number of combinations grows exponentially with the number of faults requiring huge number of models. The fifth approach is effective but still needs heavy computational load.

A contribution plot approach is adopted in the VAV terminal sensor FDD strategy developed in this study for fault isolation, which has been used recently by a few researchers in different engineering fields (MacGregor 1994, Tong and Crowe 1995, Norvilas et al. 2000). This approach compares the contribution of each variable in T^2 and *SPE* when fault(s) has been detected. The variables which make major contributions to this deviation are easily observed. This approach needs less computational load but can isolate multiple faults. It is verified effective for AHU applications (Wang and Xiao 2004a, 2004b).

Contribution plots for fault identification take into account the spatial correlations, thereby improving upon the univariate statistical techniques. The approach is based on quantifying the contribution of each process variable to T^2 statistic or *SPE*.

When the contribution plot approach is applied to a T^2 violation, the contribution calculation of each variable x_i is shown as follows:

$$T_i^2 = \sum_{j=1}^{a} \frac{x_i \cdot P(i,j) \cdot t_j}{\lambda_j} \tag{4.30}$$

$$T^2 = \sum_{i=1}^{m} T_i^2 \tag{4.31}$$

$$\eta_i = \frac{T_i^2}{T^2} \tag{4.32}$$

The variables responsible for the fault can be ordered by the contribution percentage η_i. The operators and engineers can immediately focus on those variables with higher η_i values and use their process knowledge to determine the cause of the out-of-control status.

Once a fault is detected using the *SPE*, the contribution plot can be used to diagnose the fault as well, i.e. to find out the root cause of the fault. When the *SPE* breaks the threshold, contribution of individual variable in new samples to the *SPE* can be checked as Equation 4.33 shown based on Equation 4.23. Where, e_i represents the *ith* element of the unmodeled residual vector *e*. η_i is the contribution of the *ith* variable to the total variance.

$$\eta_i = \frac{\|e_i\|^2}{\|e\|^2} = \frac{\|e_i\|^2}{SPE} \tag{4.33}$$

Because the *SPE* represents the total unmodeled variance of the process, which is the sum of squares of unmodeled variance of each variable, the variable having the largest contribution to the *SPE* is most probably relative to the fault. In general, the contribution plot helps to narrow the possible fault sources and thus focuses on a smaller range of measurements among all original variables. To diagnose manipulating sensors whose effects propagate to the whole system, more information about the process is needed.

4.3.5 Sensor Reconstruction

Since advanced supervisory control strategies need the accurate air flow measurement rates of VAV terminals, sensor recovery after FDD is important. The

recovered measurements are also used to improve the robustness of the flow sensor FDD scheme, which will be described later in this chapter.

A few studies have investigated the methods like iterative approach and optimization approach for sensor reconstruction. Both approaches are verified providing satisfactory results (Dunia 1996). The iterative approach is adopted in this study for VAV terminal flow sensor reconstruction as this approach does not need matrix inversion and even actual iteration.

The drawback of simple projection of measurements for sensor recover, $\hat{X} = XPP^T$, is that the faulty sensor contained in X is used in for the estimation. To eliminate the effect of the faulty sensor, we feed back the prediction of the ith variable ($\hat{x}_i$) to the input and iterate until it converges to a value z_i. The iterative approach can be represented by Equation 4.34 to 4.36. Where, x^T represents a row of the new observation matrix X. The subscripts $\pm i$ denote a vector formed by the first i-1 and the last m-i elements of the original vector respectively.

$$C = PP^T = \left[C_1 C_2 ... C_m\right] \tag{4.34}$$

$$c_i^T = \left[c_{1i} c_{2i} ... c_{mi}\right] \tag{4.35}$$

$$z_i^{new} = c_{ii} z_i^{old} + \left[x_{-i}^T 0 x_{+i}^T\right] c_i = \left[x_{-i}^T z_i^{old} x_{+i}^T\right] c_i \tag{4.36}$$

To guarantee the convergence of the iteration, we need to verify that c_{ii} is inside the unit circle. Using the orthogonal properties of $\boldsymbol{P}$, we have Equation 4.37 and 4.38. Eventually, the asymptotic value for z_i can be deduced as Equation 4.39 for the application in this study, which does not require matrix inversion and the reconstruction is obtained without actual iteration.

$$\left[P\tilde{P}\right]\left[P\tilde{P}\right]^T = C + \tilde{P}\tilde{P}^T = I \tag{4.37}$$

$$c_{ii} + \sum_{h=a+1}^{m} p_{ih}^2 = 1 \quad \text{thus } 0 < c_{ii} \le 1 \tag{4.38}$$

$$z_i = \frac{\left[x_{-i}^T 0 x_{+i}^T\right] c_i}{1 - c_{ii}} \tag{4.39}$$

Figure 4.6 shows the geometric interpretation of the iterative approach for the three correlated variables and one principle component. The reconstructed variable is x_3. The iterative approach projects x on the PC line and the x_3 coordinate (z_3^{new}) is used to define the new location of x. The procedure continues until x_3 converges to its final value z_3 as in Equation 4.39.

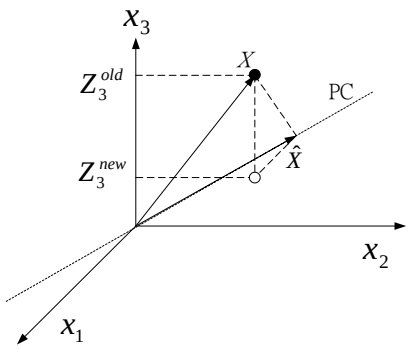

Figure 4.6 Geometric interpretation of the iterative approach

4.4 PCA Models at System Level and Terminal Level

Complete failure of VAV terminal flow sensors (Fault 6&7) results in the failure in achieving the major function of the air-conditioning systems. Air flow sensor bias (Fault 11) in a typical VAV terminal might not affect the normal control process if the readings are within certain range as it can be compensated by resetting the air flow set point. However, when sensor drift, bias or precision degradation is developed beyond

a certain level, the readings will reach minimum or maximum of the VAV terminal design flow and ruins the control process. Furthermore, advanced supervisory control strategies need the accurate air flow measurement rates of VAV terminals and soft sensor faults make the control systems fail in optimization. Therefore, flow sensor FDD and sensor recovery of VAV terminals are important to the reliability and robustness of air-conditioning system control.

A VAV air distribution system may have many VAV terminals and all terminals are interactive for system balance. It means that VAV system network characteristics are related to all terminals with many process variables involved. Instead of analyzing all the variables, PCA method focuses on analyzing principle components when monitoring the condition of a network. Therefore this dimension reduction technique is suitable to be used for VAV terminal sensor fault analysis.

For VAV terminal flow sensor fault detection and diagnosis, PCA models at two levels are developed and used in serial. They are system model and terminal models (Figure 4.7). The system level model indicates that, in a network, the hydraulic characteristics are related to the static pressure (P_{st}) of the system, the damper positions and the flow rates (F) of all VAV terminals. However, in common pressure independent VAV systems, the damper position signals may not be available. The control signal to damper (μ) typically represents the position of an actuator for position algorithm controller (Kamimura et al. 1994) and can be used instead of damper position for modeling (Figure 4.7). In HVAC applications, the control signal to damper (μ) is normally an electrical signal of 0-10V or 4-20mA, which is unlikely to deform. The static pressure is assumed correct in this study as the fault of this sensor has already been analyzed by the strategy developed by Wang and Xiao (2004a, 2004b).

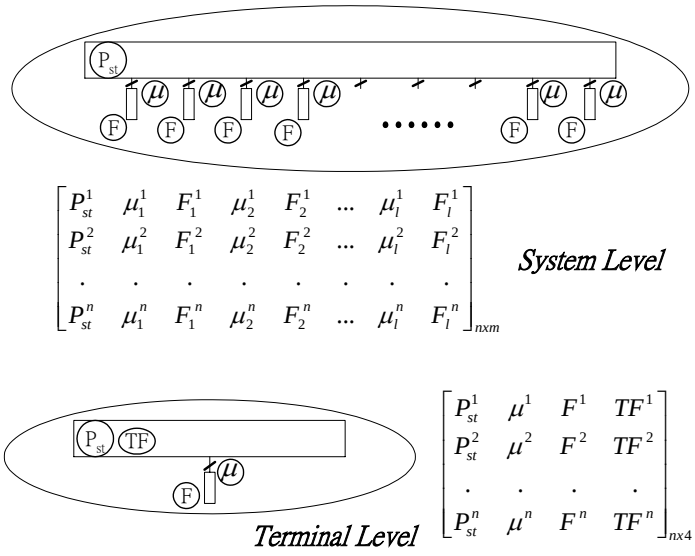

Figure 4.7 PCA models at system level and terminal level

As all VAV terminals are involved in the system level model, the reliability of fault detection and isolation may be affected by the process stability and multiple faults in the system. Therefore, terminal level PCA models are developed and used together with the system model in serial to further investigate the suspicious terminal(s), which are detected by the system level FDD scheme. For individual terminals, the PCA models involve four variables: the static pressure (P_{st}) of the system, the damper position represented by the damper control signal (μ), the terminal flow rate (F) and total flow rate (TF) of the system, which represents the overall influence of other terminals on a particular terminal (Figure 4.7).

4.5 Structure of PCA-based Terminal Sensor FDD Scheme

PCA-based FDD scheme for VAV terminal flow sensor fault is designed based on T^2 and SPE for fault detection and contribution plot for fault identification (Figure 4.8).

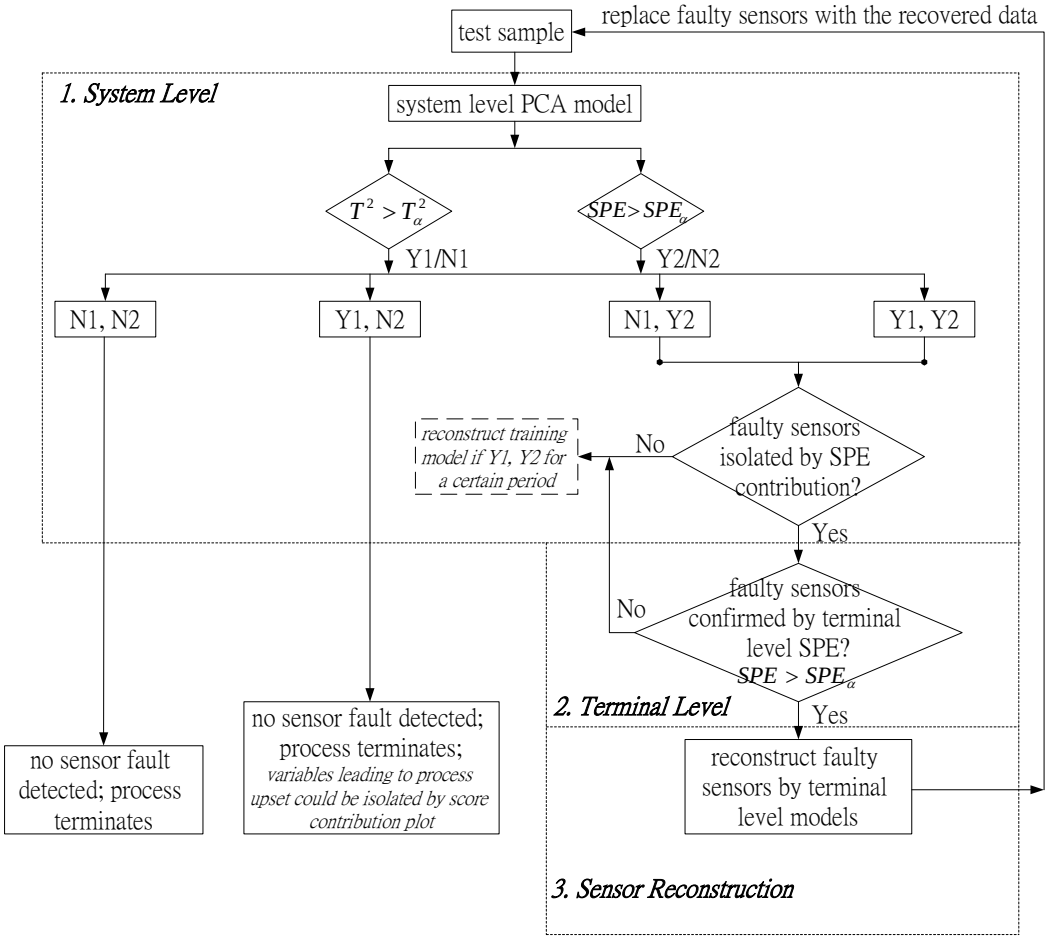

Figure 4.8 PCA-based VAV terminal sensor FDD scheme

When the *SPE* of new observations exceed the thresholds (95% confidence level is selected in the scheme, i.e. $\alpha = 0.05$), *SPE* contribution plot is applied to isolate the suspicious sensor(s). The suspicious sensors are further examined by terminal level PCA model(s) based on terminal level T^2 and *SPE*. If the faulty sensors are identified by violating terminal level *SPE* threshold, those sensors would be reconstructed based on terminal models. New system level T^2 and *SPE* could be calculated with the recovered data. If both new T^2 and *SPE* are under the thresholds, the FDD process terminates. If only new T^2 exceeds the threshold, the system is diagnosed to have a process upset but no other faulty sensors. Variables leading to the process upset could be isolated by the score contribution plot. If only new *SPE* or both new T^2 and *SPE*

exceed the thresholds, faults might exist in other sensors, the strategy repeats FDD process.

It is common for multiple faults exist but the system level FDD may not isolate all of them by contribution plot simultaneously because the significant sensor error would dominate the *SPE* contribution. The left faulty sensor(s) could be further isolated repeating the same FDD process after replacing the faulty sensor with the recovered one. The scheme terminates until T^2 and *SPE* at the system level do not indicate any more fault after all the isolated faulty sensors are recovered. Consequently, the sensitivity and robustness of the FDD scheme are enhanced significantly particularly for multiple faults.

The FDD scheme includes three major parts: 1>. System level fault detection and isolation, 2>. Terminal level fault identification, 3>. Repeating the FDD process after recovering the isolated faulty sensors.

4.5.1 System Level Fault Detection and Isolation

For VAV air distribution network, the system level measurement space is constructed by measurements from sensors and control signals (Equation 4.40).

$$Y = \begin{bmatrix} P_{st}^1 & \mu_1^1 & F_1^1 & \mu_2^1 & F_2^1 & \dots & \mu_l^1 & F_l^1 \\ P_{st}^2 & \mu_1^2 & F_1^2 & \mu_2^2 & F_2^2 & \dots & \mu_l^2 & F_l^2 \\ \cdot & \cdot & \cdot & \cdot & \cdot & \cdot & \cdot & \cdot \\ P_{st}^n & \mu_1^n & F_1^n & \mu_2^n & F_2^n & \dots & \mu_l^n & F_l^n \end{bmatrix}_{nxm} \tag{4.40}$$

Samples of variables under normal operation condition are used to construct the training matrix Y (n samples of m variables). Because different variables in the system use different units, the columns of the training matrix usually need to be normalized to zero mean and unit variance. This is important because the monitoring statistic is the

sum of squared deviations from the observed process variables, so each process variable must be in comparable magnitude to prevent a variable of larger numerical value from dominating the statistic. The training matrix is normalized using Equation 4.41 to 4.43.

$$M_i = \frac{1}{n}\sum_{j=1}^{n} Y_{j,i} \tag{4.41}$$

$$\sigma_i = \sqrt{\frac{1}{n-1}\sum_{j=1}^{n}(Y_{j,i} - M_i)^2} \tag{4.42}$$

$$X = (Y - I_n M^T)\Xi^{-1} \tag{4.43}$$

$I_n = [1,1,1...1]_n^T \in R^n$, $i=1,2\ldots m$, $j=1,2\ldots n$. $\Xi_{m\times m}$ ($\Xi = diag(\sigma_1, \sigma_2 \ldots \sigma_m)_{m\times m}$) is a diagonal matrix whose diagonal elements are the standard variances of the variables in the training matrix.

A PCA model is not represented by some equations or logic descriptions as most conventional models. A PCA model involves several elements, including the loading vectors (***P***) of the PCs which is used to decompose the measurement spaces, the mean and variance vectors which define a statistical average operation condition, and the thresholds of the T^2 and *SPE* which are used to detect faults. Therefore, the task of building a PCA model is actually to obtain all these elements.

The loading vectors (***P***) of the principal components are deduced based on the minimum VRE. The thresholds of the T^2 and *SPE* are calculated after the number of PCs has been determined according to Equation 4.22 and Equation 4.29 respectively.

Once the PCA models (including the loading vectors and the thresholds) are set up, new samples can be examined using the models. The basic scheme includes three

major function procedures: (i) pre-processing of new samples, (ii) sensor fault detection, and (iii) sensor fault diagnosis. Conclusions can be made about the performance of all sensors.

After normalized according to Equation 4.44, a new normalized sample vector (x_{new}) is projected to the principal component subspace and gets its modeled component that contains the normal variation of the process (Equation 4.45).

$$x_{new} = (y_{new} - M^T)\Xi^{-1} \tag{4.44}$$

$$\hat{x}_{new} = x_{new} PP^T \tag{4.45}$$

The T^2 and *SPE* calculated with Equation 4.21 and Equation 4.23 respectively, are used as the fault indices (Figure 4.9). A change in correlations among the variables increases their projection on the residual subspace. As a result, the magnitudes of the T^2 and/or *SPE* become lager than usual compared to those obtained during normal conditions.

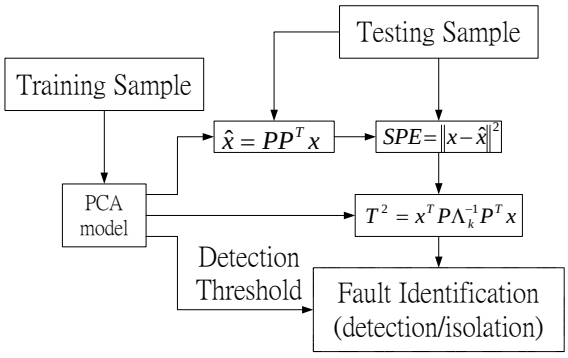

Figure 4.9 Flow chart of PCA method for fault detection

When no fault exits, the T^2 and *SPE* are below their upper limits previously defined. It means that the correlations among measurements are within normal range. On the other hand, when process upset or sensor fault occurs, the correlations among

the measurements will be destroyed, and higher values of the T^2 and/or *SPE* are detected.

The variables responsible for T^2 and/or *SPE* violation are isolated by the contribution plot. The contribution percentage of each variable to T^2 and *SPE* is calculated according to Equation 4.32 and Equation 4.33 respectively. The variable contributes most to the *SPE* is isolated as the 'suspected' sensor at the system level.

4.5.2 Terminal Level Fault Identification

The 'suspected' sensor is further investigated at the terminal level. The PCA model of each terminal is defined as Equation 4.46 as introduced previously.

$$Y = \begin{bmatrix} P_{st}^1 & \mu^1 & F^1 & TF^1 \\ P_{st}^2 & \mu^2 & F^2 & TF^2 \\ . & . & . & . \\ P_{st}^n & \mu^n & F^n & TF^n \end{bmatrix}_{nx4} \tag{4.46}$$

The terminal model is trained and applied for fault confirmation after the 'suspected' terminals have been isolated at the system level. The sensor fault can be confirmed by *SPE* limit violation at the terminal level.

4.5.3 Sensor Reconstruction for Robust FDD and Fault-tolerant Control

When the sensor fault has been detected and identified. The measurements can been recovered based on the terminal PCA model. The iteration approach introduced in Section 4.3.5 is used to recover the normalized data of the flow sensor measurements. Those normalized data would replace the faulty ones and the new T^2 and *SPE* at the system level could be calculated. The faulty sensor(s) which were not isolated by the previous FDD process could be further isolated repeating the same

process after the replacement. Thus, the FDD ability is improved significantly for multiple faults and the FDD scheme is robust.

The recovered air flow rates are retrieved from the normalized data following the reversed procedure of the normalization (Equation 4.47).

$$Y = X\Xi + I_n M^T \tag{4.47}$$

Those recovered air flow rate could be further used for advanced supervisory control, what is called fault-tolerant control.

4.6 Summary

Many VAV terminal flows are measured and controlled in a typical VAV air distribution system to realize automatic monitoring, control and optimization. Correlations exist among these variables due to the hydraulic characteristics of the network. One of the multivariate statistical process control methods, the PCA method, was chosen to describe the correlations among process variables in the network. When the correlations are disturbed by sensor faults, it can be observed by abnormal values of the statistics and the faults can be detected.

The PCA method can simplify the multivariate analysis problem by reducing the dimension of a multivariate system but retaining its major variance. Two statistics, the Hotelling T^2 and the *SPE*, were both used in the scheme for sensor fault diagnosis.

This chapter presents the PCA-based sensor FDD scheme for multiple VAV terminal flow sensor biases. Both PCA models at system level and terminal level are

constructed based on the network characteristics. The scheme employs the two models in serial, which can also improve the reliability and sensitivity of the FDD scheme.

The contribution plot is chosen for fault isolation at the system level. After the fault is confirmed at the terminal level, the faulty sensor is reconstructed based on the terminal PCA model. The robustness of the FDD scheme for multiple faults is enhanced by the recovered measurements.

CHAPTER 5 TEST FACILITIES AND ENVIRONMENTS

Test facilities in two test environments, i.e. on a dynamic simulator and in real buildings respectively, are used to validate the FDD schemes and the strategy developed in this study. This chapter briefly introduces these two test facilities and environments.

Section 5.1 briefly describes the simulated building and its VAV air-conditioning system. The first principle models of the components and the system network as well as supervisory control strategies are introduced. Section 5.2 introduces the real buildings and their VAV systems as the second test facilities for validation tests. Section 5.3 summarizes this chapter.

5.1 Dynamic Simulator of VAV Air-conditioning System

5.1.1 System Description

To study on the root faults in the pressure-independent VAV systems, a local building's VAV system is simulated (Wang 1999). The building is a 46-storey commercial building located at Central, Hong Kong. The floor under study is an open plan office of about 2300 m^2 usable floor area. Two central AHUs with VAV systems serve the floor. Each serves half of the floor. There are 40 VAV terminals and over a hundred air diffusers associated with one AHU. The VAV terminals are pressure independent VAV boxes under cascade control. The design air flow rates of the VAV

system is 6 m^3/s and the design VAV supply fan pressure at the location of pressure sensor is 650 Pa.

One AHU/VAV system covering a floor area of 1166 m^2 is simulated to carry out the validation tests. The floor area is divided into eight zones when simulating the office floor. Six of the zones are perimeter zones and the other two are interior zones. A schematic of the VAV system distribution is presented in Figure 5.1. Two variable blade angle fans are equipped as VAV supply fan and return fan, respectively. The pitch angle of the VAV supply (axial) fan is moderated to control the supply air static pressure. The return (axial) fan is used to control the ex-filtration flow rate in order to maintain positive pressure in the building. It is achieved by controlling the difference between the total supply and return air flow rates within the upper and lower limits by moderating the pitch angle of the return fan.

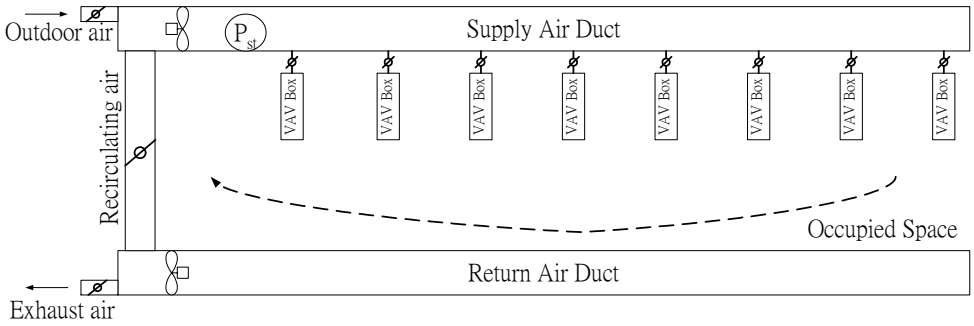

Figure 5.1 Schematic of the VAV system air distribution

This simulator is developed partly based on the work of Wang (1999). The following parts briefly present the dynamic models in the simulator.

5.1.2 First Principle Models

Simplified Building Model

A simplified building model simulates the dynamic balance of energy, moisture, CO_2 and a non-occupant generated pollutant of the zones. The model represents the open plan office floor by a network of thermal resistance, thermal capacitance and air volume. Each space is considered as a node of well-mixed air volume with uniform temperature, moisture, CO_2 and pollutant concentration. The connections between zones are the air mass exchanges caused by air flow. The external wall of each zone is represented by a node of thermal capacitance and resistance linking the zone with outside. The internal structure and furniture in each zone are represented by a node of thermal capacitance connected to the zone through a thermal resistance.

The model computes the heat load of solar radiation absorbed by the external walls by means of an equivalent 'sol-air' temperature, which takes account of the effect of the solar radiation absorbed by building external walls (including absorbency and emission) as the effect of increment of outside air temperature to building. The equivalent 'sol-air' temperature of a zone is defined as the equilibrium temperature of the zone internal node when the solar radiation absorbed by building external walls is the only heat sources of the zone (i.e. internal heat load and other external heat load are zero) and when the zone is isolated from other zones.

Each zone node employs four ordinary differential equations, describing the balance of energy, moisture, CO_2 and non-occupant generated pollutant (Equation 5.1-5.4).

$$M_i c_p \frac{dT_i}{dt} = Q_i + m_{VAV,i} c_p (T_{VAV} - T_i) + m_{\inf,i} c_p (T_{amb} - T_i) - m_{exf,i} c_p T_i + \sum_j m_{ij} c_p (T_j - T_i) + \frac{T_{w,i} - T_i}{R_{wi,i}} + \frac{T_{fut,i} - T_i}{R_{fut,i}} + \frac{T_{sa,i} - T_i}{R_{win,i}} \quad (5.1)$$

$$M_i \frac{dG_i}{dt} = GS_i + m_{VAV,i}(G_{VAV} - G_i) + m_{\inf,i}(G_{amb} - G_i) - m_{exf,i}G_i + \sum_j m_{ij}(G_j - G_i) \quad (5.2)$$

$$V_i \frac{dC_i}{dt} = CS_i + v_{VAV,i}(C_{VAV} - C_i) + v_{\inf,i}(C_{amb} - C_i) - v_{exf,i}C_i + \sum_j v_{ij}(C_j - C_i) \quad (5.3)$$

$$V_i \frac{dC2_i}{dt} = PS_i + v_{VAV,i}(C2_{VAV} - C2_i) + v_{\inf,i}(C2_{amb} - C2_i) - v_{exf,i}C2_i + \sum_j v_{ij}(C2_j - C2_i) \quad (5.4)$$

Where, *T, G, C* and *C2* are the space air temperature, humidity, CO_2 and pollutant concentrations, respectively. *Q, GS, CS* and *PS* are the total internal heat, moisture, CO_2 and pollutant generation rates, respectively, in a zone. M and V are the total air mass and volume, respectively, in a zone. *m* and *v* are the mass and volume flow rates. R_{wi} is the thermal resistance of external wall node in connection to the indoor air node of a zone. R_{fut} is the thermal resistance of internal structure and furniture node in connection to indoor air node of a zone. R_{win} is the thermal resistance of indoor air node in connection to outside.

Damper Model

The flow resistance of an individual damper at certain damper position (*H*) is calculated using Legg's exponential correlation (1986). The air flow (F_{nom}) passing through a damper at nominal pressure head is calculated using Equations 5.5 and 5.6 for damper with opposed blades and parallel blades, respectively. The flow resistance (*R*) is then calculated according to Equation 5.7.

$$F_{nom} = (1 - H) \bullet F_{leak} + H \bullet e^{4.725 \bullet (H-1)} \quad (5.5)$$

$$F_{nom} = (1 - H) \bullet F_{leak} + H \bullet e^{3.789 \bullet (H-1)} \quad (5.6)$$

$$R = \frac{R_{\min}}{F_{nom}^2} \quad (5.7)$$

Duct Model

A duct model is developed to simulate the heat loss through duct wall, dynamic effects of the duct wall and the effects of transfer delay on temperature, moisture, CO_2 and the pollutant. A duct is divided into a number of sections considering the duct length and the velocity ranges of the air flowing inside. The process of the air flowing in the duct at a simulation step is assumed consisting of three separate 'sub-processes': moving of the air segment; mixing of air within individual sections and the heat exchange with outside through duct wall.

It is assumed that the air segments reach their end positions of the step within infinitesimal time and the air within one duct section is mixed within infinitesimal time. The dynamic heat exchange process then takes place between the air with each section and the environment through the wall of relevant sections. The heat exchange of an air segment between two time simulation steps is represented by two differential equations (Equation 5.8 and 5.9). The heat exchange of the duct wall along the air flow direction is neglected.

$$C_{a,i} \frac{dT_{a,i}}{dt} = \frac{T_{w,i} - T_{a,i}}{R_{1,i}} \quad (5.8)$$

$$C_{w,i} \frac{dT_{w,i}}{dt} = \frac{T_{a,i} - T_{w,i}}{R_{1,i}} + \frac{T_{am} - T_{w,i}}{R_{2,i}} \quad (5.9)$$

Fan Models

The supply fan and return fan are axial fans, whose states are represented by three normalized variables representing the air volume flow rate (φ), fan total pressure rise (ξ) and fan absorbed power (λ), respectively. The fan performance law is fitted by a polynomial of two variables of normalized airflow rate (φ) and fan pitch angle (θ) as the following equations show.

$$\xi = \sum_{i=0}^{n_1} \left(\sum_{j=0}^{m_1} C_1(i,j) \bullet \varphi^i \bullet \theta^j \right) \tag{5.10}$$

$$\lambda = \sum_{i=0}^{n_2} \left(\sum_{j=0}^{m_2} C_2(i,j) \bullet \varphi^i \bullet \theta^j \right) \tag{5.11}$$

Cooling Coil Model

A dynamic model is developed to simulate the cooling coil. A first order differential equation is used to represent the dynamics of a coil with lumped thermal mass. The dynamic equation on the basis of energy balance ensures that the energy is conserved. The heat transfer calculation applies the classical Number of Transfer Unit (*NTU*) and heat transfer effectiveness methods. The dry regime and the wet regime are considered separately.

In dry regime, the overall heat transfer resistance (*R*) is computed as follows. Where, *A* is the total heat transfer surface area, R_a, R_m and R_w are the heat transfer resistances of air side convection, coil metal and water side convection, N_{row} is the number of row.

$$NTU = \frac{UA}{C_{\min}} = \frac{A}{C_{\min}(R_a + R_m + R_w)} \tag{5.12}$$

$$\varepsilon = f\left(N_{row}, \frac{C_{\min}}{C_{\max}}, NTU\right) \tag{5.13}$$

$$R = \frac{T_{a,in} - T_{w,in}}{Q} = \frac{1}{\varepsilon \bullet C_{\min}} \tag{5.14}$$

In wet regime, a fictitious air flow is assumed, which has a specific heat equal to the average saturation specific heat (c_s, specific heat of saturation moisture air at the average temperature of air inlet wet bulb temperature and water inlet temperature). The air capacity flow rate and air convection coefficient of the fictitious air flow (C_{af}, $h_{a,wt}$) are as follows. Where, C_{pi} is the specific heat of moisture air.

$$C_{af} = m_a \bullet c_s \tag{5.15}$$

$$h_{a,wt} = h_a \bullet \frac{c_s}{c_{pi}} \tag{5.16}$$

Then, the overall heat transfer resistance (R) is computed using the same approach. Where, subscript ‘wt’ represents wet regime, ‘f’ represents fictitious air flow.

$$NCU_f = \frac{AU}{c_{\min f}} = \frac{A}{C_{\min f}(R_{a,wt} + R_m + R_w)} \tag{5.17}$$

$$\varepsilon_f = f(N_{row}, \frac{C_{\min f}}{C_{\max f}}, NTU_f) \tag{5.18}$$

$$Q_{wt} = \varepsilon_f \bullet C_{\min f} \bullet (T_{aw,in} - T_{w,in}) \tag{5.19}$$

$$\varepsilon_{wt} = \frac{Q_{wt}}{(T_{a,in} - T_{w,in}) \bullet C_{\min f}} \tag{5.20}$$

$$R = \frac{T_{a,in} - T_{w,in}}{Q_{wt}} = \frac{1}{\varepsilon_f \bullet C_{\min f}} \tag{5.21}$$

DDC Controller Model

The 'realistic' controller model represents the following functions: DDC functions, discrete-time operation of digital controllers and supervisory control strategies.

The time scheduling of a sampling cycle is considered to be four steps: process variable sampling, control outputs computation, control signal output, and waiting time for the next sampling cycle. The PID control function used in DDC loops uses the ISA algorithm. Its discrete form is used in the models.

Actuator Model

The actuator model is used to represent the characteristics of actuators. The actuator is assumed to accelerate very quickly and then turn at constant speed. A minimum changes (e.g. the sensitivity of the actuator defined as a parameter of the model) in demanded position is required to restart the actuator. The actuator model includes the hysteresis in the linkage between actuators and valves or dampers.

Sensor Model

The dynamic first-order sensor model is used to simulate the temperature, pressure, flow rate and CO_2 sensors using the time constant method. Different time

constants are used for different sensors depending on the characteristics of the sensors and the measured variables and the locations of the sensors.

The parameters of VAV models to be used for simulation could be determined according to the VAV component characteristics given in manufacturer catalogues and/or empirical correlations given in handbooks. In this study, the VAV system performance data needed for determining the parameters of the VAV component models were obtained by monitoring the VAV system on site.

System network model

The original system network model developed by Wang (1999) considered the eight VAV terminals in parallel and neglected the pressure loss along the supply air duct. The network model is further developed in this study by incorporating 'Fluid flow rate and pressure calculation' model developed by Zhu (1993). Therefore the 'realistic' system network is described. The effect of air velocity and wind effect on the system pressure-flow balance is neglected.

The flow resistances of the AHU filter and cooling coil are considered to be constant. The constant flow resistance before VAV pressure sensor represents the resistance of the air attenuator and duct before the sensor. The resistance of the air duct after the VAV pressure sensor is considered to be constant as well. The resistances of VAV terminals and diffusers are variables, which depend on the positions of the VAV dampers. The pressure in the entire occupied space is considered to be uniform when simulating the system pressure-flow balance. The air leakage through the building envelope is computed by assuming that a constant flow resistance links the occupied space to outside. The flow resistance of return duct is considered to be constant. The resistances of the outdoor air, recycle air and exhaust air dampers

vary according to the positions of the dampers. The flow resistance of an individual damper at certain damper position is calculated using Legg's exponential correlation.

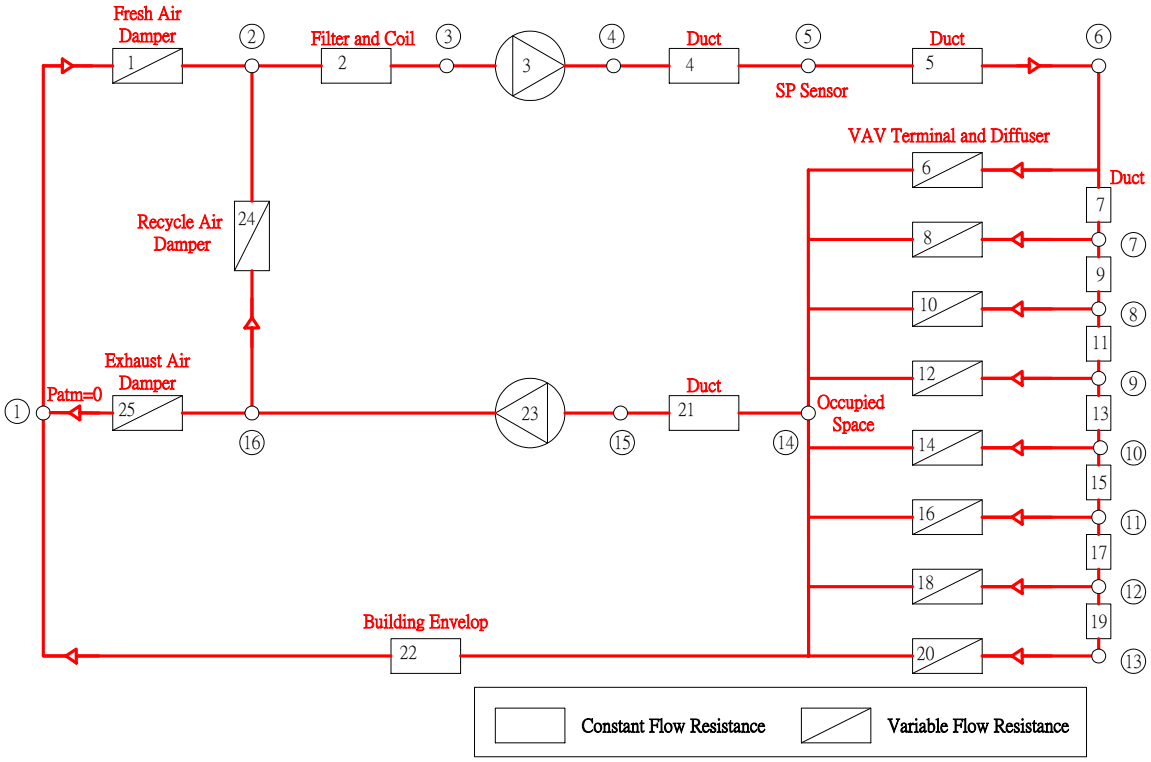

Figure 5.2 Schematic of system pressure-flow balance model

The system network model was designed for simulating the flow rate and pressure balance of a closed fluid network. Reference pressure is specified for calculating pressure of each node. The relationship of branches and nodes are specified as parameters. The flow resistance, fan/pump work characteristic and altitude difference of all branches are used as inputs to determine the flow rate and pressure distribution in the network.

Before a network is described by the model, a scheme of the network is necessary (Figure 5.2). In the scheme, the network is composed of branches with assumed flow directions and nodes. All of the branches and nodes are assigned order numbers, and both of the number series must be continuous and start from 1. Node 1 (atmospheric

pressure, which is assigned 0.0) is regarded as a reference node for pressure calculation. All of the pressures of other nodes would be the relative pressure to Node 1.

The mathematical basis of the model is that the incoming and outgoing flow of each node should be balanced and the total pressure variation along each circuit should be zero:

$$A\,G = 0 \tag{5.22}$$

$$B\,\Delta P = 0 \tag{5.23}$$

$$\Delta P_i = S_i G_i |G_i| - H_i + \Delta Z_i \tag{5.24}$$

N: number of branches

M: number of nodes

A: network relationship matrix (for nodes)

a_{ij} = 1: *j*th branch is connected to and comes from the *i*th node;

a_{ij} = -1: *j*th branch is connected to and goes to *i*th node;

a_{ij} = 0: *j*th branch is unrelated to *i*th node,

$1 \leqq i \leqq$ M-1, $1 \leqq j \leqq$ N.

B: basic circuit matrix (for circuits)

b_{ij} = 1: *j*th branch is in *i*th circuit and in the same direction;

b_{ij} = -1: *j*th branch is in *i*th circuit and in the reverse direction;

b_{ij} = 0: *j*th branch is unrelated to *i*th circuit;

$1 \leqq i \leqq$ M-1, $1 \leqq j \leqq$ N.

S: vector of resistance coefficient (S_1, S_2, … , S_n)

G: vector of flow rate (G_1, G_2, … , G_n)

H: vector of pressure increments caused by fan in the branch (H_1, H_2, … , H_n)

ΔZ: vector of pressure difference caused by altitude difference in the branch (ΔZ_1, ΔZ_2, … , ΔZ_n)

ΔP: vector of pressure difference in the branch (ΔP_1, ΔP_2, … , ΔP_n)

In order to decrease the scale of the network as much as possible, a flow resistance criterion for blocked branch is specified as a parameter. When the resistance coefficient of a branch is higher than this criterion, the branch is considered as blocked and is deleted from the network as well as the flow rate is set zero. This criterion can be set very high if the user wouldn't like to consider the state of blocking.

Providing the resistance of the system components, ducts, dampers and the delivery static pressure head of two fans, the system network model computes the flow rates and pressure at different locations of the system using Newton iteration. The Fortran program for the model is shown in Appendix A (Type57.for).

5.1.3 Supervisory Control Strategies

Local DDC Controls

The supply air temperature controller controls the air temperature at the outlet of the AHU coil by moderating the chilled water flow rate through the coil. The static pressure controller maintains the static pressure at the VAV supply duct at its set-point by moderating the fan pitch angle of the VAV supply fan. The exfiltration flow controller controls the difference between the total supply and return airflow rates in order to maintain a positive pressure in the building by moderating the pitch angle of

the return fan. The outdoor air controller controls the outdoor airflow by moderating the dampers. The zone space temperature control employs the pressure independent VAV terminal.

In order to minimize energy consumption but maintain acceptable IEQ, some common optimal control strategies could be adopted to optimize the performance of the VAV system.

Optimal outdoor air flow control

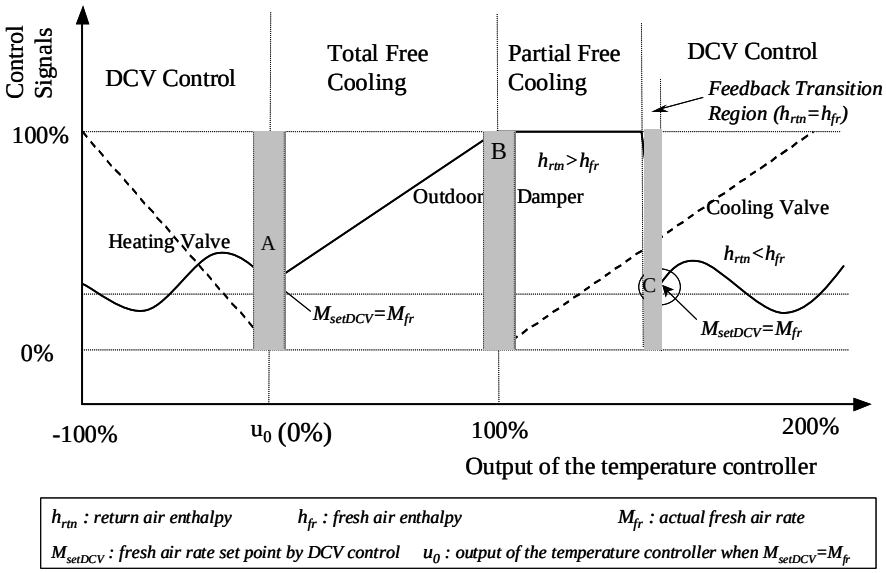

Figure 5.3 Illustration of the split-range sequencing control strategy combining DCV and economizer

The outdoor air ventilation affects both energy consumption of the VAV system and indoor air quality. The change of outdoor air ventilation flow often (but not always) results in two contrary effects on the energy consumption and indoor air quality. The optimization of outdoor airflow control is achieved by making a compromise between two control strategies, i.e. combining the enthalpy control and the occupancy-based demand control ventilation (DCV) (Wang and Jin 1998). The

outdoor air flow set-point determined by an occupancy-based demanded ventilation control strategy is used to be the low limit for outdoor air control only. The enthalpy control strategy determines an optimal outdoor air flow set-point based on the enthalpy values of outdoor air and return, total supply air flow rate and AHU supply air temperature set-point. The enthalpy control strategy aims at minimizing the coil consumption. The robust split-range sequencing control strategy combing the DCV control and the economizer was developed by Wang and Xu (2002), as shown in Figure 5.3.

On-line optimal reset of static pressure set-point

The supply fan energy consumption is minimized by minimizing the static pressure. In order to supply sufficient air to every individual zone as well as to minimize the static pressure, the static pressure is controlled to be enough and just enough for the most heavily loaded zones. The local DDC control demands can be conveniently collected from the BMS stations. The static pressure is adjusted just allowing that the VAV dampers with the highest relative cooling load among all the VAV terminals is controlled to be very close to fully open position any time, in order to ensure that all the individual zones are supplied with sufficient air and the static pressure is controlled at its lowest allowed level.

The air flow rate to a zone is reduced by closing down the VAV dampers when the load of a zone is low. Under low partial load, the total ventilation flow rate of a zone may be reduced to be very low in order to meet the reduced load. The reduction in total ventilation flow rate results in significant saving on fan power. On the other hand, a low ventilation flow rate may cause deficiencies of system performance, e.g. poor mixing of supply air and room air, inadequate room ambient air circulation and

dumping. When a minimum limit of the total ventilation flow rate is used, a space may be overcooled under low partial load if the supply air temperature is low.

AHU supply air temperature set-point reset

The proper resetting of the supply air temperature allows the VAV system to avoid the poor ventilation and save as much fan power as possible. The supply air temperature reset strategy utilizes the air flow rate set-points of the pressure independent VAV terminals as the cooling load indicators of individual zones. The minimum flow set-point is set to avoid performance deficiency in individual zones, which may have different values for different zones and needs to be selected and tuned according to actual design and situation of individual zones. The upper flow rate set-point is a parameter used only for calculating the relative load of a zone. Since different zones may have very different flow ranges, the rate of the flow set-point of each zone is normalized using the ratios of the set-point to the minimum flow set-point and upper flow set-point, respectively.

The maximum ratio to upper flow set-point among zones is selected as the indicator of the relative load of zone with most critical thermal load. The minimum ratio to minimum flow set-point among zones indicates most critical zone in terms of ventilation. If the minimum ratio indicates the flow in certain zone is too low, the supply air temperature set-point needs to be increased. On the contrary, if the maximum ratio indicates the load of a certain zone is high, the supply air temperature set-point needs to be reduced. The change rate limit is applied to the temperature set-point to ensure the stability of system control. The local and supervisory control systems are illustrated in Figure 5.4.

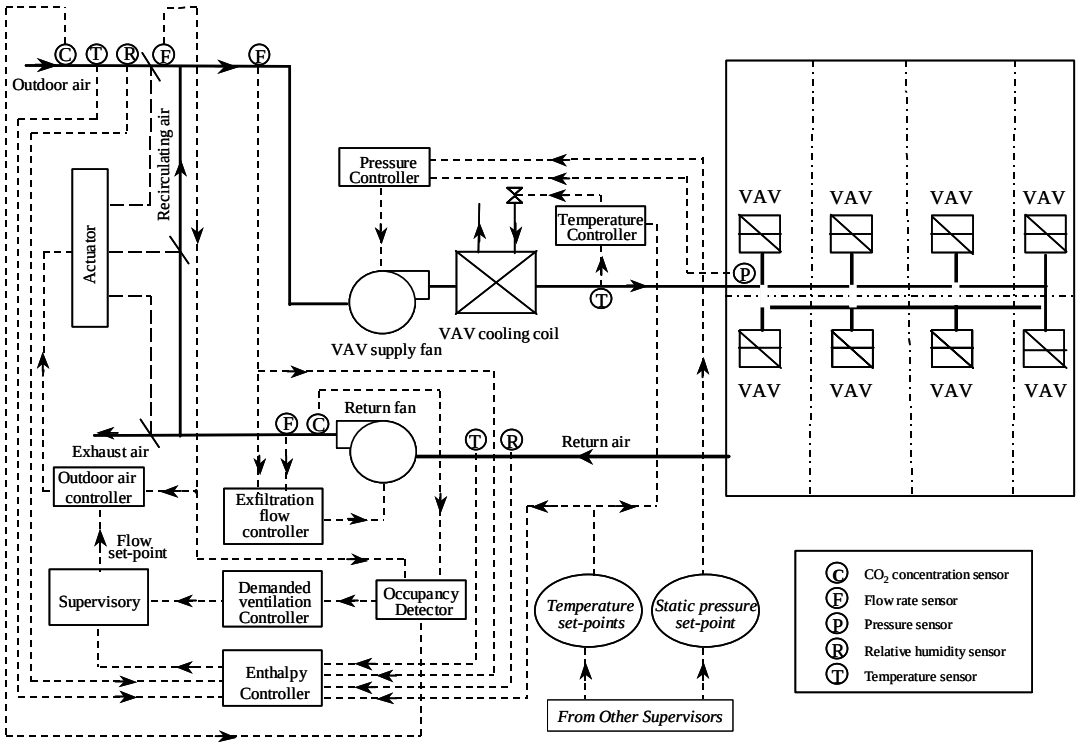

Figure 5.4 Illustration of the simulated VAV air conditioning system with its local and supervisory control systems

5.1.4 Dynamic Simulator

The dynamic simulator, which simulates one AHU/VAV system and their associated buildings, is developed using TRNSYS (Transient System Simulation Program [Klein et al. 1990]) as the simulation platform. TRNSYS is a transient system simulation program with a modular structure. It allows one to perform detailed simulations of multi-zone buildings and their equipment, as well as thermal systems in general. The modular nature of TRNSYS gives the program tremendous flexibility, and facilitates the addition to the program of mathematical models not included in the standard TRNSYS library. The above-mentioned models are added using FORTRAN. The TRNSYS "deck" integrates the models and sets up the simulation projects.

Figure 5.5 shows a schematic of the major interconnection between the component models (information flow diagram) for the system simulation. The component

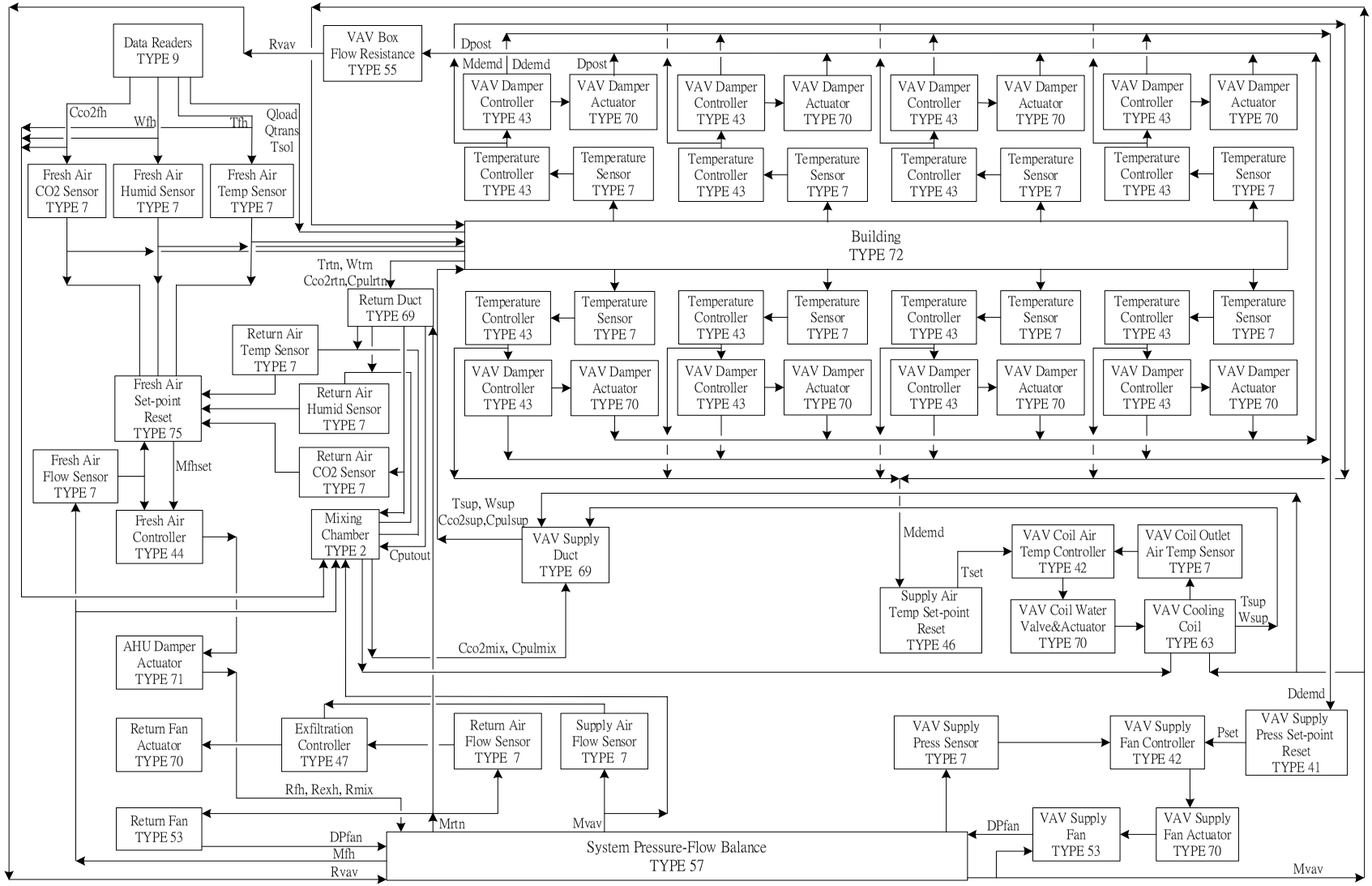

Figure 5.5 Illustration of TRNSYS simulation deck of VAV air-conditioning and control system

integration for pressure-flow balance, thermal balance, moisture and pollutant balance computation as well as the temperature control, pressure control, flow control and supervisory control are illustrated.

The occupancy, lighting and equipment loads in each zone, the solar gain of each zone transmitted through the windows, ‘sol-air’ temperature of each zone, the outdoor air temperature, humidity and CO_2 concentration are provided by data files during simulation as test conditions. The transmission solar gain and equivalent ‘sol-air’ temperature are computed by a pre-processor prior to simulation according to building construction data, the solar radiation and outdoor air temperature recorded in the selected days.

5.2 VAV Systems in Real Buildings

5.2.1 Building A

Figure 5.6 BMS workstation

The building, which was re-commissioned in 2002 as stated in Chapter 2, was chosen as one test building of the second test facility. The HVAC systems in the building are fully supported by the BMS. Figure 5.6 shows the BMS workstation.

The full set of operation data for all VAV boxes in the building were recorded during the re-commissioning exercise. The database itself could provide some in-situ data for the validation of some FDD schemes. Besides, the physical systems offer the testing field for some in-situ tests.

5.2.2 Building B

The second test building is another high-rise commercial building. The building (Figure 5.7) is located at Hong Kong Island East with a gross area of more than 70,000 m^2. It is cladded with high-performance, double-glazed, solar reflective, heat absorbing panels set in anodized aluminum frames with vertical mullions at 1.5m intervals.

Figure 5.7 Commercial building

A computer-based, automated BMS monitors and supervises all the building HVAC, fire, lift and safety systems. The BMS also controls lighting in public areas and adjusts air-conditioning temperatures to ensure environmental comfort and safety at all times while maintaining energy efficiency. The building is provided with both a dedicated 24-hour chilled water supply. Air-handling units assisted by a DDC/VAV system provide ventilation, cooling or heating to the office area. Two AHUs sever one typical floor. The set-point of the indoor air temperature can be adjusted via the BMS.

Unlike building A, the VAV systems in this building are pressure-dependent type. The damper openness signal is available and could be logged by the BMS automatically. The supervisory control of VAV static pressure reset is also implemented in the VAV systems. Most of the VAV systems are in operation for 5.5 days per week and around 12 hours per day. The AHU turn-on schedules are determined by the outdoor temperature to optimize the morning pull-down period.

5.3 Summary

This chapter briefly introduced two test facilities. They are the simulated VAV system and the VAV systems in real buildings. Both test facilities will be used to validate the FDD schemes and therefore the FDD strategy developed in this thesis.

The dynamic simulator can simulates the thermal, environmental, mechanical characteristics and energy performance dynamically of the system using the component-based dynamic simulation program, TRNSYS. A system network model

was developed based on hydraulic balance to deal with the network problems. Therefore the realistic VAV air distribution system could be simulated under different supervisory controls.

The real systems provide the realistic test platforms for strategy validation. Both BMS trend data and in-situ tests could be achieved with this test facility.

CHAPTER 6 VALIDATION OF FDD STRATEGY FOR HARD FAULTS

The FDD strategy developed in this study is validated on two test facilities, i.e. VAV systems in a dynamic simulator and in real buildings respectively. On both test facilities, the validation tests of FDD strategy for VAV hard faults (Scheme 1-7) are conducted with multiple hard faults introduced into the systems. The robustness of the FDD schemes is analyzed.

Section 6.1 presents the validation tests for the strategy for the hard faults under a simulator with signal fault as well as different hard fault combinations. The robustness of the FDD strategy is verified. Section 6.2 validates the FDD schemes and then the strategy using both the retrieved BMS data and in-situ tests in a real building. A summary of this chapter is given in section 6.3.

6.1 Validation Using Simulation Tests

Dynamic simulation of VAV systems provides a convenient and low cost tool in testing, commissioning and evaluating VAV system supervisory control and FDD strategies. Simulation tests in the FDD research have great importance. Many faults are not allowed to be introduced to a real process because they may disturb the process, and even damage machines and injure humans. However, those faults could be introduced to simulation tests and their effects could be observed. The FDD

strategy for hard faults were tested and validated using simulation tests before using real site data or experiment data.

6.1.1 Test Conditions

A dynamic simulator of a typical VAV system was described in Chapter 5. Dynamic simulation of the system is used to generate data for the validation of the FDD strategy. Both single fault and multiple faults were introduced into the simulation deck to generate the data set for single FDD scheme validation and FDD strategy validation.

The daily operation of the simulated air-conditioning system was from 07:45 to 20:00. The temperature of the chilled water through the cooling coil was a constant, i.e. 8^{o}C. The set-point of the supply air temperature was 13^{o}C and the set-point of the static pressure was 650Pa. The simulation time step was 1 second and the sampling interval was chosen to be suitable for FDD scheme validation. The weather data of one day in summer was selected as the simulation conditions, which were prepared in a data file. Operation data in this day with different faults were used for strategy validation.

6.1.2 Tests on Single Fault for FDD Scheme Validation

Scheme 1 – Fault 1 (Poor tuning of static pressure control loop)

Fault 1 (poor tuning of static pressure control) was introduced by resetting the proportional gain of the fan controller to much higher (100 times the original setting). Fault 1 is detected by the SPC model for counting excessive consecutive reversals of the filtered static pressure around its set-point over a preset period. This faulty pattern was also verified using laboratory tests by Seem et al. (1999).

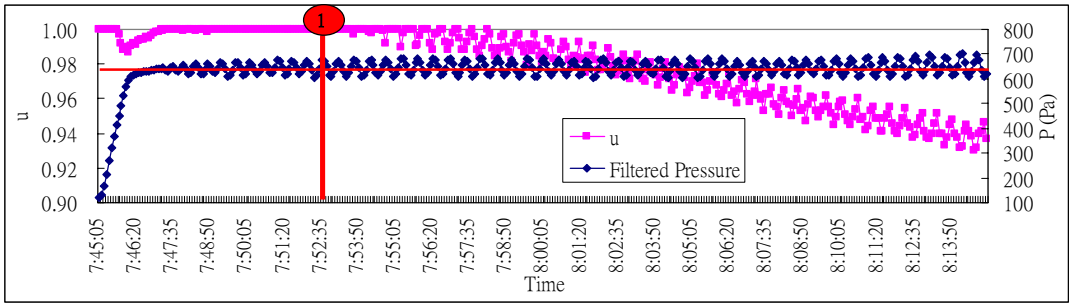

Figure 6.1 Static pressure oscillation

Figure 6.1 demonstrates the simulation results at 5-second intervals. Fault 1 is detected after counting 20 consecutive reversals of the pressure (under transient state). Figure 6.1 also shows that the duty cycle of a VAV terminal increased. It is forecasted that actuators of the VAV terminals are likely to fail prematurely due to excessive movement.

Fault detection for the fan control to maintain the proper static pressure is independent. Other faults included in this study would not affect the characteristic equations employed in Scheme 1.

Scheme 2 – Fault 2 (Zone temperature sensor reading frozen)

The simulation test was carried out by fixing the temperature sensor output of Zone 6 at 24 ^{o}C and the simulation results logged at 5-minute intervals are presented in Figure 6.2. Fault 2 (Zone Temperature Sensor Reading Frozen) could be detected under Scheme 2 by the qualitative state and the SPC models based on the CUCUM method over a pre-set period. Figure 6.2 presents the fixed flow set point and the fixed zone temperature. The fault could be detected after 5 hours.

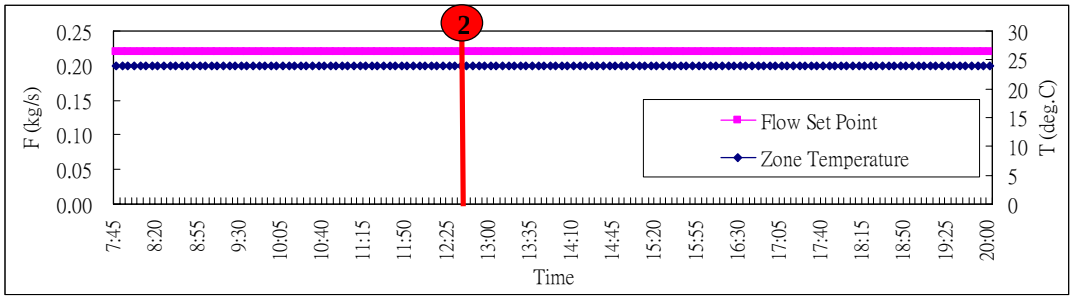

Figure 6.2 Zone temperature reading frozen

Scheme 3 – Fault 3 (VAV controller hard failure)

VAV controller hard failure was introduced into VAV terminal 6 in the simulation tests. In the first test, the flow controller output (μ) was fixed at the minimum. Fault 3 of VAV controller hard failure was detected by the characteristic equation (Equation 3.16) under Scheme 3 after the preset period (30 mins). Figure 6.3 presents the simulation results of the test.

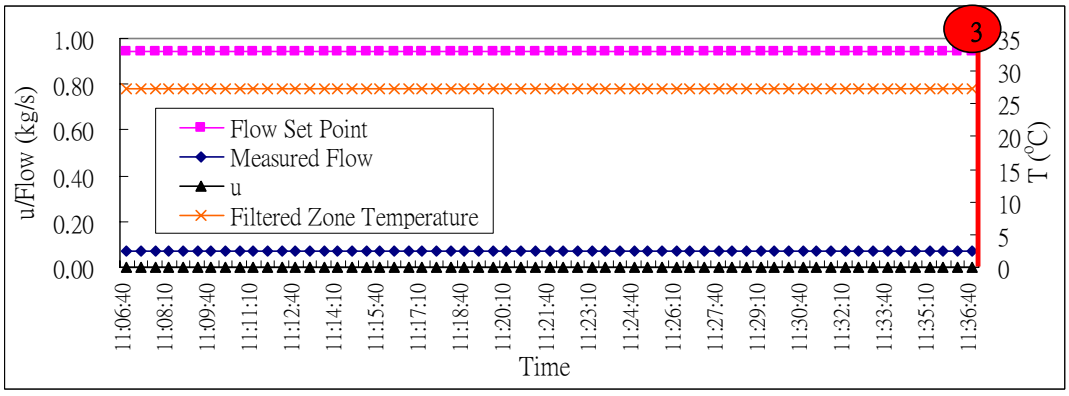

Figure 6.3 Flow controller hard fault

In the second test, the temperature controller output (the flow set point) was fixed at the minimum. Fault 3 of VAV controller hard failure was detected by the characteristic equation (Equation 3.18) under Scheme 3 after the preset period (30 mins). Figure 6.4 presents the simulation results of the test.

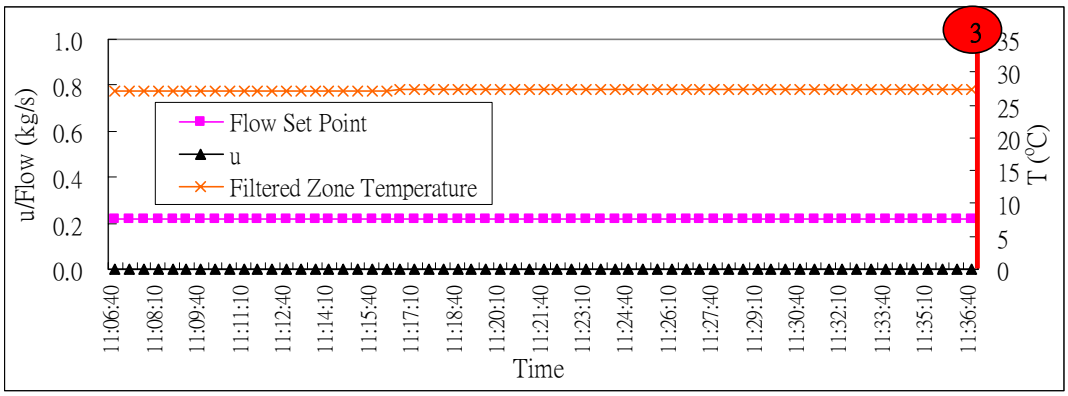

Figure 6.4 Temperature controller hard fault

Scheme 4 – Fault 4/5 (VAV terminal under or over capacity / VAV damper stuck)

By setting VAV Terminal 6 damper stuck at 50% openness (T_{set}=24°C), simulation test was conducted to verify the scheme (Scheme 4) when Fault 5 was involved. Fault 4 or 5 was detected after half an hour operation while the qualitative state for the fault was satisfied. The faulty pattern is presented at 5-minute intervals in Figure 6.5.

Similarly, Figure 6.6 presents the faulty pattern of VAV Terminal 6 under capacity by setting the zone temperature set-point at 20°C. Fault was detected after half an hour operation.

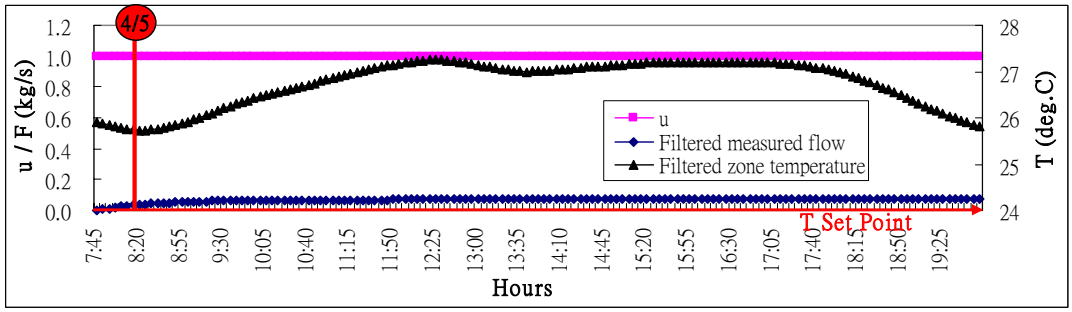

Figure 6.5 VAV terminal damper stuck

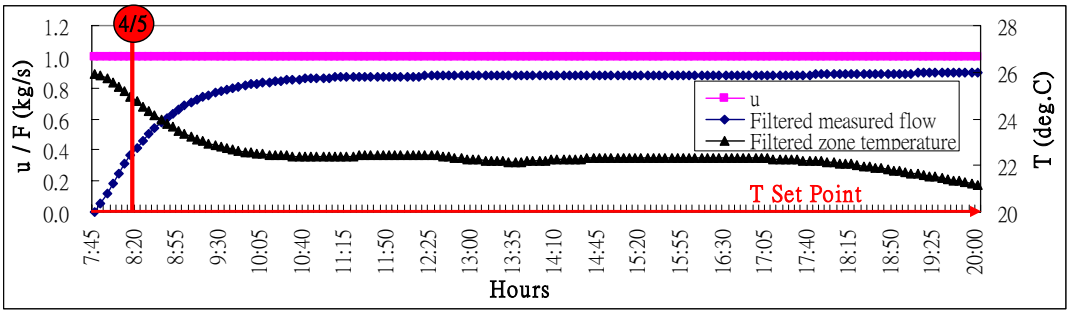

Figure 6.6 VAV terminal under capacity

As explained in Chapter 3, the differentiation of Fault 4 and 5 is not included in the automatic FDD strategy. The hardware failure of damper stuck (mechanically stuck or actuator failure) and terminal under/over capacity are recommended to be identified manually.

Scheme 5 – Fault 6 (VAV flow sensor reading frozen)

Another group of tests were carried out by fixing the flow rate reading of VAV Terminal 6. The fault of frozen sensor reading at 0.5 kg/s was chosen for the simulation result demonstration in Figure 6.7 with the flow set-point presented.

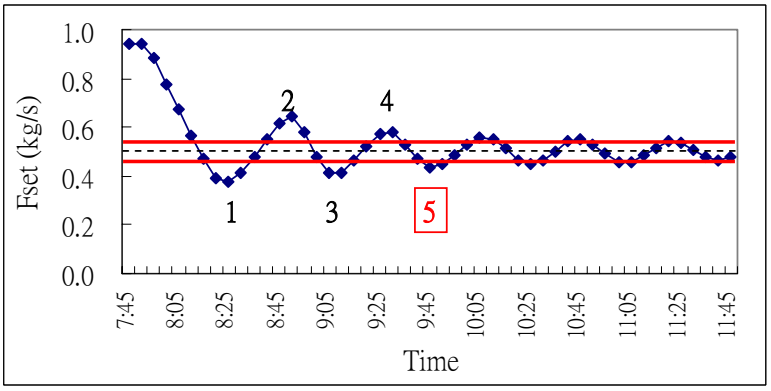

Figure 6.7 VAV flow sensor reading frozen at 0.5 kg/s

Under Scheme 5, when it was confirmed that the measured flow conformed to the qualitative state (Equation 3.23-3.25), the SPC models for flow reading frozen and

flow set-point reversal counting were used for fault detection. Fault 6 was detected when the counted number of the flow set-point reversal ($R_{F,set}$) within a preset period (t_{delt}) was over 4 while the flow reading was detected frozen using the CUSUM SPC model (Equation 3.26). It is demonstrated in Figure 6.7 that Fault 6 was detected when the SPC model counted 5 reversals.

Scheme 6 – Fault 7 (VAV flow sensor reading deviation to minimum/maximum)

Scheme 6 detects Fault 7 by the characteristic equations as shown in Equation 3.27 and Equation 3.28. Two simulation tests were devised by setting the measured flow of Terminal 6 at the minimum (0.22 kg/s) and at the maximum (0.94 kg/s) respectively. The simulation results are presented in Figure 6.8 and Figure 6.9.

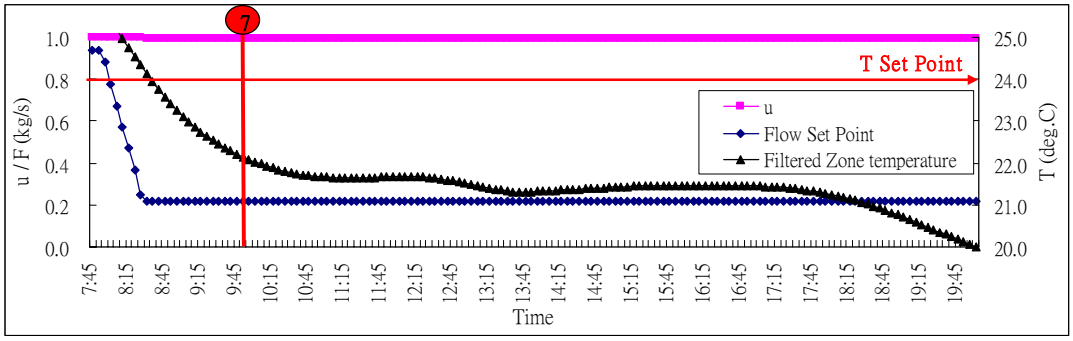

Figure 6.8 VAV flow sensor reading fixed at the minimum

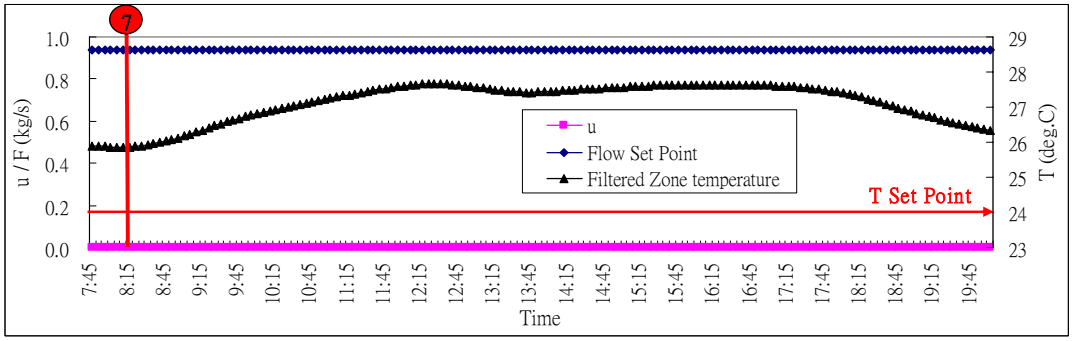

Figure 6.9 VAV flow sensor reading fixed at the maximum

In Figure 6.8, Fault 7 was detected after half an hour as from the system calculated more than 1.5 ^{o}C temperature error under the conditions of $\mu=\mu_{max}$ and $F_{set}=F_{min}$. In Figure 6.9, Fault 7 was detected after half an hour as from the system calculated more than 1.5 ^{o}C temperature error under the conditions of $\mu=\mu_{min}$ and $F_{set}=F_{max}$.

Scheme 7 – Fault 8/9/10 (Poor tuning of VAV controllers / VAV damper sticking / VAV damper hysteresis)

Again, simulation exercises were carried out to verify Scheme 7. Tests on the faulty performance were conducted by adjusting the controllers, adding damper sticking and damper hysteresis errors of VAV Terminal 6 respectively. The data were collected every two seconds as sampling frequency is an important issue when trying to unravel the true behavior of an unstable control loop (House et al. 2003). As the real system with forty VAV boxes was simulated by an eight-terminal-system, the dominant time constants of the simulated system are different from the actual ones. Therefore, the limit values of common VAV terminals are not applicable to these simulation exercises. The air flow controller maximum permissive time (t_{delt}) of the simulation case was set at five times the limit of normal settling time (*2min X 5 = 10min*) and the threshold of air flow rate control (F_{th}) was chosen as 0.05 kg/s.

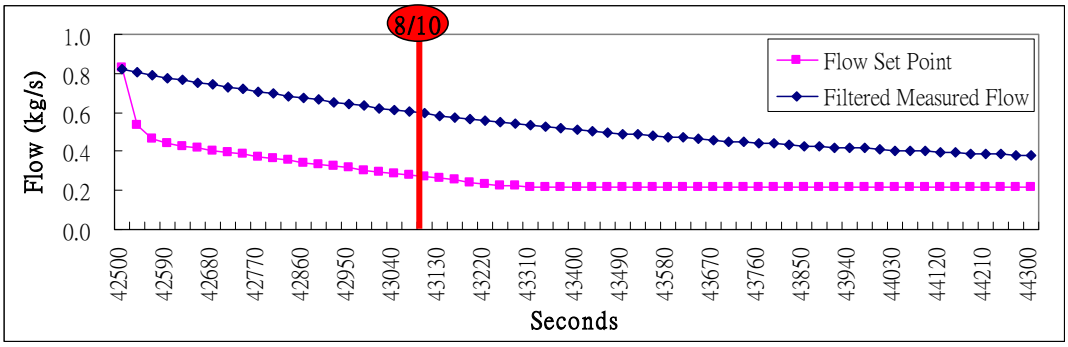

Figure 6.10 Flow sluggish response

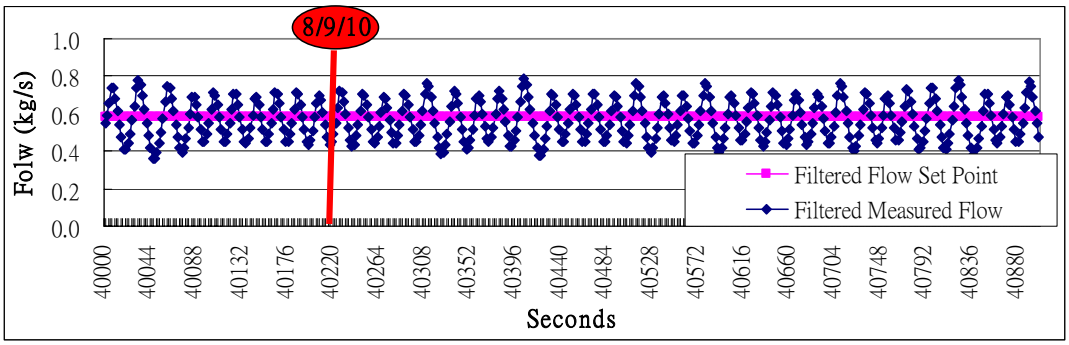

Figure 6.11 Flow oscillation

Two tests were conducted to verify Scheme 7 when Terminal 6 flow control faults exist, which were introduced by using too small and too large proportional gains for the flow controller respectively. Figure 6.10 shows the simulation results of flow controller sluggish response. Fault was detected since the measured flow could not reach the flow set-point within the time limit (10 mins). Figure 6.11 indicates the simulation results of flow oscillation. After counting 20 consecutive reversals of the measured flow by the SPC model, the alarm of Fault 8/9/10 was generated.

Another group of tests were conducted when Terminal 6 temperature control faults exist, which were introduced by using too small proportional gain and too small integral time for the temperature controller respectively. Figure 6.12 shows the simulation results of temperature controller sluggish response. Fault was detected since the zone temperature could not reach the set-point within the time limit (30 mins). Figure 6.13 indicates the simulation results of flow set-point oscillation due to improper temperature controller setting. After counting 15 consecutive reversals of the flow set-point within half an hour by the SPC model, the alarm of Fault 8 was generated.

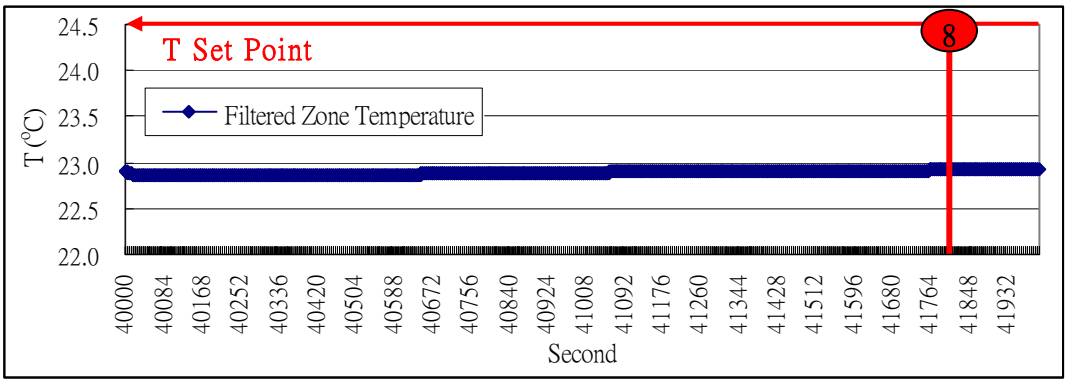

Figure 6.12 Temperature sluggish response

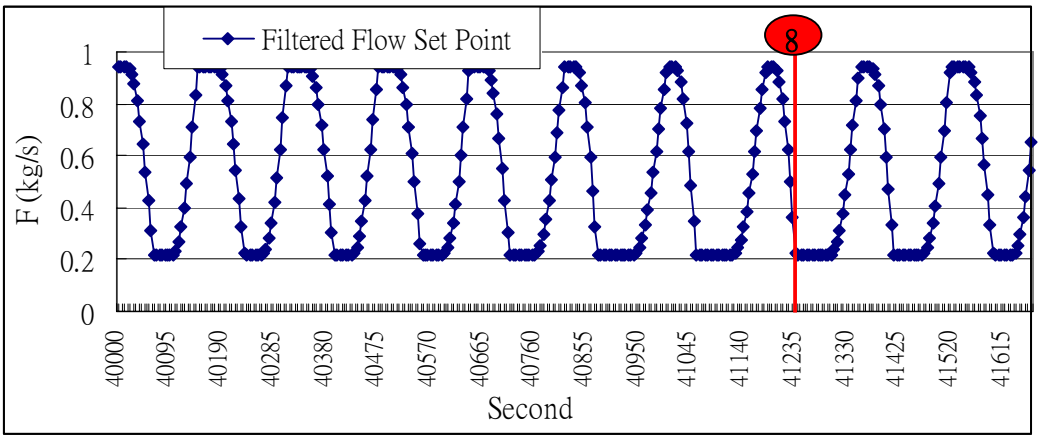

Figure 6.13 Flow set-point oscillation

However, the existence of Fault 1-7 would affect the FDD ability of Scheme 7 as mentioned in Chapter 3. The fault(s) could only be detected when the Scheme receives the fault free signal from Scheme 1-6.

Damper sticking or hysteresis would cause oscillation or sluggish response as the faulty flow controller caused. To distinguish the mechanical faults from the poor flow controller setting, pattern recognition indices are proposed in Chapter 3 (Equation 3.31 and Equation 3.32) to characterize the different response patterns.

To test on the fault identification ability of the proposed recognition indices, simulation exercises were designed by adjust the hysteresis and sticking parameter of

Terminal 6's actuator model to add the fault of damper hysteresis and sticking respectively.

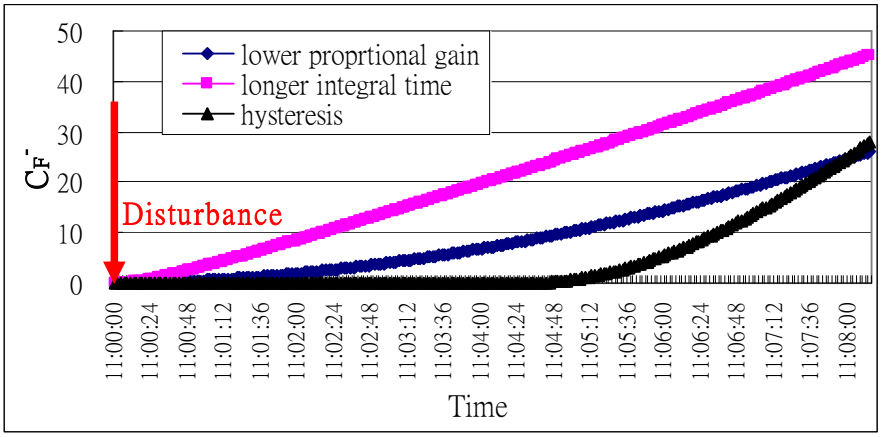

Figure 6.14 Pattern recognition index for sluggish response

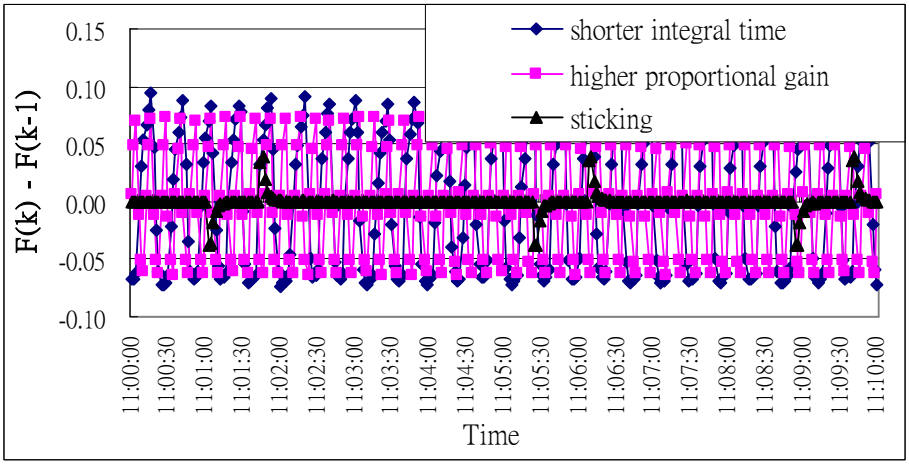

Figure 6.15 Pattern recognition index for oscillation

The pattern recognition index, $C_{\bar{F}}^{-}$, for sluggish response and the pattern recognition index, ($\bar{F}_k - \bar{F}_{k-1}$), for oscillation to characterize the patterns of poor controller tuning, hysteresis and sticking are shown in Figure 6.14 and Figure 6.15 respectively. At the beginning of the sluggish response tests, Zone 6 temperature set-point was adjusted from 24°C to 21°C. As presented in Figure 6.14, the $C_{\bar{F}}^{-}$ kept

almost unchanged for a certain period then deviated when the root cause of the sluggish response was damper hysteresis. The oscillation caused by damper sticking was distinguished from controller poor tuning based on the dominated zeroes ($\overline{F}_k - \overline{F}_{k-1} \approx 0$) of the pattern recognition index as indicated in Figure 6.15.

6.1.3 Tests on Multiple Faults for FDD Strategy Validation

The above simulation tests validated the individual FDD schemes (Scheme 1-7) for hard faults detection. However, as described in Chapter 3, the existence of multiple faults will affect the fault detection results of some FDD schemes. The interaction amongst the faults were carefully studied when developing the strategy and the problem was solved by considering the seven schemes simultaneously with the essential exchange of the FDD output as shown in Figure 3.8.

FDD Scheme 1, 2, 5 and 6 are independent as their fault detection results would not be affected by the existence of multiple faults. Different combinations of multiple faults were introduced into the simulation deck to generate the test data to evaluate the independence of those schemes.

The simulation tests with Fault 1 by resetting the proportional gain of the fan controller to much higher (100 times the original setting) and different combination of other hard faults were carried out. The simulation results showed that those other faults included in this study did not affect the characteristic equations employed in Scheme 1 and Fault 1 was detected by the same faulty pattern of single fault as shown in Figure 6.1. The simulation tests with zone temperature sensor fault (fixed at 24 ^{o}C) (Fault 2) and other hard faults were carried out as well. The robustness of fault detection ability of Scheme 2 for Fault 2 was verified by the same simulation results with or without other faults (Figure 6.2). Similarly, the independence of Scheme 5 and

Scheme 6 were testified by the simulation data with different combinations of hard faults.

Under Scheme 3 and Scheme 4, zone temperature is a key parameter for fault detection. The existence of Fault 2 would give the counterfeit fault detection results of both Scheme 3 and Scheme 4. However, the existence of other faults would not affect these two schemes. The simulation tests of multiple hard faults except Fault 2 validated the both schemes. As the pattern of Fault 3 is self-explanatory, in-situ tests for Scheme 3 is omitted.

The existence of Fault 1-7 would affect the FDD ability of Scheme 7 as mentioned in Chapter 3. The fault(s) could only be detected when the Scheme receives the fault free signal from Scheme 1-6. The scheme's FDD ability for single fault has been validated before.

The above validation tests with different groups of simulation data verified the FDD ability of the developed FDD strategy for the hard faults. The strategy's FDD ability for the soft fault (VAV flow sensor biases) is achieved by PCA-based flow sensor FDD scheme (Scheme 8) at the second step, which will be validated in the next chapter.

6.2 Validation Using In-situ Tests

6.2.1 Test Conditions

The other test facility is the real VAV systems in Building A as described in Chapter 5. The in-situ validation was conducted based on some VAV faulty

performance recorded on the site investigation during the re-commissioning exercise and the particular FDD tests in the same building.

In-situ tests were also carried out in the building by introducing faults into the real system in the vacant area. The FDD schemes are validated by the tests in the real building as well.

6.2.2 Tests on Existing Faults

According to the performance pattern of the VAV Terminal 35 at the 31st floor, the zone temperature sensor frozen (Fault 2) could be detected by the SPC models after 5 hours by Scheme 2. Figure 6.16 demonstrates the performance pattern of the VAV terminal, where the zone temperature sensor frozen (Fault 2) was confirmed on site. The FDD ability of Scheme 2 was verified.

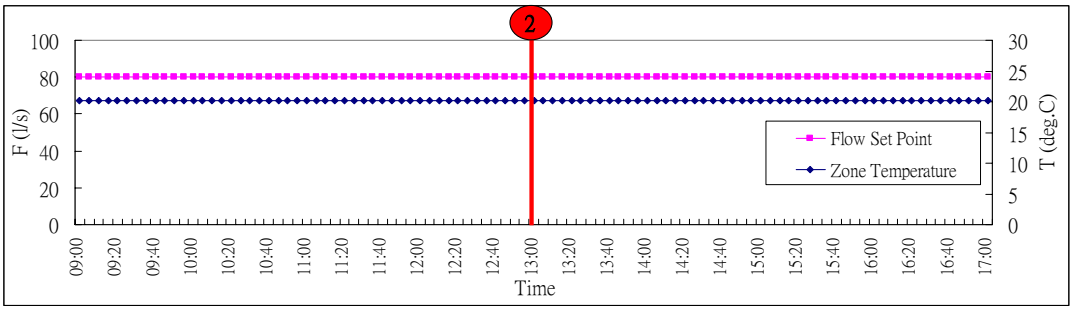

Figure 6.16 Zone temperature reading frozen

According to the site investigation, Fault 4 and Fault 5 were common. However, the database obtained during the site investigation did not give the full data set of the FDD scheme (Scheme 4) required as the control signal μ was not logged. Since μ cannot be logged by the existing BMS in this building, an in-situ test on damper stuck (Fault 5) was carried out on a stuck VAV damper (VAV Terminal 2 at the 38th floor) by manual recording the damper control signal (0-10V DC) using a portable digital voltage meter.

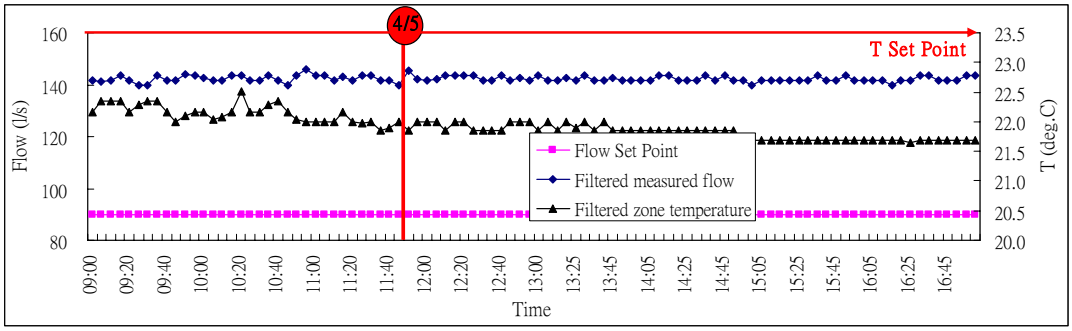

Figure 6.17 VAV terminal damper stuck

Figure 6.17 explains the faulty performance (T_{set} = 23.5°C) of VAV terminal 2 at the 38th floor with a confirmed fault of damper stuck. The damper control signal (μ) recorded by the portable digital voltage meter was fixed at the minimum. The scheme detected the fault after analyzing 30 minutes data record by the qualitative state.

It was observed that VAV flow sensor reading fixed at minimum/maximum (Fault 7) happened on many of the 33 VAV terminals at the 26th floor after roughly checking on the BMS logged data. The manual measurement on damper control signal, μ, of five suspected VAV terminals were conducted besides BMS data logging of the other variables required by the Scheme 6. Using the data record, the scheme successfully diagnosed the sensor faults (fixed at minimum/maximum) which were further confirmed by manual checking.

Figure 6.18 shows a sample of the fault by demonstrating the trend data of VAV Terminal 32 (F_{max} = 250 l/s, T_{set}=20°C). The damper control signal measured by the portable digital meter was fixed at the minimum. The fault was detected by Scheme 6 after half an hour.

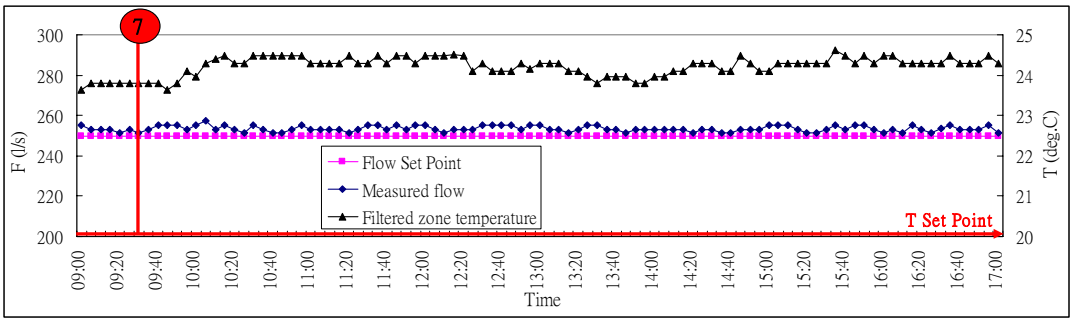

Figure 6.18 VAV flow sensor reading fixed at the maximum

6.2.3 Tests on Physically Introduced Faults

For VAV flow sensor reading frozen (Fault 6), the in-situ test was carried out by replacing the flow sensor signal of VAV Terminal 30 at the 18th floor with an emulated control signal of 4V DC, which represented 200l/s of the reading. Under the temperature set-point of 21.5°C, the trend data of the flow set-point were recorded at 1-minute intervals for an hour afterwards. The FDD scheme (Scheme 5) detected the fault after counting five consecutive reversals of the filtered flow set-point as shown in Figure 6.19.

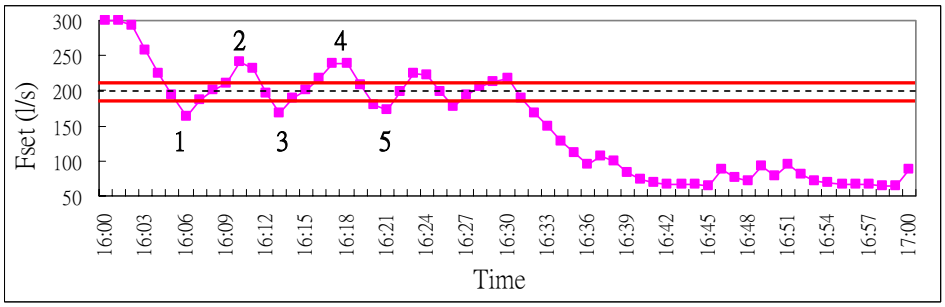

Figure 6.19 VAV flow sensor reading frozen at 200 l/s

To verify Scheme 7, the controllers of a VAV terminal at the 18th floor were studied. The settings of the temperature controller of the terminals were built in, which could not be adjusted without a password. Thus the in-situ tests were focused on the terminal flow control by resetting the proportional gain and the integral time of

Johnson Controls' PI flow control. The existing BMS could not log the data at intervals shorter than 1 minute, which means that the logged measurements could not reflect the full-scale faulty patterns as some essential data between two samples were missing from the records.

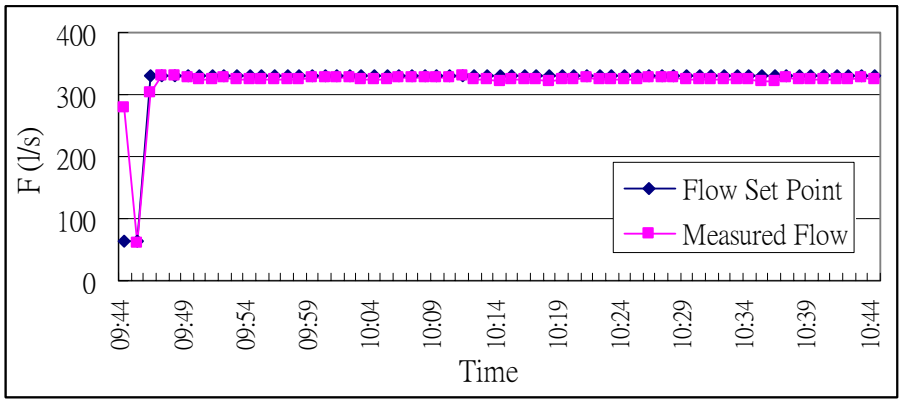

Figure 6.20 Flow sluggish response

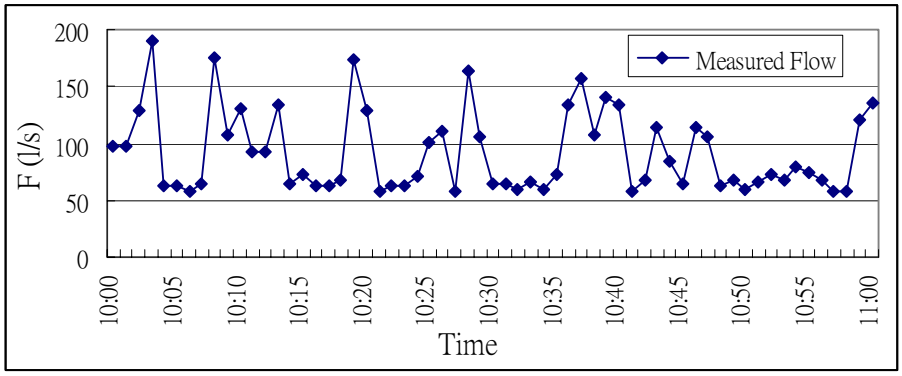

Figure 6.21 Flow oscillation

Figure 6.20 shows the test results of sluggish response which was introduced by resetting the zone temperature set-point from 21°C to 18.5°C and resetting the proportional gain from 5 to 0.1. The data were logged at 1-minute intervals as frequently as possible. Although the full-scale faulty pattern could not be presented, the sluggish response could be observed at the beginning of the test as shown in

Figure 6.20. Figure 6.21 demonstrates the test results of sluggish oscillation which was introduced by resetting the integral time from 5 to 0.1. The data were logged at 1-minute intervals also. The pattern of oscillation is obvious.

Two in-situ tests involving VAV damper mechanical faults (sticking and hysteresis) were conducted as well. The fault of damper sticking was introduced by mechanically tightening up the actuator mechanism of the same VAV terminal at the 18^{th} floor in the first test and the fault of hysteresis was introduced by slacking off the damper actuator connection of the VAV terminal in the second test. The temperature set-point was kept fixed (T_{set} = 21^{o}C) for the sticking test and was adjusted to 18.5^{o}C at the beginning of the hysteresis test respectively. The data trends of the flow set-point, the measured flow and the zone temperature were logged at 1-minute intervals for the both tests as the existing BMS could not log the trend more frequently. Nevertheless, the pattern of flow oscillation for sticking (Figure 6.22) and the pattern of flow sluggish response for hysteresis (Figure 6.23) were obvious. The logged flow measurements also showed that the flow measurement kept unchanged at the beginning of the hysteresis test and it was fixed most time during sticking test. The pattern recognition indexes for fault isolation among Fault 8, Fault 9 and Fault 10 were supported by the in-situ test results as well.

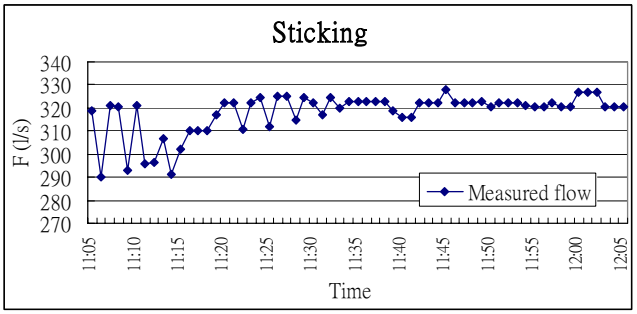

Figure 6.22 In-situ test results of damper sticking

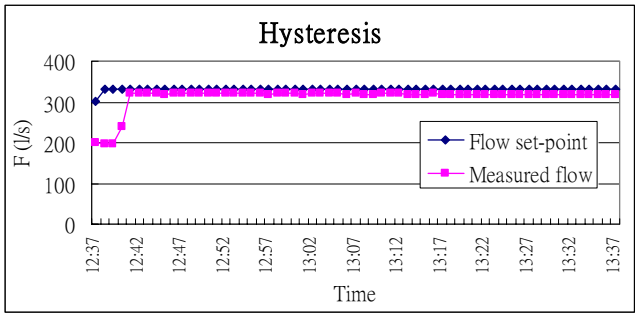

Figure 6.23 In-situ test results of damper hysteresis

The above sets of in-situ tests validated the FDD schemes for hard faults proposed in Chapter 3, which validated the FDD strategy for the hard faults. The validation of the FDD strategy for soft fault (VAV flow sensor biases) using PCA-based flow sensor FDD scheme (Scheme 8) will be explained in the next chapter.

6.3 Summary

Validation test results of the FDD strategy concerning hard faults are presented in this chapter using both simulation tests, BMS database recorded during site investigation of a real building and designed in-situ tests in the same building. By introducing different fault combinations into the tests, both FDD schemes (Scheme 1-7) and the interference between the schemes are verified. The FDD schemes designed within the frame of qualitative/quantitative reasoning demonstrated their effectiveness of FDD ability through the tests.

Considering the interaction among the FDD schemes, the FDD strategy should be carefully studied for real application. Fault 3 under Scheme 3 and Fault 4/5 under Scheme 4 could only be detected when Scheme 2 gives its ‘fault free’ signal. Similarly,

Fault 8/9/10 could only be detected by Scheme 7 when the strategy confirms that the system is free of Fault 1-7. Scheme 8 for terminal flow sensor bias would be put into operation when the system is free of Fault 1-10, which will be validated in the next chapter.

CHAPTER 7 VALIDATION OF PCA-BASED FLOW SENSOR FDD SCHEME

The VAV flow sensor bias FDD scheme based on the PCA method was validated using both simulation tests and site data retrieved from the BMS of a real building. The FDD strategy's ability for soft faults is therefore verified.

Various sensor faults are introduced into both the simulation tests and the in-situ tests. Section 7.1 presents the validation tests with both single fault and multiple faults. The robustness of the FDD scheme is analyzed in this section. Section 7.2 validates the FDD scheme using site data retrieved from the BMS of a real building. The sensitivity of this scheme is analyzed in this section. A summary of this chapter is given in section 7.3.

7.1 Validation Using Simulation Tests

The dynamic simulator of a typical VAV system was described in Chapter 5. Two categories of simulation tests were conducted to validate the sensor bias FDD scheme: normal operation without fault and operation under different sensor faults. The VAV flow sensor FDD scheme was used to monitor the air distribution process under different conditions to evaluate its robustness in sensor FDD.

7.1.1 Test Conditions

The daily operation of the simulated air-conditioning system was from 07:45 to 20:00. The simulation time step was 1 second and the sampling interval was chosen as 300 seconds (5 minutes) for FDD scheme validation. The temperature of the chilled water supplied to the cooling coil was a constant, i.e. 8^{o}C. The set-point of the supply air temperature was 13^{o}C and the static pressure was under the supervisory control of static pressure reset. The weather data of one day in summer was selected as the simulation conditions, which were prepared in a data file. Operation data in one day were used to construct the training matrixes of the PCA models at both system level and terminal level. Different sensor faults introduced into Terminal 6 and Terminal 4 were simulated to test the sensor bias FDD scheme.

Table 7.1 Proportion of variance explained

Principal Component	Eigenvalue	Variance (%)	Cumulative Variance (%)
1	11.73	69.00%	69.00%
2	4.052	23.83%	92.83%
3	0.8318	4.89%	97.72%
4	0.2544	1.50%	99.22%
5	0.0858	0.50%	99.73%
6	0.03118	0.18%	99.91%
7	0.00503	0.03%	99.94%
8	0.00335	0.02%	99.96%
9	0.00258	0.02%	99.97%
10	0.00135	0.01%	99.98%
11	0.00099	0.01%	99.99%
12	0.00065	0.00%	99.99%
13	0.00055	0.00%	99.99%
14	0.00042	0.00%	100.00%
15	0.00034	0.00%	100.00%
16	0.00014	0.00%	100.00%
17	0.000059	0.00%	100.00%

The PCA models were trained using the measurements of 17 variables (including 8 VAV terminal flow rates, 8 terminal damper control signals and one static pressure)

under normal operation obtained from the simulation test of a day. Both system level training data matrix and terminal level training data matrix (for Terminal 6 and Terminal 4) were collected from the test. Because the variables were of different units, the data in each column were normalized to zero mean and unit variance. An eigenvalue decomposition of the covariance matrix of the training sample gave the loading vectors and the eigenvalues which explained the system variances captured by the relevant loading vectors (Table 7.1).

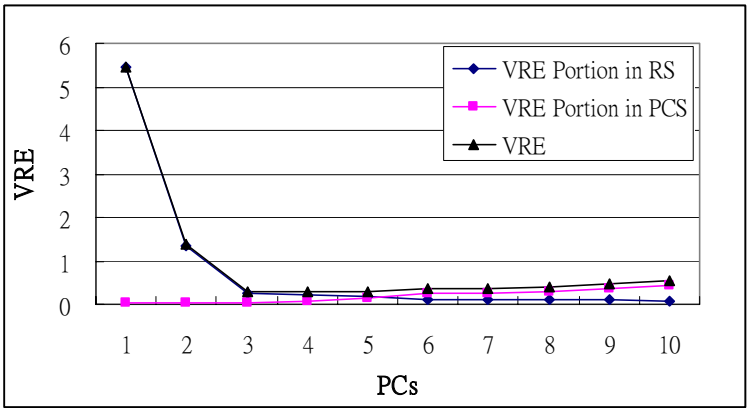

Figure 7.1 VRE Index

Three PCs for the system PCA model were retained based on training data matrix (*33x17*) using the VRE method (Figure 7.1), which captured 97.7% of the total variance of the training data matrix (Table 7.1). The thresholds of T^2 statistic and *SPE* at 95% confidence level were calculated to be 9.53 and 1.172 respectively. As for terminal level training matrixes (*33x4*) of Terminal 6 and Terminal 4, the VRE method retained three PCs for both terminal PCA models.

The results of the validation tests in two days are presented here below. Single sensor fault and multiple sensor faults were introduced in two tests respectively. In the first test, a bias error was introduced into the flow senor of Terminal 6 gradually

starting from 11:06AM. The bias increased with a rate of 9% of the sensor reading per hour. In the second test, besides the same bias error was introduced to flow sensor of Terminal 6, a fixed bias error of (-0.2kg/s) was introduced to Terminal 4 at the time 13:53PM. In the both tests, the system started to operate at 7:45AM.

7.1.2 Test A – Single Fault

The measurements of 17 variables (including 8 VAV terminal flow rate, 8 terminal damper control signals and one static pressure) were used by the scheme to examine the condition of the system at each sampling interval. The scheme examined the system at a predefined interval (300 seconds) by deducing both T^2 statistic and *SPE*. The T^2 statistic and *SPE* plot are presented in Figure 7.2.

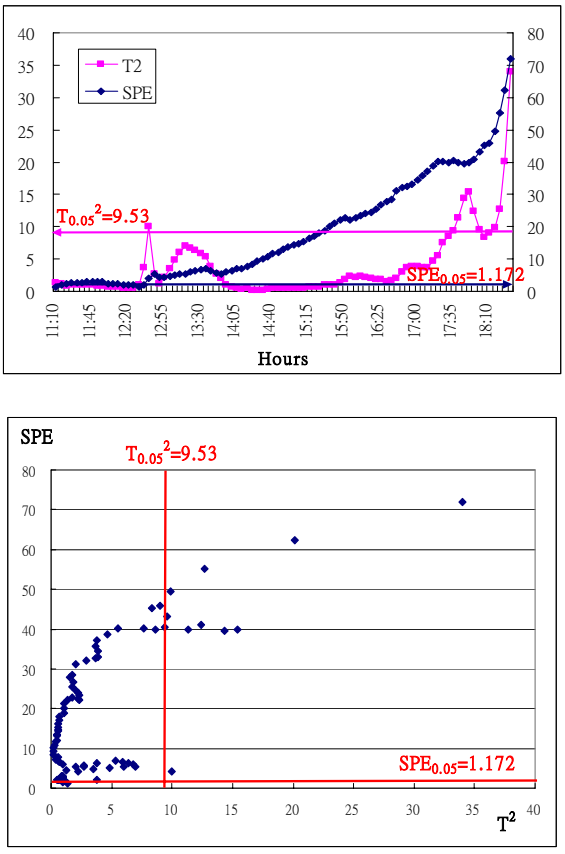

Figure 7.2 T^2 and *SPE* plots at system level when single developing senor bias in Terminal 6

It is found that most of the points were within the limit of T^2 statistic but quickly out of control on *SPE* as the flow sensor error developed. When the bias expanded to a significant level, both limits of T^2 and *SPE* were violated. The results (Figure 7.2) strongly indicate the existence of sensor bias.

To isolate the faulty sensor, *SPE* contribution of all 17 variables were calculated at a predefined interval as from 11:40AM. 10 groups of contribution plots (with an interval of 40 minutes) are presented in Figure 7.3. Obviously, flow rate of Terminal 6 (C13) had a major contribution (over 80%) to *SPE* and was therefore isolated as the faulty one. Further looking into Terminal 6 by the terminal level PCA model (9.53 for $T_{0.05}^2$ and 0.006177 for $SPE_{0.05}$) confirmed that the flow sensor of Terminal 6 was faulty (Figure 7.4). This faulty sensor was reconstructed within its PCA terminal model by iterative approach and the recovered data tally with the real flow rates (Figure 7.5).

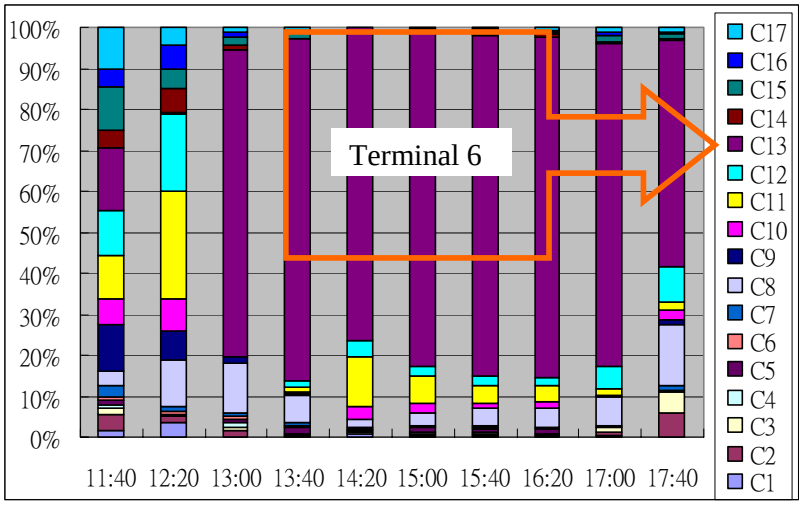

Figure 7.3 *SPE* contribution of all variables when single fault in Terminal 6

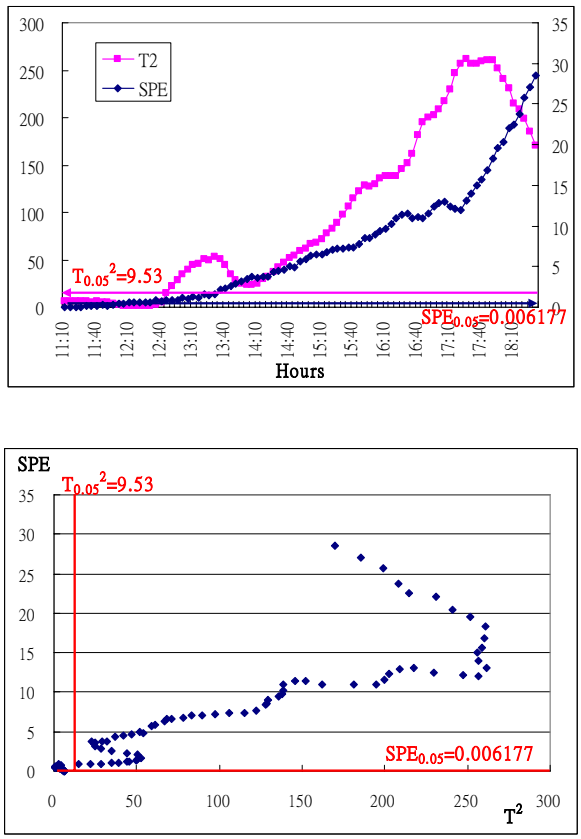

Figure 7.4 T^2 and *SPE* plots at terminal level when developing senor bias in Terminal 6

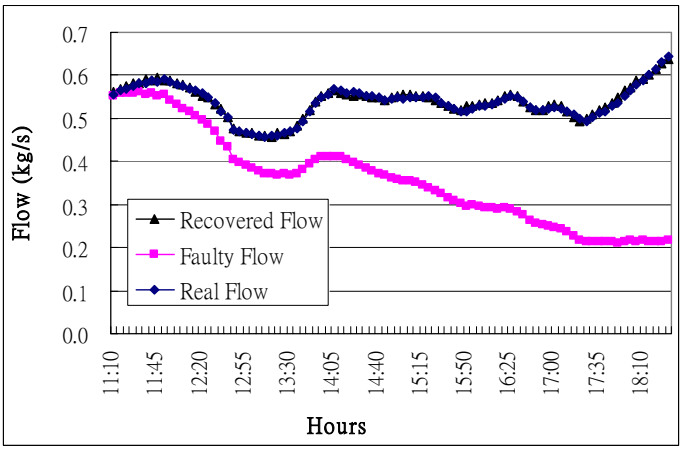

Figure 7.5 Biased and recovered flow measurements of Terminal 6

With the new T^2 and *SPE* calculated using the recovered measurements, both new T^2 and *SPE* were within the limits indicating the system was "fault free". The FDD

process terminated. The accuracy and reliability of Terminal 6 flow sensor were improved significantly using the recovered data, which can therefore assist in realizing the fault-tolerant control.

7.1.3 Test B – Multiple Faults

With the flow sensor bias of Terminal 6 and Terminal 4, similarly the existence of faulty sensors was confirmed by the violation of the *SPE* limit at system level (Figure 7.6).

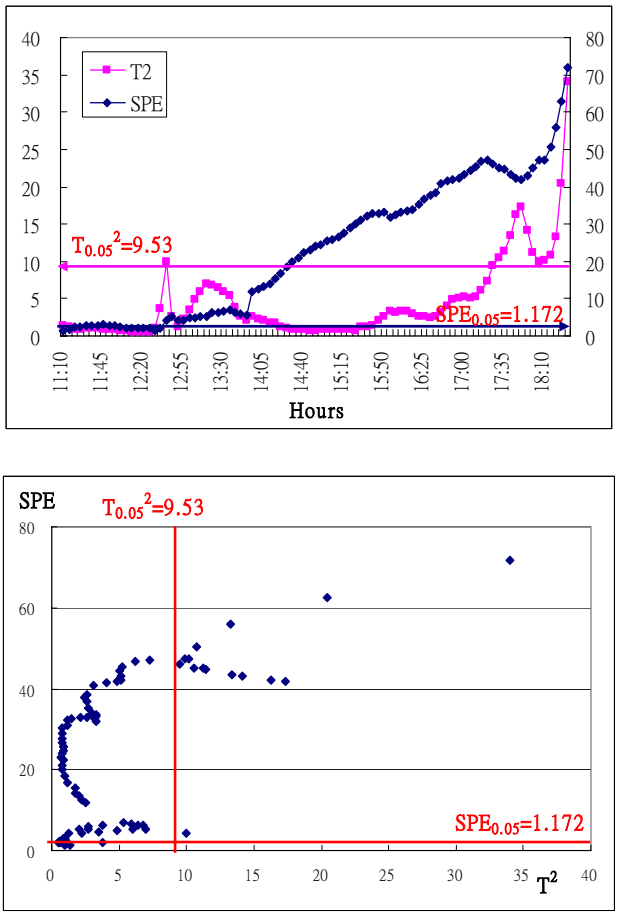

Figure 7.6 T^2 and *SPE* plots at system level when multiple faults in Terminal 4 and 6

Ten groups of contribution plots (with an interval of 40 minutes) as from 11:40AM were presented in Figure 7.7 for fault isolation. Flow rate of Terminal 6

(C13) and flow rate of Terminal 4 (C9) contributed significantly to *SPE* and were therefore isolated as the faulty ones.

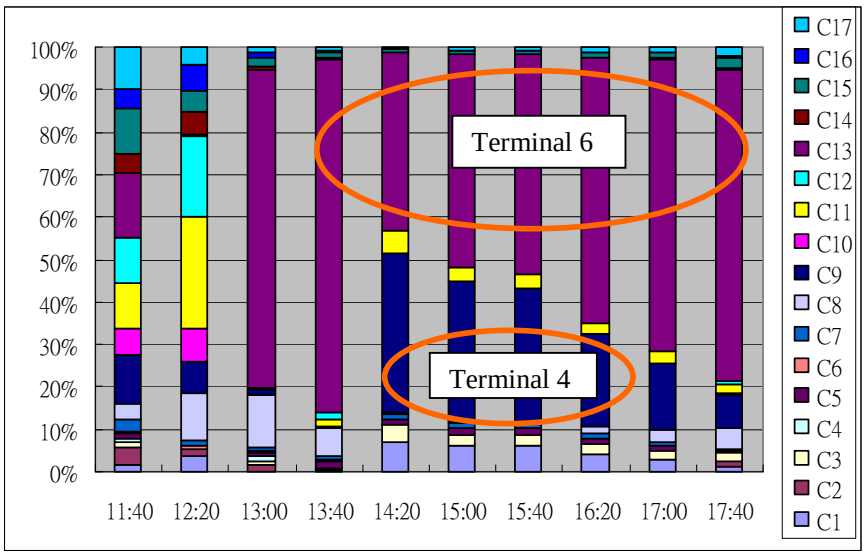

Figure 7.7 *SPE* contribution of all variables when multiple faults in Terminal 4 and 6

Compared with the above-mentioned case of single fault, the pattern of fault detection was similar. However, isolation of the multiple faults should be studied carefully. In Figure 7.7, we can find that Terminal 6 dominated the *SPE* contribution while Terminal 4 contributes a significant portion at the later stage. Further investigation on T^2 and *SPE* plots of Terminal 4 and 6 at terminal level confirmed that flow sensors of both Terminal 4 and 6 were faulty after 13:53PM.

If the sensor fault of Terminal 4 was not isolated at this stage, the recovered sensor measurements of Terminal 6 can help further isolate the faulty sensor(s) by repeating the same FDD procedure. With the faulty flow measurements of Terminal 6 replaced by the recovered data, the FDD process repeated. The fault of Terminal 4 was detected by the violation of the system level *SPE* (Figure 7.8) and isolated by the *SPE* contribution of Terminal 4 flow sensor (Figure 7.9).

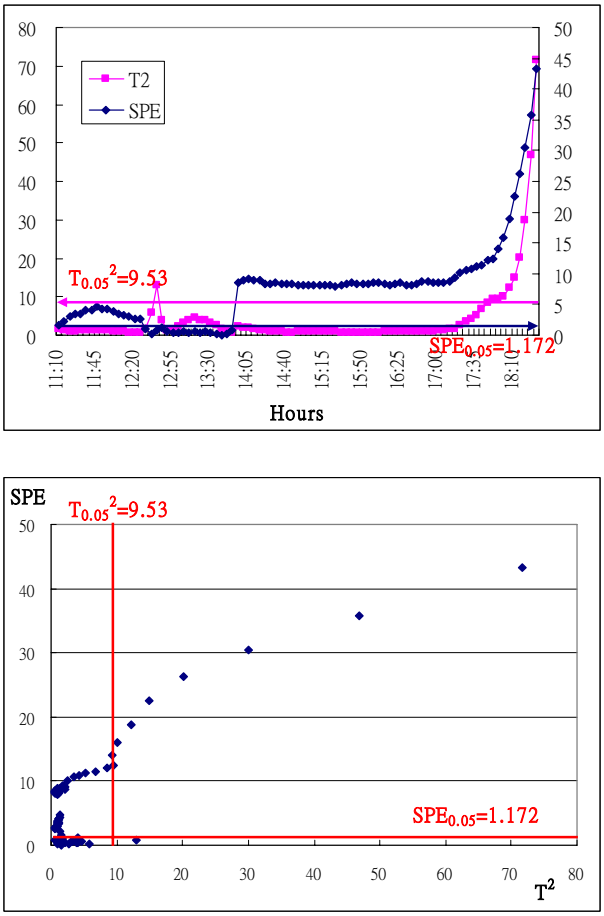

Figure 7.8 T^2 and *SPE* plots at system level when multiple faults in Terminal 4 and 6 with recovered flow sensor of Terminal 6

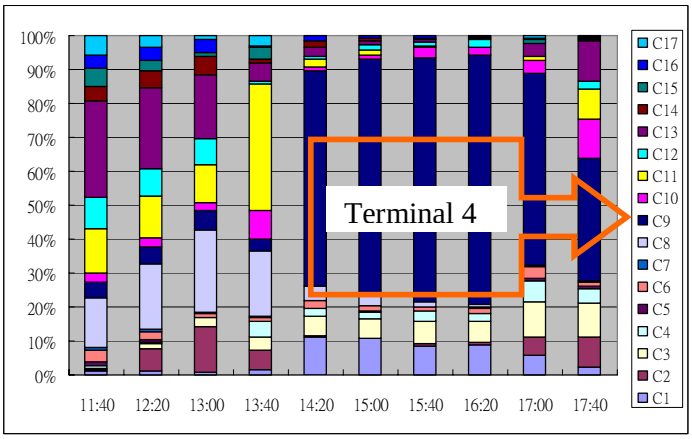

Figure 7.9 *SPE* contribution of all variables when multiple faults in Terminal 4 and 6 with recovered flow sensor of Terminal 6

Further investigating terminal level T^2 and *SPE* plots on Terminal 4 revealed that sensor fault occurs at 13:53PM (Figure 7.10). Using the recovered measurements of both Terminal 6 and Terminal 4, both new T^2 and *SPE* were recalculated. The new T^2 and *SPE*, which were within the limits, indicated that the system was "fault free". The FDD process then terminated.

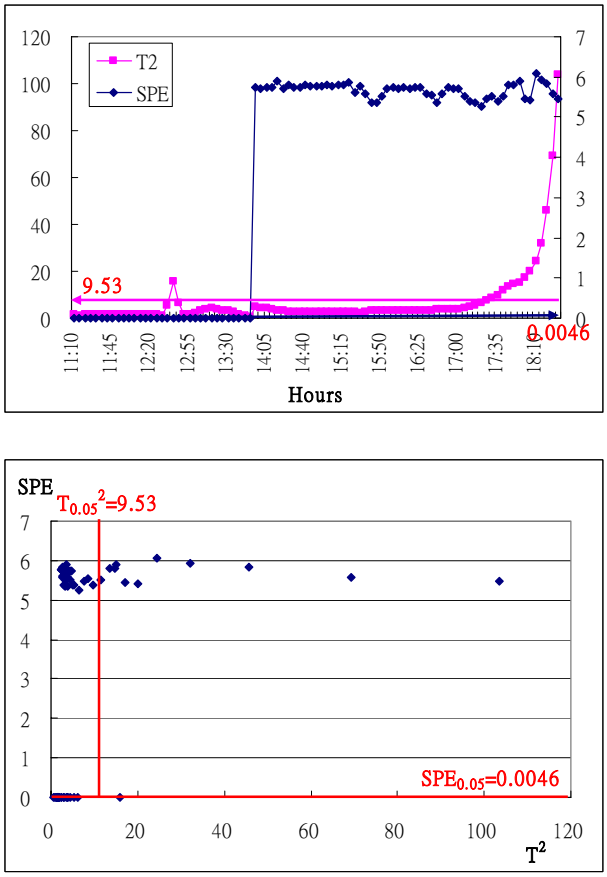

Figure 7.10 T^2 and *SPE* plots at terminal level with fixed bias in Terminal 4

7.1.4 Robustness Analysis of PCA-based FDD Scheme

A system level PCA model may involve many VAV terminal flows in a typical VAV air distribution system. The fault detection and isolation ability of the PCA-based method may be affected by the process stability and multiple faults in the

system. The scheme adopts PCA models at two levels and iteration approach to enhance the robustness.

PCA models at two levels improved the reliability of the FDD scheme as the models at the terminal level further confirms the fault detected at the system level. For multiple faults, the iteration approach with the recovered measurements used could isolate the faulty sensor(s) which are not isolated previously. The scheme terminates only when the T^2 and *SPE* at the system level do not indicate any more fault after all the isolated faulty sensors are recovered. Thus, the robustness of the FDD scheme is guaranteed particularly for multiple fault detection.

7.2 Validation Using Site Data from a Real Building

7.2.1 Test Conditions

The second test facility is the HVAC system in Building B as described in Chapter 5. Operation data of one typical VAV system serving the 24th floor was used for FDD scheme evaluation. The air-conditioning system serves half floor open office. The system operated 12 hours (8:00~20:00) during working days. The control and performance monitoring are implemented by the BMS. As it is a pressure dependent VAV system, the VAV damper position signal is available and could be logged by the BMS. The data retrieved from the central workstation were used for the PCA-based VAV terminal flow sensor FDD scheme evaluation.

The VAV system hydraulic characteristics were monitored by logging the system static pressure, damper openness (signal of damper position) and air flow rate of all 31

VAV terminals of the system. There are 2 static pressure measurements (SP1&SP2) in the system as all the terminals are distributed at two air duct branches. 14 terminals (1-14) are located at Branch 1 under the control using SP1 and 17 terminals (15-31) are located at Branch 2 under the control using SP2. The VAV terminals at Branch 2 were studied in the validation tests.

7.2.2 Data Preprocess

Measurements at 30-minute intervals of a week (5 working days) were recorded by the BMS system. After initial checking on the data of VAV boxes at Branch 2, Box 15, 16, 18, 23 and 25 were left out of the training matrix as the signal of damper openness and the flow measurements were observed to be abnormal. The data of the first three days under normal operation are used to construct the training data matrix for the PCA models. Applying a filter based on T^2 statistic, outliers in the measurements of the first three days were eliminated. 72 samples were used to construct the training matrix (*72X25*). To minimize the VRE (Figure 7.11), first five PCs representing 84.6% of the total variance of the system were retained. The detection thresholds of 95% confidence level were calculated to be 12.7 for T^2 and 8.4 for *SPE*.

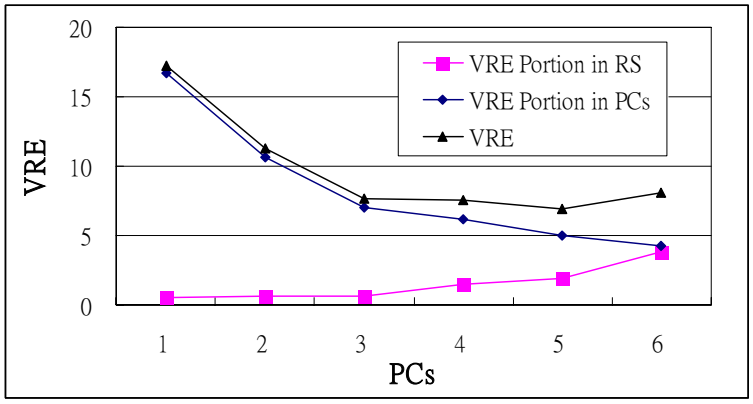

Figure 7.11 VRE Index

Three tests were carried out using the measurements of the fourth and fifth days. In the first test, the measurements of VAV terminal box 19 were added with fixed bias (+100l/s, Error I for Test I). In the second test, it was added with a developing bias (increment rate of 4l/s per hour, Error II for Test II) into the flow sensor of the same terminal. In the third test, it was added with another fixed bias (+50l/s, Error III for Test III) into the flow sensor of the same terminal.

7.2.3 Test I – Fixed Bias

Figure 7.12 shows the T^2 and *SPE* plots in case of Error I. The operation process was under control since T^2 plot was obviously below the threshold. The existence of flow sensor bias was detected by *SPE* as all sample points are above the threshold line in the figure.

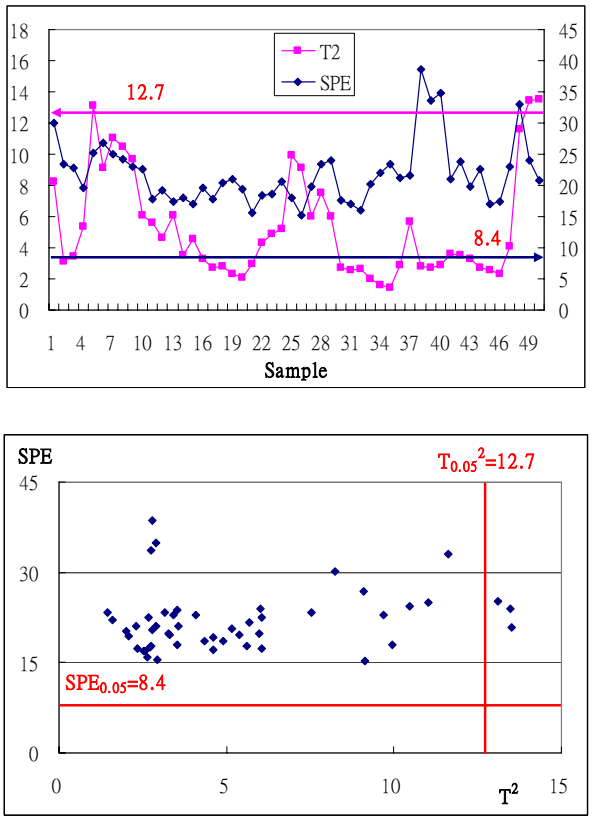

Figure 7.12 T^2 and *SPE* plots at system level of Error I (4th and 5th days)

SPE contribution plot approach was used to isolate the faulty sensor. In Figure 7.13, the variables' average *SPE* contributions of 50 samples were compared. The flow rate of Terminal 19 in the test data matrixes was isolated as it had a major *SPE* contribution. Studying on terminal 19 at terminal level revealed that flow sensor of Terminal 19 was faulty as its *SPE* exceeded the threshold (Figure 7.14). In Figure 7.14, it is also noticeable that the T^2 exceeded its threshold significantly at Sample 1 and 25. The reason was that the operating conditions were significantly different at morning pull-down period at both 4^{th} and 5^{th} days. Using the terminal level PCA model, the faulty flow sensor of Terminal 19 was reconstructed (Figure 7.15). Multiple VAV terminal flow sensor FDD could be achieved by replacing the faulty measurements with the recovered ones.

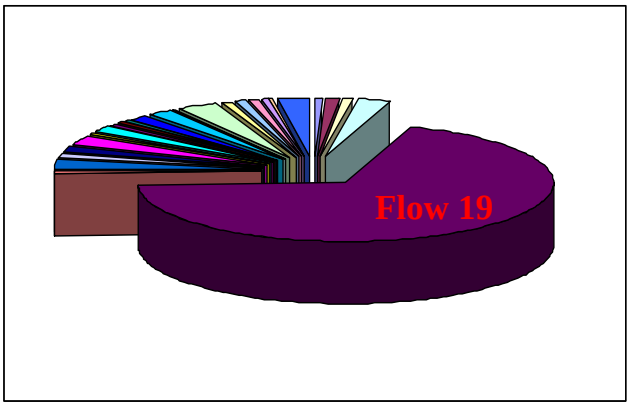

Figure 7.13 *SPE* contribution plot in Test I (4^{th} and 5^{th} days)

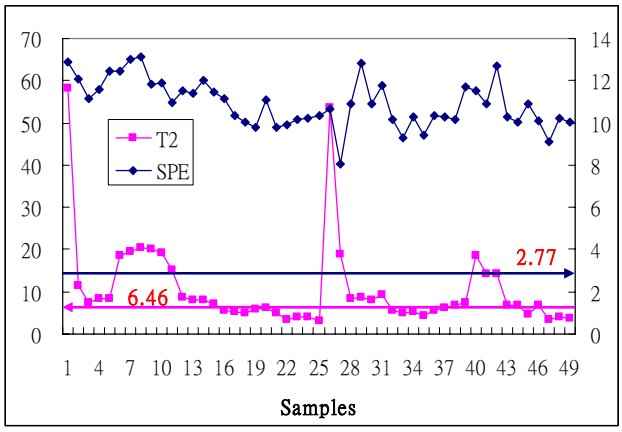

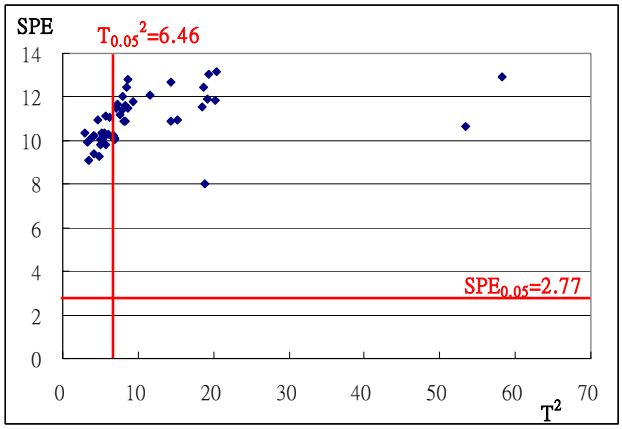

Figure 7.14 T^2 and *SPE* plots at terminal level of Error I (4th and 5th days)

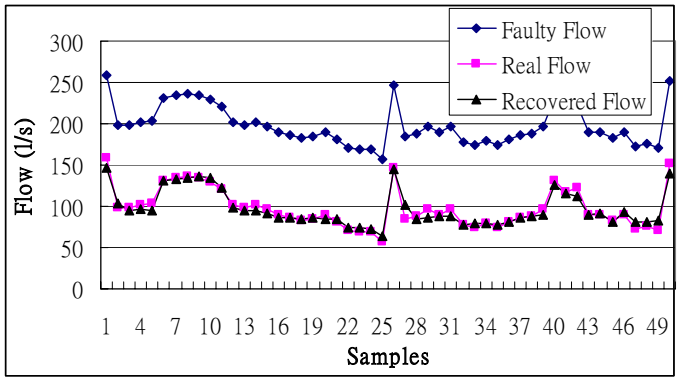

Figure 7.15 Biased and recovered flow measurements of Terminal 19

Using the recovered flow measurements of Terminal 19, both new T^2 and *SPE* at system level were recalculated. The new T^2 and *SPE*, which were within the limits, indicated that the system was "fault free" then. The FDD process terminated.

7.2.4 Test II – Developing Bias

Figure 7.16 shows the T^2 and *SPE* plots in case of Error II about the developing bias. The operation process was under control since the T^2 plot was obviously below the threshold. The developing bias was only detected by *SPE* later when the bias was significant. The test indicated that a small bias may not be detected by the scheme.

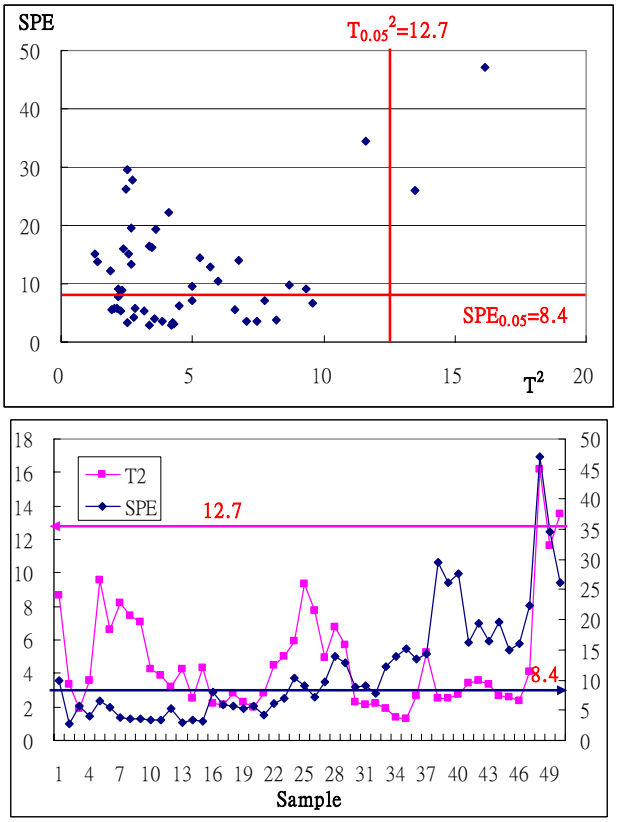

Figure 7.16 T^2 and *SPE* plots at system level of Error II (4th and 5th days)

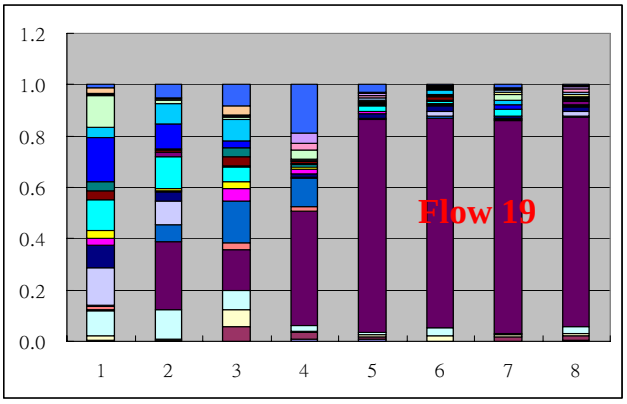

Figure 7.17 *SPE* contribution plot in Test II (4th and 5th days)

To isolate the faulty sensor, *SPE* contribution plot approach was used. For the developing bias test (Error II), the *SPE* contribution of each variable is compared at 3-hour intervals (Figure 7.17). The flow rate of Terminal 19 in the test data matrixes

dominated the *SPE* contribution in the last four data groups. Terminal 19 was therefore isolated. Further studying on terminal 19 plotted the terminal level's T^2 and *SPE* in Figure 7.18. The developing sensor bias of Terminal 19 was confirmed later when the *SPE* exceeded the threshold.

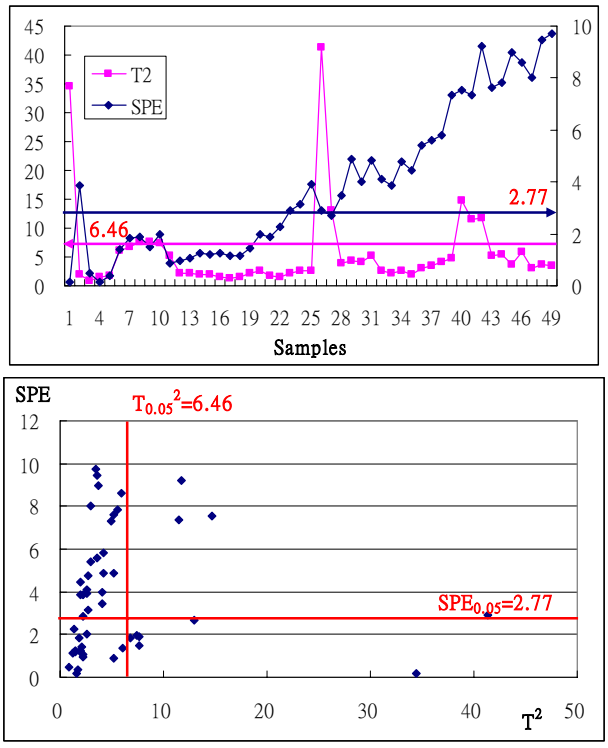

Figure 7.18 T^2 and *SPE* plots at terminal level of Error II (4th and 5th days)

7.2.5 Test III – Another Fixed Bias

For Test III, Figure 7.19 shows the T^2 and *SPE* plots at system level. Similarly, the operation process was identified as normal since T^2 plot was obviously below the threshold. In previous tests, the fixed bias of +100l/s (Error I) was detected apparently. However, the developing bias of Error II could only be detected when the bias was significant. As shown in Figure 7.19, the *SPE* points are around its threshold in this

test. The fault detection ability of the scheme for the fixed bias of +50l/s (Error III) was marginal in this VAV system.

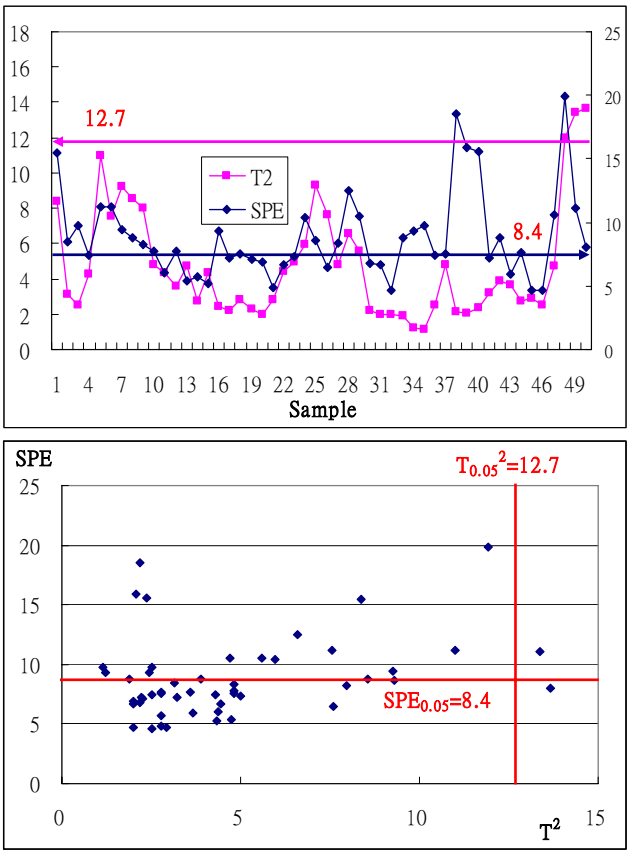

Figure 7.19 T^2 and *SPE* plots at system level of Error III (4th and 5th days)

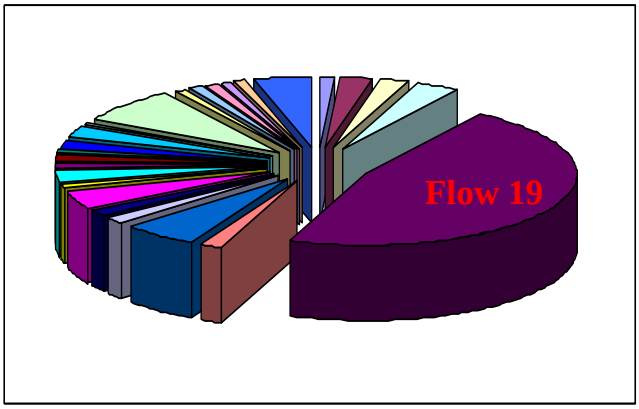

Figure 7.20 *SPE* contribution plot in Test III (4th and 5th days)

Again, *SPE* contribution plot approach was used to isolate the faulty sensor. In Figure 7.20, the variables' average *SPE* contributions of 50 samples were compared. The flow rate of Terminal 19 in the test data matrixes could be isolated as it had a major *SPE* contribution. Studying on terminal 19 with its terminal level PCA model worked out the T^2 and *SPE* of the tested terminal matrix, which were plotted in Figure 7.21. The flow sensor of Terminal 19 was confirmed faulty as the *SPE* exceeded the threshold in most cases.

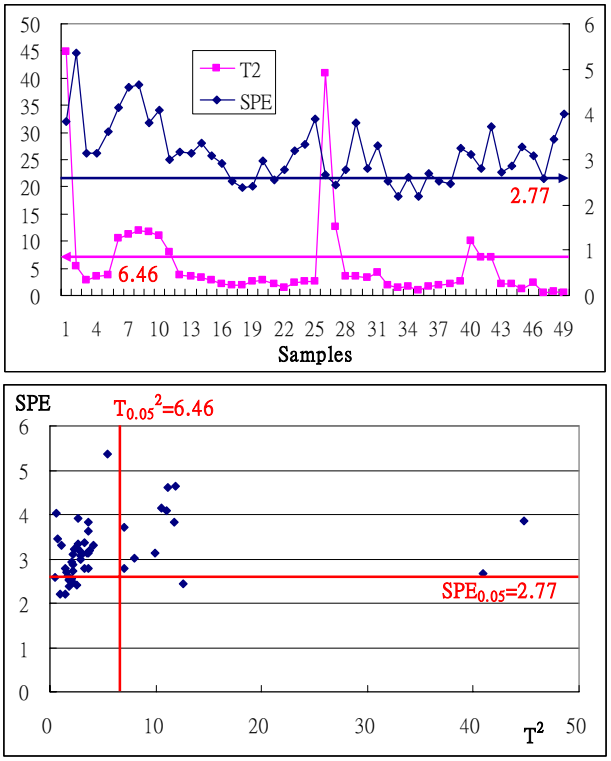

Figure 7.21 T^2 and *SPE* plots at terminal level of Error III (4th and 5th days)

7.2.6 Sensitivity Analysis of PCA-based FDD Scheme

The validation tests demonstrated that when the sensor was biased by +100l/s (Error I), it could be easily detected in Test I. However, the developing bias (Error II) could only be detected when the bias was significant in Test II. Test III also

demonstrated that the bias of +50l/s (Error III) was marginally detectable. In the tests, the air flow rate of the concerned VAV terminal (Terminal 19) was within the range of 70~150l/s. The tests indicate that the sensor biases could only be detected when biases exceeded a certain level in practical applications. As a small sensor bias would not affect the normal control process, the sensitivity of the FDD strategy is acceptable.

The sensitivity of the PCA-based FDD method is also relative to the quality of the training data. In the case of the studied system, if only the measurements of the first working day are used to construct the training matrix, the faults could not be isolated as the training matrix does not cover the characteristics of the system at sufficient operating conditions, which actually leaded to extreme high values of both T^2 and *SPE* of the test matrix.

The PCA method aims at capturing as much as possible normal variation in the process from the training data. If the training data are insufficient, the PCA model could not capture the system characteristics. But if the training data spread in too large range, the sensitivity of the PCA model would be affected because the variations caused by the sensor faults are not significant compared with modeling error. Therefore, there must be sufficient training data to capture the correlations while training data must not spread in too large range when the operation condition is concerned.

Experiences show, when applying PCA-based flow sensor FDD scheme to real buildings, the training matrix should be carefully constructed. As the operating condition varies according to the weather conditions, occupancy and internal loads, the training matrix selected should represent appropriate coverage of system operating conditions.

7.3 Summary

This chapter presented the validation of the PCA-based VAV flow sensor FDD scheme presented in Chapter 4 using both simulation tests and site data retrieved from the BMS of a real building in Hong Kong. Both fixed bias and developing bias were introduced in the simulation tests. The sensor FDD scheme detected both of them successfully with the faulty sensor reconstructed. The normal operation data retrieved from the BMS showed that the PCA model can capture most of the normal variances in the VAV air distribution system. Artificial sensor faults of both fixed bias and developing bias were successfully detected using the scheme.

In practical applications, the construction of training matrix is the most important part of the FDD process. The fault(s) could not be identified if the training matrix does not capture the operating characteristics of the system under certain operating conditions. Test of the scheme at sufficient typical operating conditions is recommended before actual applications. The training matrix should be reconstructed if both thresholds of T^2 and *SPE* are exceeded for a certain period under those typical operating conditions while the system is fault free.

CHAPTER 8 AUTOMATIC COMMISSIONING SOFTWARE AND ITS APPLICATION

This chapter presents the implementation of the FDD strategy developed in the previous chapters for VAV air distribution systems automatic commissioning using a software package developed as an automatic commissioning tool. The commissioning tool can be integrated with BMSs, improve their performance in healthy components and reliable measurements. It is implemented in both simulated and real buildings.

Section 8.1 briefly introduces the automatic commissioning tools in HVAC field. Section 8.2 structures the software package as an automatic commissioning tool for VAV air distribution systems. Section 8.3 demonstrates the application of the commissioning tool in both simulated and real buildings. Section 8.4 describes the integration of the commissioning tool with BMS for continuous commissioning and Section 8.5 summarizes this chapter.

8. 1 Critical Review on Automatic Commissioning Tools

Commissioning has played an important role in improved building comfort and reduced energy consumption. As buildings are subject to change, continuous commissioning is neither a “start-up” of a building nor a punch-list check-out. Continuous commissioning in HVAC systems is a process to: 1. optimize the operation of existing systems to improve building comfort and reduce building energy cost, 2. solve existing comfort and IAQ problems, 3. guarantee continuous optimal

operation by operational staff in future years, and 4. provide optimal energy retrofit suggestions to owners to minimize the project costs.

Commissioning tools are under developing nowadays due to 1) Energy and environmental reasons. Global warming has increased the pressure to reduce energy use in buildings and many countries are willing to develop green buildings 2) Business reason. Many companies are developing new services to diversify their activities in the building and energy industries 3) Technological reasons. Building automation systems are now standard in recent buildings and are being installed in many older ones. These systems automatically collect building and plant operating data, and offer possibilities for innovative commissioning services.

There are mainly three commissioning procedures. They are manual commissioning procedures, BMS assisted commissioning tools and model-based commissioning tools. The IEA working group (Annex 40) is working on developing, validating and documenting tools for commissioning buildings and building services systems. These tools include guidelines on commissioning procedures and recommendations for improving commissioning processes, as well as prototype software that could be implemented as stand-alone tools and/or embedded in BMSs. The methods used for developing the automatic commissioning tools are classified into the following seven categories:

1) expert rules
2) other artificial intelligent techniques
3) simulation models
4) graph technology
5) statistics
6) simple engineering calculation

7) combination of methods

Although automatic control is an important element in the commissioning of HVAC systems, few studies have been conducted about using automatic control for commissioning. Haves et al. (1996) developed a basic commissioning tool to verify the performance of HVAC control systems that combined a Close Loop Test and an Open Loop Test. They reported the results of a laboratory experiment for the tool application to verify the functions of HVAC control systems through a simulation method, but their approach has not yet reached the stage of practical application. Tsubota et al. (Annex 40) successfully developed a prototype of "HVAC Control Logic Tracer" for supporting the commissioning of HVAC control systems. The Tracer could show the control algorithm of an HVAC control system as a flowchart, and displayed how control was actually taking place on the flowchart using visual images. The failure could be diagnosed by identifying the causes traceable to the system control. It was concluded that the tool precisely traced the actual control history within the operation data range selected in this study.

The automatic commissioning tools are mostly developed from system design models. Commissioning, or more specifically, the subtask of functional testing, involves evaluating the installed performance of a piece of equipment and comparing this performance with expectations or design intent (Kelso and Salsbury, Annex 40). Thus the model-based commissioning is broken down into twp parts: 1) Characterization of installed performance. 2) Translation of design intent into performance expectations for conditions at the time of the test, which is commonly realized by system design models. If the model is structured properly so that its parameters would be expected to be relatively invariable for changes in conditions, the parameterized model could then be used to predict performance for a new set of non-

design conditions. Kelso and Salsbury used the design model of a heat exchanger for commissioning. The results from the tests at the Iowa Energy Center showed that the proposed commissioning approach based on system identification and design models were workable. It was also clear that the presented methodology could easily be automated as part of a stand-alone tool or be embedded in the control system.

Model-based commissioning procedures use mathematical models of components and systems to link design, commissioning and operation. To develop the automatic tool for functional tests, both suitable models and test sequences are the key elements. Supporting software is necessary to implement the test sequences and analyzing the results using the models. A group of researchers are focusing on identifying and refining suitable models and defining the test sequences required to verify acceptable performance when detect/diagnose selected faults.

Implementing automatic commissioning procedures in software and hardware raises specific questions. Two types of procedures are possible. Passive monitoring procedures use the BMS to collect data about building and HVAC system behaviour. Then algorithms are applied on these data to determine if the behaviour is correct or not. Active testing procedures techniques not only monitor data but send test signal to the HVAC systems. Such procedures could include, for example, stopping and starting up plants, opening or closing dampers… These procedures enable a much thorough testing of the system behaviour but imply a two way interaction with the system which is more complex to implement. Solutions to implement passive monitoring as well as active testing procedures are under studying within Annex 40 framework.

Commissioning tools are usually designed to serve as the interface between the end-user and BMSs by Annex 40 working group. They monitor building control data, storing them in their structured database to be used on-line or upon request. Data

resulting from standardized test procedures invoked manually or automatically are also stored in the database. The database functions as a server to reasoning algorithms that perform intelligent analyses of the monitored data, carrying out additional automated tests of components and systems, identifying and diagnosing faults, and evaluating potential improvement in energy efficiency. The common architecture of the tools is shown in Figure 8.1.

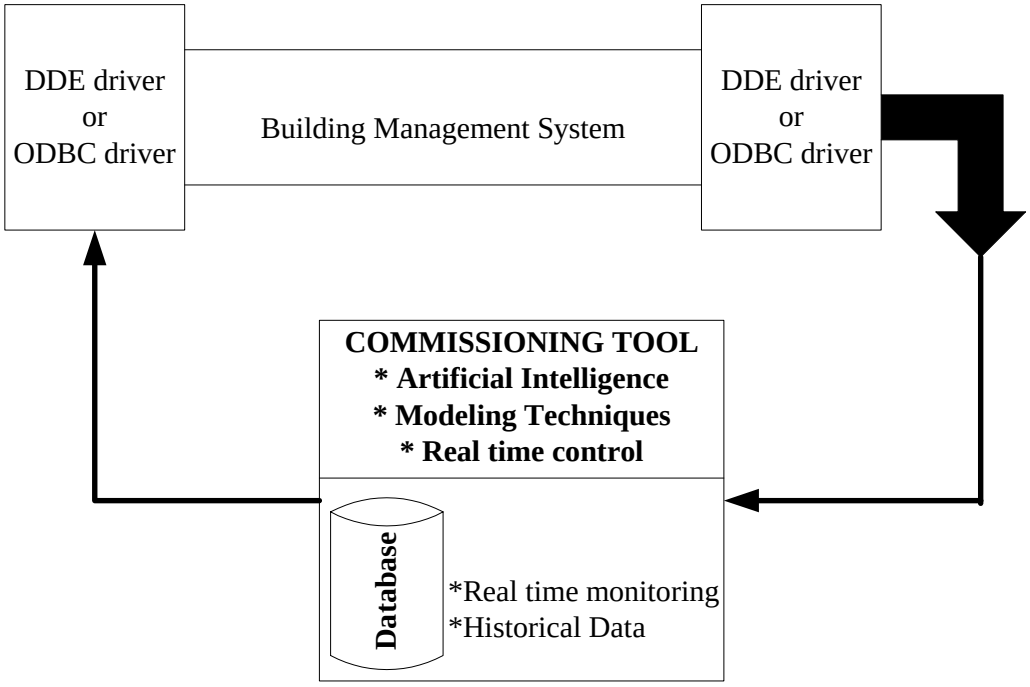

Figure 8.1 Common architecture of commissioning tools

Software installation is done on a personal computer (usually the Building Operating Station) where a link to the BMS is possible. As BMS and commissioning tools may not share the same communication protocol, some kind of communication translator (Driver or Server) has to be installed. For propriety communication protocols, these devices can only be provided by the control manufacturer while for standard protocol should be provided by either a control manufacturer or a third party.

A recent survey conducted in Japan showed that BMS data were used for commissioning in more than 80% buildings. However, more than 2/3 of them were used for verification check and less than 1/3 were used for functional tests. It also revealed that for the most buildings, it was difficult to complete entire commissioning. The automatic commissioning tools are therefore expected to document and multilaterally analyze the data collected from BMSs. The FDD strategy developed in this study is valuable to be converted to an automatic commissioning tool.

8.2 Automatic Commissioning Software Package

The automatic commissioning tool for VAV air distribution systems is developed from the FDD strategy presented in the previous chapters. Based on the BMS database, the human machine interface (HMI) is set up to read in the data from the BMS, run the commissioning software package and generate the FDD results. The structure schematic of the automatic commissioning tool is presented in Figure 8.2.

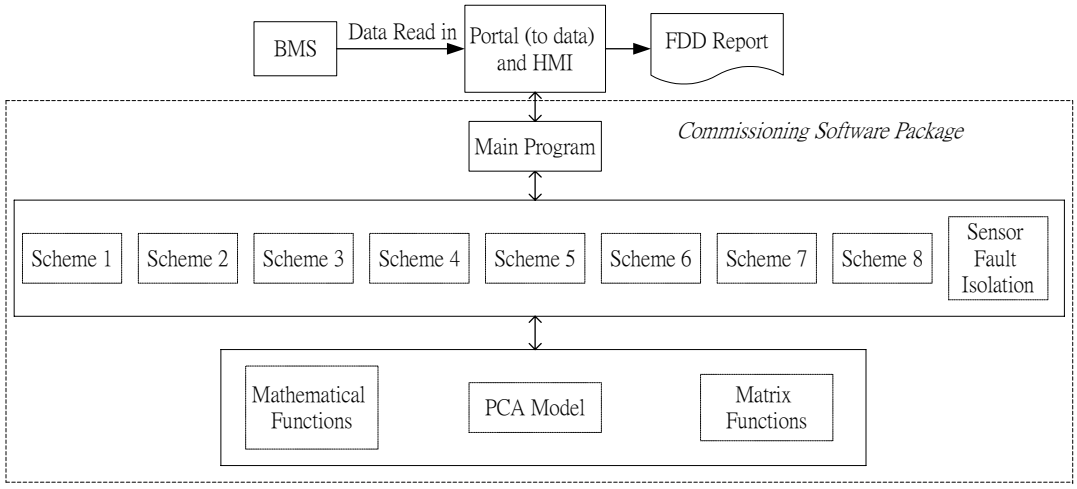

Figure 8.2 Structure schematic of the automatic commissioning tool

The commissioning software package was developed on the platform of FORTRAN 90, which included a FDD main program, eight functional modules (subroutines) for eight schemes, VAV flow sensor fault isolation module (subroutine) and some mathematical modules (subroutines) as shown in Figure 8.2. The functional packages implementing the fault detection within the scheme and fault grouping is conducted in the main program.

FDD Main Program

The FDD main program defines the system configuration and read in the data files. The data are also filtered within the main program. The program is responsible for arranging the relationship of the eight functional schemes. Configuration information, including the system configuration, measurement positions in the system and samples, is prepared in text files through HMI and can be read in by the program. The system configuration of pressure-independent VAV systems is different from that of pressure-dependent VAV systems, so the data file defines which measurements are used. The configuration of PCA models at both system level and terminal level are also figured out in the main program. The software is initialized by starting the main FDD program. The main program configured for the simulated system is shown in Appendix B (FddVAV.for).

As a typical VAV system involves many VAV terminals, the main program should also read in the number of terminals in the system and arrange the fault detection sequence of all the terminals. The VAV terminals are designed to be checked for multiple hard faults (Fault 1-10) one after another by going through Scheme 1 module to Scheme 7 module. Scheme 8 module and the relevant modules are activated by the main program when it is confirmed that the system is free of hard faults.

The functional module of Scheme 8 fulfills both system level and terminal level PCA modeling for detecting flow sensor faults. When new samples are available, the monitoring results, including the T^2, *SPE* and their thresholds at system level are calculated within Scheme 8 module. After the sensor fault(s) are detected by both T^2 and *SPE*, the functional module of sensor fault isolation is called by the main program to isolate the faulty sensor(s). The isolated fault(s) are then checked using relevant terminal PCA model(s) by calling the subroutine Scheme 8. The structure of the subroutine arrangement in the software package is illustrated in Figure 8.3.

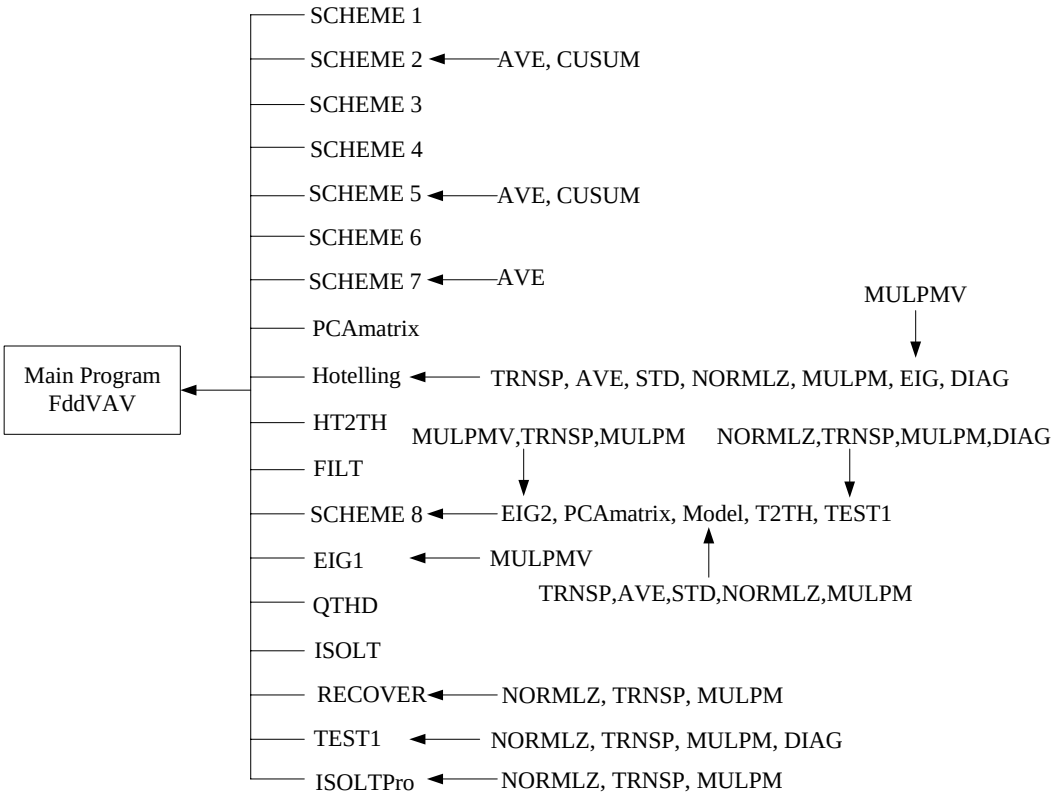

Figure 8.3 Structure of the software package

Scheme 1-7 work together to detect Fault 1-10 by giving the output (‘0’ or ‘1’) of their relevant fault detection indices (FF1-7 for Scheme 1-7), where the output ‘0’ indicates fault free and ‘1’ indicates fault detected. Under Scheme 7, Fault 8, Fault 9

and Fault 10 are involved. The faulty pattern could be sluggish response and oscillation, where flow sluggish response is briefed by the index, FF7FS, flow oscillation is briefed by FF7FO, temperature sluggish response is briefed by FF7TS and temperature oscillation is briefed by FF7TO. Similarly, the index output of "0" indicates fault free and the output of "1" indicates fault detected.

Functional Modules

Scheme 1 module is called by the main program to detect Fault 1 by exporting the result of the fault detection index, FF1. It is developed based on the SPC model described previously to count the reversals and compare the counted one with the pre-defined limit (20). It reports the counted reversals and the result of the fault detection index, FF1, to the main program.

Scheme 2 module is called by the main program to detect Fault 2. It obtains the trend data of the individual VAV terminals' measured temperature and flow set-point with fixed intervals from the main program. The time counting is achieved by counting the intervals of the data sample. The functions of Average and CUSUM are called by this subroutine to detect both temperature and flow set-point frozen. The subroutine also transfers the result of fault detection index, FF2, to the main program.

Scheme 3 module is called by the main program to detect Fault 3 by exporting the result of the fault detection index, FF3. Fault 3 could only be detected under condition that the main program gives fault free output (FF2=0) of Scheme 2. The subroutine is easily built up by some IF-THEN statements.

Scheme 4 module is called by the main program to detect Fault 4/5. This module is similar to Scheme 3 module. The fault could only be detected when the main program

gives fault free output (FF2=0) of Scheme 2. The result of the FDD index, FF4, is reported to the main program.

Scheme 5 module is called by the main program to detect Fault 6. This subroutine is kind of combination of Scheme 1 module and Scheme 2 module. Reversal counting of flow set-point is written based on the SPC model and the flow measurement frozen is programmed by calling the functions of Average and CUSUM. Similarly, the result of the FDD index, FF5, is reported to the main program.

Scheme 6 module is called by the main program to detect Fault 7 by giving the result of the FDD index, FF6. In this subroutine, the characteristic equations for fault detection are written by some IF-THEN statements.

Scheme 7 module is called by the main program to detect Fault 8/9/10 by exporting the fault detection index, FF7. As explained previously, Fault 8, Fault 9 and Fault 10 are involved within this module. The subroutine is programmed to identify the faulty patterns of flow sluggish response, flow oscillation, temperature sluggish response and temperature oscillation only. It is written by filtering the read-in data first. The sluggish response is detected by counting the excessive time of the filtered variables out of pre-defined control limits. The reversal is counted by the same method described previously. However, the faults could only be detected when the main program gives the output of '0' for FF1, FF2, FF3, FF4, FF5, and FF6.

Scheme 8 is activated by the main program when it is confirmed that the system is free of hard faults (output '0' for FF1-7). Scheme 8 module is the core module in Scheme 8 as the core functions are programmed in this subroutine. The basic module of the subroutine is the matrix functions modules, which includes multiple subroutines of multiplication, transpose, matrix normalization, eigenvalues derivation, etc. The accuracy of matrix computation results determines the reliability of the PCA-based

method. Results calculated using the matrix functions were compared with those calculated using the MATLAB. The results were the same when they were rounded up to four decimal digits.

The sequence of measurements in the training matrix and new samples must be the same, which will also be used to isolate the faulty sensor when the fault occurs. Their positions in the matrix are defined using numbers. For example, the variables in the first column of the training matrix are the measurements of the system static pressure, so the first column in the file is numbered '1', which is also the index of the system static pressure in the FDD software. Training data are expected to be prepared as a text file. If they are not prepared, the first day' data will be used as the training data.

The training matrix is read in from a text file which is produced from the fault free BMS data. The data are filtered by Hotelling T^2 filter in the main program. Scheme 8 module is then called for fault detection. After the PCA matrix is built up by a subroutine (PCAmatrix.for), the PCA modeling subroutine (model.for) conducts the main function to build PCA models by calling the matrix calculation functions as shown in Figure 8-3.

The new samples for test are read in group by group. The index, FINDEX, counts the consecutive exceeding of *SPE* threshold and the index, FT2, counts the consecutive exceeding of T^2 threshold. If FINDEX is greater than 9, the fault isolation subroutine is called by the main program to isolate the fault. The relevant terminal level PCA model(s) is further used to confirm the fault by counting the consecutive exceeding (FINDEXb) of terminal level *SPE* threshold(s). If FINDEXb is greater than 9, the fault is confirmed and the index of Scheme 8 (FF8) is given the output of '1' to indicate the fault. The subroutine for data recovery is then called by the main program

to retrieve the real flow. The recovered data are stored in a text data file as part of the FDD results, which could be used for commissioning and fault-tolerant control.

8.3 Application of the Commissioning Tool

8.3.1 Application in the Simulated Building

Exercises of the software application were conducted using both the simulated data and real building data. Several groups of the simulated data were prepared in text files, which could be read in by the main program. Different faults were introduced in each group of the simulated data, which were detected by the software as the main FDD report showed '1' of the relevant fault detection indices.

The simulation data files were collected based on the simulation data (Excel files) used for strategy validation in Chapter 6 and Chapter 7. Those Excel files were converted to text files. The name of the text data files were defined previously, which should be the same as those to be opened in the main program.

Table 8.1 A sample of main FDD report for hard fault in the simulated building

Main FDD Report								
	FF1	FF2	FF3	FF4	FF5	FF6	FF7	FF8
Terminal 1	0	0	0	0	0	0	0	0
Terminal 2		0	0	0	0	0	0	
Terminal 3		0	0	0	0	0	0	
Terminal 4		0	0	0	0	0	0	
Terminal 5		0	0	0	0	0	0	
Terminal 6		0	0	0	0	1	0	
Terminal 7		0	0	0	0	0	0	
Terminal 8		0	0	0	0	0	0	

Table 8.1 shows a main FDD report for Fault 7 (FF6=1) of Terminal 6. Terminal 6 flow sensor deviation to the maximum was added to the simulation data which were prepared in the text files. As the simulated system has eight VAV terminals, the fault detection process from Scheme 1 to Scheme 7 was repeated eight times. The fault was detected when the main program opened the data files of Terminal 6.

Table 8.2 A sample of main FDD report for sensor bias in the simulated building

Main FDD Report								
	FF1	FF2	FF3	FF4	FF5	FF6	FF7	FF8
Terminal 1	0	0	0	0	0	0	0	1
Terminal 2		0	0	0	0	0	0	
Terminal 3		0	0	0	0	0	0	
Terminal 4		0	0	0	0	0	0	
Terminal 5		0	0	0	0	0	0	
Terminal 6		0	0	0	0	0	0	
Terminal 7		0	0	0	0	0	0	
Terminal 8		0	0	0	0	0	0	

Table 8.2 demonstrates a main FDD report of Terminal 6 flow sensor bias. The system was hard fault free as Scheme 1-7 did not detect any fault. Scheme 8 detected and isolated the faulty sensor, which was confirmed by the terminal level PCA model. The recovered flow sensor readings were stored in a text file under the FDD report. No further flow sensor bias was detected by the iteration process with the recovered data.

8.3.2 Application in A Real Building

As introduced previously, the common pressure-independent VAV systems only provide four measurement points (temperature set-point, zone temperature, flow set-point and flow measured) for each VAV terminal. The signals of VAV damper openness are usually not available. However, a VAV retrofitting project provides the

VAV damper position signals to BMS, which offers the potential to apply the automatic commissioning tool.

A Retrofitting Project

A commercial building, which comprises 40 storeys of approximately 860,000 square feet, was developed in 1988. Located in the hub of Hong Kong, the building is equipped with sophisticated architecture and communication technologies that satisfy the further developing requirements of tenants. However, the existing pneumatic VAV control system inhibits the implementation of new technologies through direct digital control (DDC) in air-side systems. Also, many problems in pneumatic system were found by the maintenance team:

a) air leakage, it is very difficult to check out the exact point of air leakage especially for minor leakage at connection joints.

b) air compressors must be maintained in good condition, otherwise, the whole pneumatic system will be broken down. Annual overhaul and running cost of the compressors will increase the maintenance cost.

c) the set point of the pneumatic thermostat will shift easily because it is a mechanical device, any external force, transferred from the air duct and VAV box itself, added on the thermostat will shift the set-point.

During the past years, the advantage of new software and computing technologies had already moved the standard of BMS to another level. The more reliable and high performance hardware and additional management software make BMS a must tool for facility management. As a part of BMS, the pneumatic VAV control systems in the building are subject to upgrade.

With the control methods of VAV boxes changed from pneumatic type to direct digital type, the control flexibility and accuracy are improved. By using DDC control, control algorithms could be modified if necessary. This is very useful for implementing new energy saving strategies and automatic commissioning tools. The total cost of BMS upgrading is HK$10,621,218.00 including the following works:

1) upgrade the existing JC SDC8016 BMS by the JC Metasys BMS including hardware and software.

2) all existing BMS points will be connected: HVAC, fire, pump&drainage, electrical, security and miscellaneous facilities.

3) replace the existing pneumatic VAV controllers and thermostat by intelligent DDC type VAV controllers and thermostat.

4) replace CAV boxes for AHU rooms and lift lobbies.

5) replace inlet-guide vane control by VFD control for AHU at tenants' floors.

6) replace existing pneumatic cooling valves by electrical valves

7) addition of Web Server for intranet and internet connection

8) addition of M-alarm Server for remote alarm via mobile, pager, fax and email.

9) addition of SQL(structured query language)-Historian Server for export trend data and SQL database.

Before the commence of large-scale upgrading, a pilot study aimed at verifying the difficulties and requirements of the work had been carried out in one system covering half of the 13th floor and completed at early December of Year 2004. The works were basically divided into two types: works in AHU/BMS rooms and works in tenant's

office. Works in tenant's area must be carried out in weekends. The facilities involved were the west side AHU (AHU-13-1) and total 28 nos. of VAV box (Figure 8.4). VAV box controller installation in tenant's office was carried out in two weekends. Since the VAV controller must be workable after installation, testing and commissioning were done right after the installation. To shorten the T&C time, all VAV box controllers were tested and set using dummy boxes before the installation. The pilot study was completed on schedule successfully. The whole building upgrading then started system (half-floor) by system (half-floor).

Figure 8.4 VAV terminal and its controller

New VAV control systems are under pressure-independent cascade control, which can monitor the information of actual zone temperature, temperature set-point, VAV box damper position and actual air flow rate etc. via the BMS network to figure out whether the VAV box is in good condition or the demand load is large. The set-point can be remotely adjusted to fulfill the temporary requirement and this could shorten

the time in troubleshooting. Remote connection methods include the operating workstation in the BMS room, any PC via internet and mobile phone etc.

To set up the data bank of the whole building, all the trend data of available VAV BMS points are stored at both SQL and Excel formats in the additional SQL-Historian Server. Those data could be used for VAV automatic commissioning.

Real System Automatic Commissioning

The commissioning tools, that perform intelligent analyses of the monitored data, carry out automated functional tests of components and systems, identify and diagnose faults, rectify faults if possible, and evaluating potential improvement in energy efficiency, are implemented through software application based on the database. The above mentioned retrofitted system has a dedicating server (SQL-Historian server) serving for the database. The associated Microsoft SQL server 2000 database software can provide large number of trend data collected from Network Control Modules (NCMs) and/or N30 supervisory controllers (N30s). Numerous features are also available to automatically or manually coordinate database file management. It provides the full set of database and offers the potential for on-line application of continuous commissioning.

The VAV automatic commissioning tool developed in this study is for off-line application only although it could be upgraded to on-line tool. To carry out the automatic commissioning exercises, a full set of BMS data of the upgraded system at the 13^{th} floor was managed. This VAV system comprises 28 VAV terminals. The data set includes the static pressure, temperature set-point at each VAV zone, temperature measurement at each VAV zone, each VAV box flow measurement and each VAV damper openness. The data were taken at 1-minute intervals on 11 August 2005 from

00:00 to 23:59. The preset maximum flow and minimum flow of each VAV box are available in the T&C report.

Since the system was put into operation at 7:30AM, the logged data from 7:30AM onwards were used for commissioning. The VAV flow set-point was not a direct BMS output. It was calculated based on the temperature error and the known PI control algorithm. Besides, the VAV damper position signal is available in the system. The damper control signals were therefore replaced by the damper position signals for the commissioning. FDD Scheme 4 was then modified a little bit as real damper openness signals were used instead of control signals.

The control signal to a damper may not present the real damper position if there is component or controller fault. But it is normally an electrical signal of 0-10 V or 4-20 mA, which is unlikely to deform. The damper position signal is more straightforward for fault detection as it presents the real position of the damper. However, the error of the position signal itself may affect the FDD results. This error was not included in the commissioning test.

The commissioning started when the main program read in the total number of VAV boxes (N=28). The software configured the system with 28 VAV terminals and began to read in the required group of data and implement FDD schemes in an iterating way. Scheme 8 for flow sensor bias analysis was not activated as hard faults were detected and specified. The commissioning results are shown in Table 8.3.

It is indicated in the main FDD report (Table 8.3) that totally eight terminals (28.6%) were faulty. The percentage of faulty VAV terminals was at the similar level as 20.9% observed during the site survey explained in Chapter 2. However, all the faults were detected under the same scheme (Scheme 4). The reason could be that this system was just upgraded and commissioned eight months before the commissioning

test. The settings of maximum and minimum flow of the terminals may not be adjusted to the suitable limits. Furthermore, the data were logged at 1-minute intervals, the fault of VAV controllers could not be discovered.

Table 8.3 Commissioning results of the real system

Main FDD Report								
	FF1	FF2	FF3	FF4	FF5	FF6	FF7	FF8
Terminal 1	0	0	0	0	0	0	0	0
Terminal 2		0	0	1	0	0	0	
Terminal 3		0	0	0	0	0	0	
Terminal 4		0	0	0	0	0	0	
Terminal 5		0	0	1	0	0	0	
Terminal 6		0	0	1	0	0	0	
Terminal 7		0	0	1	0	0	0	
Terminal 8		0	0	0	0	0	0	
Terminal 9		0	0	0	0	0	0	
Terminal 10		0	0	0	0	0	0	
Terminal 11		0	0	0	0	0	0	
Terminal 12		0	0	1	0	0	0	
Terminal 13		0	0	0	0	0	0	
Terminal 14		0	0	0	0	0	0	
Terminal 15		0	0	1	0	0	0	
Terminal 16		0	0	0	0	0	0	
Terminal 17		0	0	0	0	0	0	
Terminal 18		0	0	0	0	0	0	
Terminal 19		0	0	0	0	0	0	
Terminal 20		0	0	0	0	0	0	
Terminal 21		0	0	0	0	0	0	
Terminal 22		0	0	1	0	0	0	
Terminal 23		0	0	0	0	0	0	
Terminal 24		0	0	0	0	0	0	
Terminal 25		0	0	0	0	0	0	
Terminal 26		0	0	1	0	0	0	
Terminal 27		0	0	0	0	0	0	
Terminal 28		0	0	0	0	0	0	

In-situ Validation

The site investigation was conducted according to the report. It was found that the minimum flow was set at 35% of the maximum flow for all the VAV terminals. Under

the pre-set maximum and minimum flow, Terminal 5 and 6 were defined as under capacity and Terminal 2, 7, 12, 15, 22 and 26 were defined as over capacity. The maximum flow of Terminal 5 and 6 were reset to increase by 20% and the minimum flow of Terminal 2, 7, 12, 15, 22 and 26 were reduced to 25% of their maximum then. After those maximum/minimum flows reset, the terminals resumed their normal performance and achieved their temperature set-points. The commissioning tool defined all the faults correctly, which would improve VAV system operation. It is also planned to refine the tool to read in the required data set automatically instead of preparing the data files manually.

8.4 Integration of Commissioning Software Package with BMS for Continuous Commissioning

Building services including heating, ventilation and air conditioning, electrical systems, lighting systems, fire systems and security systems (Figure 8.5). In industrial buildings they may also include the compress air, steam and hot water systems used for the manufacturing process. A BMS is used to monitor and control all or just some of these services. The technical installation in a building incorporate a large number of measuring, control and regulating functions, which annunciate deviations from desired values and standards and, if possible, take automatic corrective actions.

Different suppliers provide different programming environments for configuration including graphic/symbolic form, table form and high level language free programming. Figure 8.6 shows an example of graphic display. Most modern BMS systems provide very convenient and powerful (window-based) user interface (Figure 8.7) for BMS network setup, controller setup, control strategy programming and

system monitoring. Some systems share the same platform for both configuration and monitoring but others designed the different platform for monitoring and development.

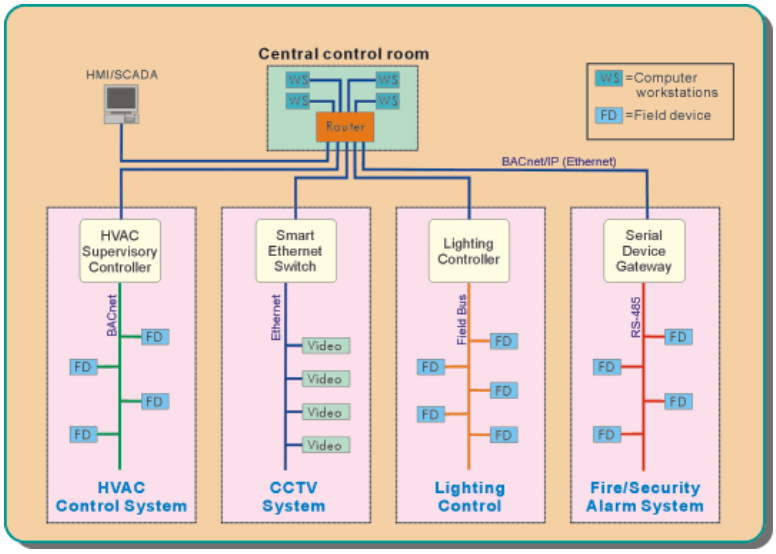

Figure 8.5 A typical schematic of BMS

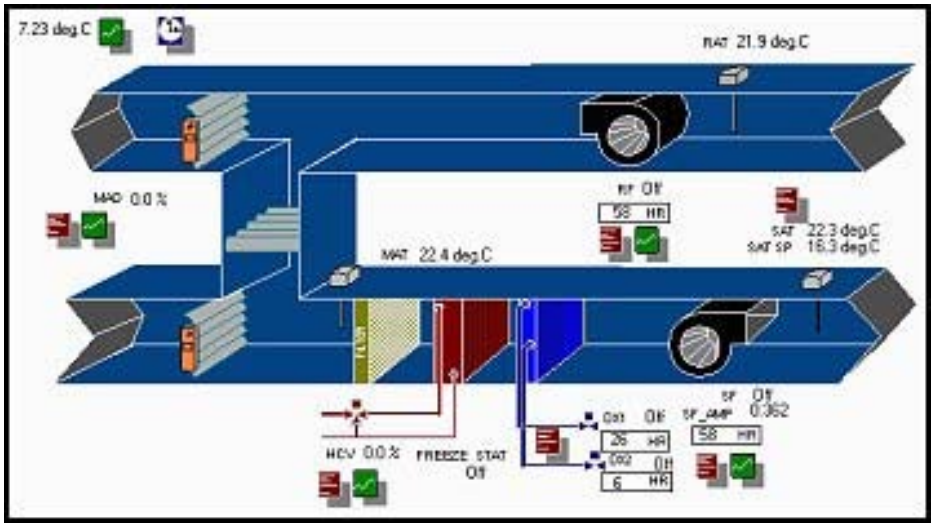

Figure 8.6 Example of graphic display

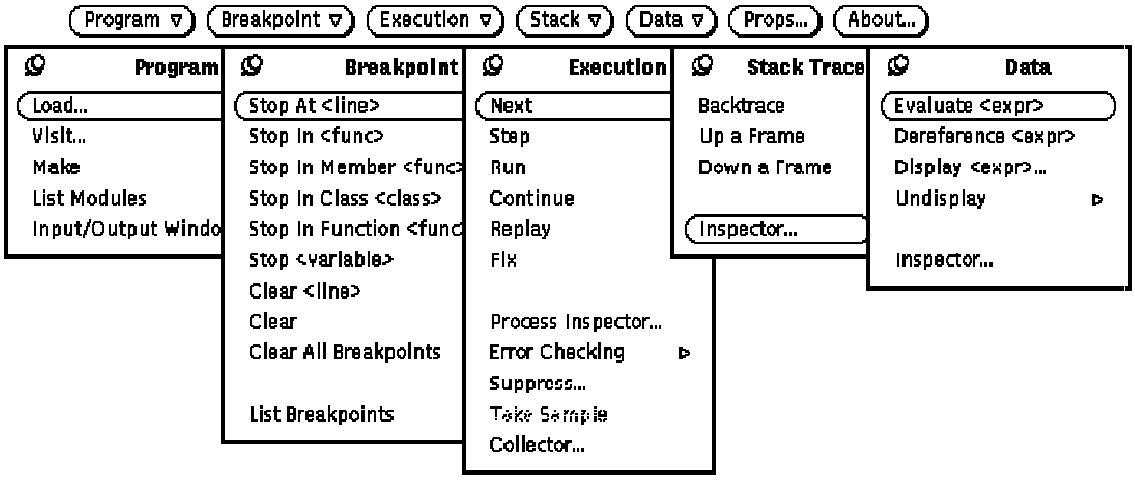

Figure 8.7 Example of window-based interface

The BMS, which was called ‘building brain’, could fulfill many building management functions. Those functions include energy management functions, risk management functions, information processing functions. With the development of information processing functions, FDD technologies, smart maintenance schedule and automatic commissioning tools were worked out recently. FDD technologies could be applied on-line or off-line. Automatic commissioning is the further developed technology of FDD. Off-line process is carried out based on the recorded monitoring data as demonstrated in the above section. On-line technology is more advanced, which could detect/analyze faults when the system is running and produce the report concurrently. Applying this technology could not only detect fault, but also reflect the analysis results to the system for better control or even data recovery and fault-tolerant control.

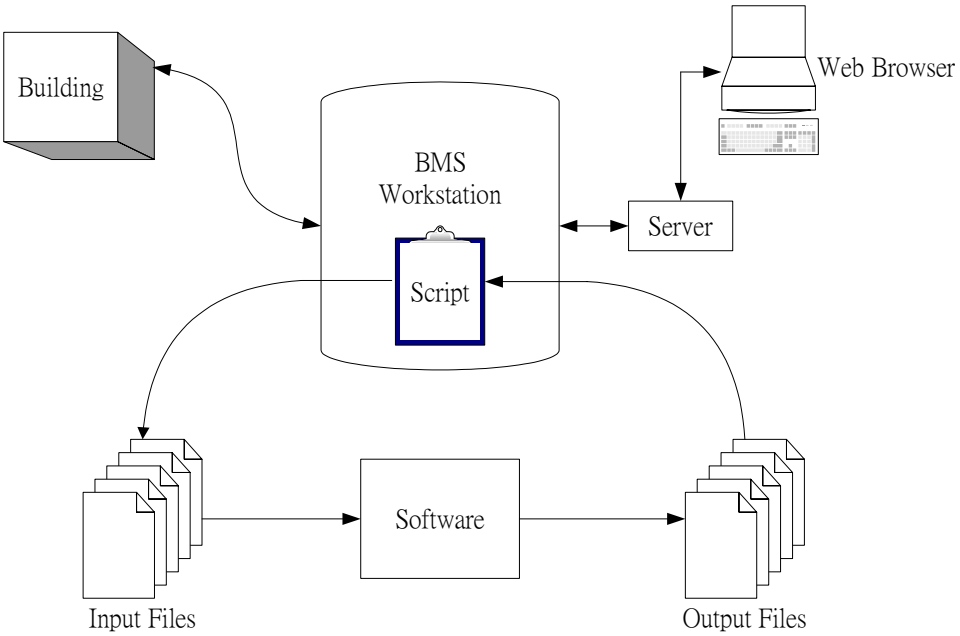

Figure 8.8 Schematic of integration of the software with BMS

The commissioning software package developed in this study could also be implemented for on-line commissioning with the assistance of the BMS by integrating the software package with the BMS automatically. Figure 8.8 shows the schematic of integration of the automatic commissioning software package with the BMS. Computer and network techniques should be employed to build various standard interfaces between the BMS, the commissioning software as well as buildings or remote clients.

A script should be coded and added to the BMS to customize the application. The script mainly assumes functions of scheduling and communication. It sends variables to be monitored to the commissioning application software in the text file format with the pre-defined names as the software demands, and then sends back the FDD results to the BMS. The FDD results should include a main FDD report and all output text files. The main FDD report list the fault detection indices (FF1-8) of the terminals and

the output text files include the characteristic data for fault detection and recovered data for fault-tolerant control.

A commissioning schedule is pre-set according to the VAV system on/off schedule. When the time is out of the schedule, the commissioning application will not be executed. When it is within the schedule, the commissioning of VAV air distribution systems is implemented automatically by sending a command to the system through the interface. The remote users/clients can also open a web page to view the results using internet techniques.

8.5 Summary

The software package to implement the automatic commissioning tool in real VAV systems was developed. The application of the software package was tested using both the simulated data and real building data. The inputs of the software package are in the format of text files. The software package could not only detect the faults, but also recover the VAV flow sensor readings, which was stored in a output text file. The reliability of the VAV system operation would be improved by applying this commissioning software package.

The commissioning tool is also planned to be connected to BMSs, buildings and the remote users. Thus the commissioning of VAV air distribution systems could be implemented automatically by sending a command to the system.

CHAPTER 9 CONCLUSION AND RECOMMENDATION

To ensure the proper control, all components and sensors are playing essential roles in VAV systems. FDD technologies and automatic commissioning tools, which ensure that systems are designed, installed, tested and capable of being operated and maintained to perform in conformity with design intent automatically, are of great interest. VAV air distribution systems suffer from component failure and sensor failure easily. However, manual commissioning for the operating VAV systems is impractical as many VAV terminals are involved and most of them are inaccessible. The automatic commissioning tools developed from the FDD strategies are desirable.

Literature survey shows that study on the faults of VAV terminals is far from sufficient, particularly concerning the system integrating a large number of VAV terminals. Most significant technical problem perceived in VAV systems is interaction among VAV units equipped with a control loop, where information exchange takes place between several control strategies.

Sensors play essential roles in BMSs to realize automatic monitoring and control of HVAC systems. Reliable sensors are necessary for reliable monitoring and control. At the same time, the performance of FDD methods applied in HVAC systems depends strongly on the quality and reliability of sensor measurements. However, sensors may suffer from both hard fault (complete failure) and soft fault (bias or drift), which may give wrong FDD results. Therefore, sensor fault detection and diagnosis are essential to achieve the reliable FDD results. The study on sensor FDD of VAV air distribution systems is insufficient too.

BMSs are widely employed in modern buildings. The huge amount of data available on BMS central stations and outstations provide rich information for monitoring, optimization and FDD of HVAC systems. Also, BMS provides essential and rich information for VAV air distribution system fault detection and diagnosis, which offer the hardware basis for the application of the automatic commissioning tool to the systems.

Conclusions on the FDD Strategy and Its Main Contributions

This thesis presented a robust FDD strategy for typical pressure-independent VAV air distribution system with eleven root faults are of concern. The FDD ability of FDD schemes within the strategy and the interaction among the FDD schemes were tested and validated using dynamic simulation data, real BMS data and in-situ tests. The automatic commissioning software package was developed from the FDD strategy. This commissioning tool was applied to both the simulated building and the real building. The major contribution of this thesis is that an applicable automatic commissioning tool for VAV air distribution system is developed and validated.

These eleven root faults analyzed by the FDD strategy were summarized through physical system analysis and site investigation, which covered both component faults and sensor faults of VAV air distribution systems. The strategy deals with the root faults in VAV air distribution systems, which were extracted from practical pressure-independent VAV systems and their faulty patterns observed during a re-commissioning exercise of all VAV terminals in a large-scale commercial building.

When system interaction is of concern, the conventional FDD based on quantitative models suffers from the lack of ability to handle qualitative knowledge especially under complex circumstances like VAV air distribution systems. As

integrating quantitative models with qualitative knowledge helps to solve decision making problems more effectively and efficiently, an overall architecture integrating system structure, qualitative reasoning and quantitative models are adopted for VAV FDD. The architecture consists of two levels of frames. The first level presents the physical knowledge about the system structure. On the second level, the qualitative/quantitative reasoning is conducted.

Integration of qualitative reasoning and quantitative computation in fault diagnosis was widely used in some fields like artificial intelligence, chemical engineering. Recently, some researchers (Zhou et al. 1994) constructed an intelligent system for operation planning in HVAC processes using important expertise, qualitative reasoning and quantitative computation. Thus qualitative/quantitative reasoning was introduced into the HVAC field. However, the application of qualitative/quantitative reasoning in HVAC FDD has not been well developed. The FDD strategy developed in this thesis fully uses the available BMS information and takes benefits from both qualitative reasoning and quantitative computation.

The FDD strategy for multiple VAV faults forms within the overall architecture. The FDD structure is set up based on the conceptual system model by fault grouping and ordering. The eleven faults are classified into eight groups. Eight FDD schemes are then developed for the eight groups of faults.

Scheme 1 for Fault 1 and Scheme 7 for Fault 8/9/10 are set up based on quantity analyzers. SPC models are finally used to detect the faults. Scheme 2 for Fault 2, Scheme 5 for Fault 6 and Scheme 8 for Fault 11 are built up based on qualitative structure supplemented with SPC models. Under these schemes, the relevant faults could be detected by the SPC models when the qualitative values are within the range

defined by the landmark points. The detection of Fault 3 by Scheme 3 and the detection of Fault 7 by Scheme 6 are easier as causality analyzer works for them. The detection of Fault 5 by Scheme 4 could be achieved by analyzing its qualitative state.

Under Scheme 8, SPC models for fault detection are constructed based on PCA method. PCA produces a lower dimensional representation in a way that preserves the correlation structure between the process variables. For VAV terminal flow sensor bias detection, PCA models at both system and terminal levels are built and employed. Sensor faults are detected using both T^2 statistic and *SPE* and isolated using *SPE* contribution plot. With the measurements recovered based on the terminal model, the sensitivity and robustness of the FDD scheme is enhanced by iteration process(es).

The interaction among the faults and FDD schemes are carefully studied. To construct the efficient commissioning tool from the FDD strategy, the schemes for hard fault detection are put at Step 1 and the scheme for sensor bias detection is put at Step 2 in the strategy. The information of the fault detection results under individual schemes are shared by all the schemes to ensure the robustness of the FDD results.

Based on the BMS database, the input data files were prepared to run the commissioning software and generate the results. The commissioning software was developed on the platform of FORTRAN 90, which included a FDD main program, eight functional modules (subroutines) for eight schemes, VAV flow sensor fault isolation module (subroutine) and some mathematical modules (subroutines). The reconstructed flow sensor readings were stored in a text file, which could be used for fault-tolerant control.

The IEA working group (Annex 40) is working on developing and validating prototype software that could be implemented in stand-alone tools and/or embedded in

BMSs. The commissioning tool developed in this thesis is different from those prototype software as it developed from qualitative/quantitative reasoning rather than system identification models. The effectiveness of the commissioning tool was testified by the simulated system and real systems.

Summary on Performances of FDD Schemes and Commissioning Tool

The SPC research involves two major stages, the univariate process control and the multivariate process control. Traditional univariate statistical control chart, the Shewhart chart, is used to monitor the process control in this study. Two very effective alternatives to the Shewhart control chart are also used when small shifts are of interest: the cumulative sum (CUSUM) control chart, and the exponentially weighted moving average (EWMA) control chart. Reversal counting and sensor frozen detection are based on these SPC techniques. PCA method is applied in multivariate process monitoring. Object-oriented numerical models based on statistical process control techniques are set up to finally identify the fault(s) when pure qualitative reasoning could not provide enough information to affirm the fault(s) under some FDD schemes (Scheme 1/2/5/7/8) of the strategy.

The faulty patterns of faults under other schemes (Scheme 3/4/6) of the strategy are straightforward. Therefore the faults could be detected directly by characteristic equations or qualitative states. Scheme 3 and 4 work when they receive the result of "No" from Scheme 2 while Scheme 6 is independent. The schemes and strategy were validated by both simulation and in-situ tests respectively.

Scheme 1/2/5 take both advantage of qualitative knowledge and SPC models for reversal counting and sensor reading frozen detection. All these three schemes are robust and independent as the fault detection results of the other schemes would not

affect their fault detection ability. The robustness of the schemes was verified by both simulation and in-situ tests.

Scheme 7 deals with the fault detection and diagnosis of Fault 8 (poor tuning of VAV controllers), Fault 9 (damper sticking) and Fault 10 (damper hysteresis). Because cascade control is used in VAV pressure-independent systems, poor tuning of VAV controllers include poor tuning of flow controllers and poor tuning of temperature controllers. Therefore, four main faulty patterns are involved in this scheme. They are temperature set-point not satisfied, airflow set-point not satisfied, instability of airflow set-point and instability of the measured flow.

With multiple faults involved in Scheme 7, FDD should be studied carefully. The airflow control loop is analyzed first and the temperature control loop is analyzed afterwards. Both quantity analyzer and SPC models are employed for FDD. As Fault 1-7 might affect the FDD results under Scheme 7, this scheme is effective when it receives "fault free" signals from Scheme 1-6. The FDD ability of this scheme is verified by the simulation tests and further supported by the in-situ tests.

The basic method employed in Scheme 8 was the PCA method. The PCA method was chosen because it is quite suitable for detection and diagnosis of VAV terminal flow sensor faults. On the one hand, although correlations exist among variables in VAV air distribution systems due to hydraulic balance, it is not easy to precisely represent the correlations using physical equations. The PCA method uses the covariance or correlation matrix to depict correlations among variables in a process. It does not require complex physical models of the dynamic and nonlinear air-conditioning system and its components, nor does it need to train complex mathematic

models such as black-box models. Problems caused by model uncertainty and training complexity are avoided.

In order to apply the PCA method to detect terminal flow sensor biases, PCA models at the system level and the terminal level were built and used in serial to reduce the effects of multiple faults and other disturbance. The advantage of both T^2 statistic *SPE* was utilized by employing the statistics together to isolate the sensor fault from the process upsets. When no fault exists, T^2 and *SPE* are less than the thresholds. On the contrary, when faults exist, the correlation among the measurements of variables will be destroyed, higher value(s) of T^2 and/or *SPE* is detected. The VAV terminal FDD scheme is developed by using both statistics. Because the PCA method is a pure data-driven method and uses no knowledge about the concerned processes, its weakness in fault diagnosis is inevitable. It was found that multiple hard faults (Fault 1-10) should be cleared up before applying the PCA models for terminal flow sensor bias analysis.

The contribution plot approach has been widely used to isolate the faulty sensor after the *SPE* detects an abnormality. The approach compares the contribution of each variable in T^2 and *SPE* when fault(s) has been detected. The variables which make major contributions to this deviation are easily observed. This approach needs less computational load but can isolate multiple faults. Although its isolation ability is weak when dealing with sensor faults whose effects may propagate to other parts of the process, the approach is applicable in this study as terminal flow sensors are not used to control other processes. Because physical knowledge about the system hydraulic balance was planted into the data-driven PCA method, the PCA-based sensor FDD scheme became more understandable, and provided much better fault detection and isolation results.

It is common for multiple sensor faults existence but the system level FDD may not isolate all of them by contribution plot simultaneously because significant sensor errors dominate the *SPE* contribution. The left faulty sensor(s) can be further isolated by the iterative FDD process after replacing the faulty sensor with the recovered one. The scheme terminates until T^2 and *SPE* at the system level not indicating any more sensor faults after all the isolated faulty sensors are recovered. Consequently, the sensitivity and robustness of the FDD scheme are enhanced significantly particularly for multiple faults.

Both the simulation tests and site data from the BMS of a real building in Hong Kong proved that the scheme was effective. The robustness of the scheme against multiple sensor faults was also checked and validated.

The major weakness of the PCA-based FDD methods is that the PCA model, once built from the training data, remains unchanged, while air distribution processes are time varying due to the changing operating conditions. Although the PCA method aims at capturing as much as possible normal variation in the process from the training data, the PCA model could not capture the system characteristics if the training data are insufficient. But if the training data spread in too large range, the sensitivity of the PCA model would be affected because the variations caused by the sensor faults are not significant compared with modeling error. Therefore, there must be sufficient training data to capture the correlations while training data must not spread in too large range when the operation condition is concerned.

It is inappropriate to use a time-invariant model to monitor a time varying process with normal shifts. Experiences show that, when applying PCA-based flow sensor FDD scheme to real buildings, the training matrix should be carefully constructed. As

the operating condition varies according to the weather conditions, occupancy and internal loads, the training matrix selected should represent appropriate coverage of system operating conditions.

The FDD strategy provides a simple and effective tool for automatic commissioning of VAV air distribution systems, which was realized by a software package developed using FORTRAN 90. The software was developed with a hierarchical structure and could be further integrated with BMSs. The commissioning tool was implemented in both the simulated building and the real building. The applicability was testified by in-situ validation after the real building implementation.

Further Investigation

It is worth making further investigations into a few aspects of the research presented in this thesis. The strategy developed in this thesis has a powerful ability in detecting and diagnosing multiple faults in pressure-independent VAV air distribution systems. The BMS assisted commissioning tool developed from the FDD strategy realized the automatic continuous commissioning of the system. However, the automatic controller tuning processes are not included in the study. Many researchers had been working on the controllers intensively. Automatic tuning is now a quite mature technique and could be incorporated into the commissioning package developed in this study.

In this thesis, some FDD schemes work only under condition that they receive the "fault free" signals from the other associated schemes. Although the probability is small, there is a chance that more than one associated faults exist in the system. Some FDD schemes may not detect the relevant fault(s) as they receive the signals of "fault detected" from the associated schemes. Thus the multiple faults may not be detected

simultaneously by the strategy developed. Therefore, it would be valuable to improve the robustness of the strategy with regard to detecting all faults. Furthermore, more field case studies would be valuable to increase confidence in the developed schemes and strategy and to promote it for practical applications.

PCA-based terminal flow sensor bias detection scheme (Scheme 8) not only detects the faulty sensor(s), but also retrieves the measurements for the faulty sensor(s). These reconstructed data could be further used for basic VAV terminal control and some advanced supervisory control to save energy. Fault-tolerant control strategies are worth studying.

Finally, the commissioning tool for real building application could be improved. As a typical VAV air distribution system may have many VAV terminals and a large-scale building own many VAV systems, huge amount of data transfer is required for automatic commissioning tool implementation. To improve the reliability and the flexibility of the commissioning tool, Scheme 1-7 for VAV terminal hard fault (Fault 1-10) detection are recommended to floor level BMS control stations as an online version. Additional works and further cooperation with manufacturers are needed to develop the online versions.

REFERENCES

Ahn, B.C., Mitchell, J.W. and Mclntosh, I.B.D. 2001. Model-based fault detection and diagnosis for cooling towers. ASHRAE Transactions, Vol.107 (Part 1), pp: 839-846.

Annex 40 work program, http://www.commissioning-hvac.org/

Astrom, K. and Hagglund, T. 1995. PID Controllers: Theory, Design, and Tuning. Instrument Society of America.

Bailey, M.B. 1998. The Design and Viability of a Probabilistic Fault Detection and Diagnosis Method for Vapor Compression Cycle Equipment. Ph.D. Thesis, School of Civil Engineering, University of Colorado.

Brambley, M., Pratt, R., Chassin, D., Katipamula, S. and Hatley, D. 1998. Diagnosis for outdoor air ventilation and economizers. ASHRAE Journal Oct., pp: 49-55.

Braun, J.E. 1988. Methodologies for the design and control of central cooling plants. Ph.D. thesis, University of Wisconsin, Madison.

Breuker, M.S. and Braun, J.E. 1998a. Common faults and their impacts for rooftop air conditioners. International Journal of HVAC&R Research, Vol.4(3), pp: 303-318.

Breuker, M.S. and Braun, J.E. 1998b. Evaluating the performance of a fault detection and diagnostic system for vapor compression equipment. International Journal of HVAC&R Research, Vol.4(4), pp: 401-425.

Choiniere, D. and Beaudoin, S. 2000, Fault detection and diagnosis tool for VAV boxes. IEA Annex 34 Meeting, 12th to 14th of April 2000, Liege, Belgium.

CIBSE 1996, Commissioning Code, Air distribution systems, Code A.

Claridge, D., Liu, M.S. and Turner, W.D. 1999. Whole Building Diagnostics. http://poet.lbl.gov/diagworkshop/proceedings.

Comstock, M.C. and Braun, J.E. 1999. Development of Analysis Tools for The Evaluation of Fault Detection and Diagnostics in Chillers. Report #HL99-20. Purdue University, Ray W. Herrick Laboratories, West Lafayette, IN.

Crawley, D.B., Pedersen, C.O., Lawrie, L.K., and Winkelmann, F.C. 2000. EnergyPlus: Energy Simulation Program. ASHRAE Journal Apr., pp: 49-56.

Dean, R.H. and Ratzenberger, J. 1985. Stability of VAV terminal unit controls. Heating, Piping & Air Conditioning, Vol.57(10), pp: 79-90.

Desborough, L. and Harrris, T. 1992. Performance assessment measures for univariate feedback control. Can. J. Chem. Eng., Vol.70, pp: 1186-1197.

Dexter, A.L., and Benouatets, M. 1996. A generic approach to identifying faults in HVAC plants. ASHRAE Transactions, Vol.102 (Part 1), pp: 550-556.

Dexter, A.L. and Ngo, D. 2001. Fault diagnosis in air-conditioning systems: a multi-step fuzzy model-based approach. International Journal of HVAC&R Research, Vol.7(1), pp: 83-102.

Dexter, A.L. and Pakanen, J. 2001. ANNEX 34 Final Report. International Energy Agency.

Dodier, R.H., Curtiss, P.S. and Kreider, J.F. 1998. Small-scale on-line diagnosis for an HVAC System. ASHRAE Transactions, Vol.104(Part 1), pp: 530-539.

Doymaz, F., Romagnoli, J.A. and Palazoglu, A. 2001. A strategy for detection and isolation of sensor failures and process upsets. Chemometrics and Intelligent Laboratory Systems Vol.55, pp: 109-123.

Dunia, R., Qin, S.J., Edgar, T.F. and McAvoy, T. 1996. Identification of faulty sensors using principal component analysis. AIChE Journal, Vol.42(10), pp: 2797-2812.

Fasolo, P. S. and Seborg, D. E. 1995. Monitoring and fault detection for an HVAC control system. International Journal of HVAC & R Research, Vol.1(3), pp: 177-193.

Fornera, L., A.S. Glass, P.Gruber and J. Todtli. 1996. Qualitative fault detection based on logical programming applied to a variable air volume air-handling unit, Control Engineering Practice, Vol.4(1), pp: 105-119.

Ghiaus, Cristian. 1999. Fault diagnosis of air conditioning systems based on qualitative bond graph. Energy and Buildings, Vol.30(3), pp: 221-232.

Glass, A.S., Gruber, M.R. and Todtli, J. 1995. Qualitative model-based fault detection in air-handling units. IEEE Control Systems Magazine, Vol.15(4), pp: 11-22.

Gordon, J. M. and Ng, K. C. 1995. Predictive and diagnostic aspects of a universal thermodynamic model for chillers. International Journal of Heat and Mass Transfer, Vol.38(5), pp: 807-818.

Han, C.Y., Xiao, Y.F. and Ruther, C.J. 1999. Fault detection and diagnosis of HVAC systems. ASHRAE Transactions, Vol.105(Part 1), pp: 568-578.

Haves, P., Jorgensen, D.R., Salsbury, T.I. and Dexter, A.L. 1996. Development and testing of a prototype tool for HVAC system commissioning, ASHRAE Transactions, Vol.102(Part 1), pp: 467-475.

Haves, P. 1999. Overview of diagnostic methods. Proceedings of diagnostics for commercial buildings: from research to practice. San Francisco, CA.

House, J.M. and Kelly, G. (NIST). 1999. An Overview of Building Diagnostic. http://poet.lbl.gov/diagworkshop/procedings.

House, J.M., Lee, W.Y. and Shin, D.R. 1999. Classification techniques for fault detection and diagnosis of an air-handling unit. ASHRAE Transactions, Vol.105(Part 1), pp: 1087-1100.

House, J.M., H. Vaezi-Nejad, J.M. Whitcomb. 2001. An expert rules set for fault detection in air handling units/discussion. ASHRAE Transactions, Vol.107(Part 1), pp: 858-871.

House, J.M., Lee, K.D. and Norford, L.K., 2003. Controls and diagnostics for air distribution systems. Journal of Solar Energy Engineering, Transactions of the ASME, Vol.125(3), pp: 310-317.

Hung, C.Y.S., Lam, H.N. and Dunn, A. 1999. Dynamic performance of an electronic zone air temperature control loop in a typical variable-air-volume air conditioning system. International Journal of HVAC&R Research, Vol.5(4), pp: 317-337.

Hyvärinen, E. J. and Kärki, S. 1996. Building Optimization and Fault Diagnosis Source Book. IEA Annex 25, Technical Research Center of Finland.

Jackson, J.E. 1991. A User's Guide to Principal Components, John Wiley & Sons INC.

Kalogirou, S.A., Neocleous, C.C. and Schizas, C.N. 1997. Heating load estimation using artificial neural networks. Proc. CLIMA 2000 Conf., Brussels, Belgium.

Kamimura, K., Yamada, A., Matsuba, T., Kimbara, A., Kurosu, S. And Kasahara, M. 1994. CAT (computer-aided tuning) software for PID controllers. ASHRAE Transactions, Vol.100 (Part 1), pp: 180-190.

Katipamula, S., Pratt, R.G., Chassin, D.P., Taylor, Z.T., Gowri, K. and Brambley, M.R. 1999. Automated Fault Detection and Diagnosis for Outdoor Air Ventilation System and Economizers: Methodology and Results from Field Testing. ASHRAE Transactions, Vol.105(Part 1), pp: 555-567.

Kelso, R.M. and Salsbury, T.I. Commissioning via System Identification and Design Models. http://www.commissioning-hvac.org/

Klein, S.A. et al. 1990. TRNSYS-A Transient Simulation Program, User manual Version 13.1.

Kuipers, Benjamin 1994. Qualitative Reasoning Modeling and Simulation with Incomplete Knowledge. The MIT Press, Cambridge, Massachusetts, London, England.

Lee, W.Y., House, J.M. and Shin, D.R. 1997. Fault Diagnoses and Temperature Sensor Recovery for an Air-Handling Unit. ASHRAE Transactions, Vol.103(Part 1), pp: 621-633.

Legg, R.C. 1986. Characteristics of single and multi-blade dampers for duct air systems. Building Services Engineering Research and Technology, Vol.7(4), pp: 129-145.

Li, M. and Levermore, G. J. 2000. Stability analysis for a vav test rig. Building Services Engineering Research and Technology, Vol.21(4), pp: 225-232.

Linder, R. and Dorgan, C. B. 1997. VAV systems work despite some design and application problems. ASHRAE Transactions, Vol.103 (Part2), pp: 807-813.

Liu, X.F. and Dexter, A. 2001. Fault-tolerant supervisory control of VAV air-conditioning systems. Energy and Buildings, Vol.33, pp: 379-389.

MacGregor, J.F., Jaeckle, C., Kiparissides, C. and Koutoudi, M. 1994. Process Monitoring and Diagnosis by Multiblock PLS Method. AIChE Journal, Vol.40(5), pp: 826-838.

McGhee, J., Henderson, I.A. and Baird, A. 1997. Neural Networks Applied for the Identification and Fault Diagnosis of Process Valves and Actuators. Measurement, Vol.20(4), pp: 267-275.

McIntosh, I.B.D., Mitchell, J.W. and Beckman, W.A. 2000. Fault detection and diagnosis in chillers, part 1: model development and application. ASHRAE Transactions, Vol.106 (Part 2), pp: 268-282.

Montgomery, D.C. 2001. Introduction to Statistical Quality Control. John Wiley & Sons, Inc.

Ngo, D. and Dexter, A.L. 1999. A robust Model-based Approach to Diagnosing Faults in Air-handling units. ASHRAE Transactions, Vol.105(Part 1), pp: 1078-1086.

Norford, L.K., Wright, J.A., Buswell, R.A., Luo, D. et al. 2002. Demonstration of Fault Detection and Diagnosis Methods for Air-Handling Units (ASHRAE 1020-RP). International Journal of HVAC&R Research, Vol.8(1), pp: 41-71.

Norvilas, A., Negiz, A., DeCicco, J. and Cinar, A. 2000. Intelligent Process Monitoring by Interfacing Knowledge-based Systems and Multivariate Statistical Monitoring. Journal of Process Control, Vol.10, pp: 341-350.

Piette, M.A., Kinney, S.K. and Philip, H. 2001. Analysis of An Information Monitoring and Diagnostic System to Improve Building Operation. Energy and Buildings, Vol.33 (8), pp: 783-791.

Qin, S. J. and Dunia, R. 2000. Determining the number of principal components for best reconstruction. Journal of Process Control, Vol.10, pp: 245-250.

Rossi, T.M. and Braun, J.E. 1996. Minimizing operating costs of vapor compression equipment with optimal service scheduling. International Journal of HVAC&R Research, Vol.2(1), pp: 3-26.

Rossi, T.M. and Braun, J.E. 1997. A statistical, rule-based fault detection and diagnostic method for vapor compression air conditioners. International Journal of HVAC&R Research, Vol.3(1), pp: 19-37.

Russell, E.L., Chiang, L.H. and Richard, D.B. 2000. Data-Driven Techniques for Fault Detection and Diagnosis in Chemical Process. London: Hong Kong, Springer.

Salsbury, T.I. 1999. A practical algorithm for diagnosing control loop problems. Energy and Buildings, Vol.29, pp: 217-227.

Schein, J. and House, J.M. 2003. Application of control charts for detecting faults in variable-air-volume boxes. ASHRAE Transactions, Vol.109(Part 2), pp: 671-682.

Seem, J.E. 1997. Implementation of a new pattern recognition adaptive controller developed through optimization. ASHRAE Transactions, Vol.103(Part 1), pp: 494-506.

Seem, J.E. 1998. A new pattern recognition adaptive controller with application to HVAC system. Automatica, Vol.34(8), pp: 969-982.

Seem, J.E., House, J.M. and Monroe, R.H. 1999. On-line monitoring and fault detection. ASHRAE Journal Jul., pp: 21-26.

Shaw, S.R., L.K. Norford, D. Luo, and S.B. Leeh. 2002. Detection and diagnosis of HVAC faults via electrical load monitoring. International Journal of HVAC & R Research, Vol.8(1), pp: 13-40.

Stylianou, M. and Nikanpour, D. 1996. Performance monitoring, fault detection, and diagnosis of reciprocating chillers, ASHRAE Transactions, Vol.102(Part1), pp: 615-627.

Stylianou, M. 1997. Application of classification functions to chiller fault detection and diagnosis. ASHRAE Transactions, Vol.103(Part1), pp: 645-656.

Tong, H. W. and Crowe, C. M. 1995. Detection of gross errors in data reconciliation by principal component analysis. AIChE Journal Vol.41(7), pp: 1712-1722.

Tsubota, Y., Shioya, M. and Sagara, N. Development of an HVAC control system commissioning tool “HVAC Control Logic Tracer”, http://www.commissioning-hvac.org/

Visier, J.C. et al. 2005. ANNEX 40 Final Report. International Energy Agency.

Wang, S.W. 1999. Dynamic simulation of building VAV air-conditioning system and evaluation of EMCS online control strategies. Building and Environment, Vol.34, pp: 681-705.

Wang, S.W. and Chen, Y.M. 2001. Fault-tolerant control for outdoor ventilation air flow rate in building based on neural network. Building and Environment, Vol.37(7), pp: 691-704.

Wang, S.W. and Cui, J.T. 2005. Sensor fault detection, diagnosis and estimation in centrifugal chiller systems using Principal Component Analysis Method, Applied Energy, in print.

Wang, S.W. and Jiang, Z.M. 2004. Valve fault detection and diagnosis based on CMAC neural networks. Energy and Buildings, Vol.36(6). pp 599-610.

Wang, S.W. and Jin, X.Q. 1998. CO_2-based occupancy detection for on-line outdoor air flow control. Indoor and Built Environment, Vol.7(3), pp: 165-181.

Wang, S.W. and Wang, J.B. 1999. Law-based sensor fault diagnosis and validation for building air-conditioning systems. International Journal of HVAC&R Research, Vol.5(4), pp: 353-380.

Wang, S.W., Wang, J.B. and Burnett, J. 2001. Validating BMS sensors for chiller condition monitoring. Transactions of the Institute of Measurement and Control, Vol.23(4), pp: 201-225.

Wang S.W. and Wang, J.B. 2002. Robust sensor fault diagnosis and validation in HVAC systems. Transactions of the Institute of Measurement and Control, Vol.24(3), pp: 231-262.

Wang, S. W. and Xiao, F. 2004a. AHU sensor fault diagnosis using principal component analysis method. Energy and Buildings, Vol.36, pp: 147-160.

Wang, S. W. and Xiao, F. 2004b. Detection and diagnosis of AHU sensor faults using principal component analysis method. Energy Conversion and Management, Vol.45, pp: 2667-2686.

Wang, S.W. and Xu, X.H. 2002. A robust control strategy of combined DCV and economizer control for air-conditioning systems. Energy Conversion and Management, Vol.43(18), pp: 2569-2588.

Wang, Y. and Chen, J. 1995. Framework of decision analysis integrating qualitative reasoning and quantitative models. Proceedings of the IEEE International Conference on Systems, Man and Cybernetics, Vol.1, pp: 346-350.

Yoshida, H., Iwami, T., Yuzawa, H. and Suzuki, M. 1996. Typical Faults of Air-conditioning Systems and Fault Detection by ARX Model and Extended Kalman Filter. ASHRAE Transactions, Vol.102(Part 1), pp: 557-564.

Yoshida, H., and Kumar, S. 1999. ARX and AFMM model-based on-line real-time data base diagnosis of sudden fault in AHU of VAV system. Energy Conversion and Management, Vol.40, pp: 1191-1206.

Yoshida, H., Kumar, S. and Morita, Y. 2001. Online fault detection and diagnosis in VAV air handling unit by RARX modeling. Energy and Buildings, Vol.33(4), pp: 391-401.

Yu, C.C. and Lee, C. 1991. Fault diagnosis based on qualitative/quantitative process knowledge. AIChE Journal, Vol.37(4), pp: 617-628.

Zhang, Z. and Nelson, R. M. 1992. Parametric analysis of a building space conditioned by a VAV system. ASHRAE Transactions, Vol.98 (Part 1), pp: 43-48.

Zhou, H., Rao, M. and Chuang, K.T. 1994. Integrated operation planning: intelligent system approach for HVAC processes. Journal of Intelligent and Robotic Systems: Theory & Applications, Vol.10(1), pp: 59-78.

Zhu, Y. X. 1993. TRNSYS model: Fluid Flow Rate and Pressure Calculation, Tsinghua University, Beijing.

APPENDIX A – NETWORK BALANCE MODEL

(Type57.for)

```
C*******************************************************************
C
      SUBROUTINE TYPE57(TIME,XIN,OUT,T,DTDT,PAR,INFO)
C
C          TYPE 57 : FLUID FLOW RATE AND PRESSURE CALCULATION
C
C          Author:    Yingxin Zhu, the cooperating researcher of Nagoya Univ., Japan
C          Address: Dept. of Thermal Engineering, Tsinghua Univ., Beijing, China
C          Date:       May, 1993
C          Modified by Jean Qin in April 2003
C          PAR(I)--parameters
C               I=1 the pressure of reference node (node 1) (Pa)
C                  2 MODE: 1--AIR, 2--WATER
C                  3 resis. coef. criterion for fully blocked branch [Pa/sq.(m3/s)]
C                  4 amount of flow branches in this network: N
C                  5 amount of pressure nodes in this network: M
C                  6 number of branches with varied flow resistance coefficient
C                                                          i.e. damper/valve: K
C                  7 number of branches with pump/fan: L
C                  8 (inlet node index)*100+(outlet node index) of branch 1(-)
C                     .....
C                  7+N (inlet node index)*100+(outlet node index) of branch N(-)
C                  7+N+1 fixed flow resistance coefficient of branch 1 [Pa/sq.(m3/s)]
C                     .....
C                  7+2N fixed flow resistance coefficient of branch N [Pa/sq.(m3/s)]
C                  7+2N+1 height of outlet above inlet of 1st branch(m)
C                     .....
C                  7+3N height of outlet above inlet of Nth branch(m)
C                  7+3N+1 order number of the 1st branch with varied flow resis. coeff.
C                     .....
C                  7+3N+K order number of the Kth branch with varied flow resis. coeff.
C                  7+3N+K+1 order number of the 1st branch with fan/pump
C                     .....
C                  7+3N+K+L order number of the Lth branch with fan/pump
```

```
C
C       XIN(I)--inputs
C           I=1 varied resistance coefficient of the 1st branch with varied resistance
C                .....
C             N varied resistance coefficient of the mth branch with varied resistance
C             N+1 the pressure rise accross the 1st branch with fan/pump
C                .....
C             N+L the pressure rise accross the Lth branch with fan/pump
C             N+L+1 dP/dG of the 1st branch with fan/pump
C             N+2L  dP/dG of the Lth branch with fan/pump
C
C       OUT(I)--outputs
C           I=1  Supply air total flow rate (Kg/s)
C             2  Supply air total flow rate (Kg/s)
C             3  Supply air total flow rate (Kg/s)
C             4  Return air flow rate (Kg/s)
C             5  Fresh air flow rate (Kg/s)
C             6  Recycled air flow rate (Kg/s)
C             7  Exhaust air flow rate (Kg/s)
C             8  Exfiltration air flow rate (Kg/s)
C             9  Pressure before VAV 1 (Pa)
C             10 Pressure before VAV 2 (Pa)
C             11 Pressure before VAV 3 (Pa)
C             12 Pressure before VAV 4 (Pa)
C             13 Pressure before VAV 5 (Pa)
C             14 Pressure before VAV 6 (Pa)
C             15 Pressure before VAV 7 (Pa)
C             16 Pressure before VAV 8 (Pa)
C             17 Static Pressure at sensor location (Pa)
C             18 Pressure at the occupied space (Pa)
C             19 Pressure at sensor location (Pa)
C             20 Flow rate of VAV Zone 1 (Kg/s)
C             21 Flow rate of VAV Zone 2 (Kg/s)
C             22 Flow rate of VAV Zone 3 (Kg/s)
C             23 Flow rate of VAV Zone 4 (kg/s)
C             24 Flow rate of VAV Zone 5 (Kg/s)
C             25 Flow rate of VAV Zone 6 (Kg/s)
C             26 Flow rate of VAV Zone 7 (Kg/s)
C             27 Flow rate of VAV Zone 8 (Kg/s)
```

```
C
C          IBMAX---the maximum number of branches in a network
C          NODMAX---the maximum number of nodes in a network
C          ISMAX---the maximum number of branches with varied resis. coeff.
C          IFANMAX---the maximum number of branches with fan/pump
C
C          G(I)--- flow rate of branch I (m3/s)
C          S(I)--- flow resistance coefficient of branch I [Pa/Sq.(m3/s)]
C          P(I)--- pressure of node I (Pa)
C          Z(I)--- position difference of outlet over inlet of I branch (m)
C          IA(I,J)---    J: order number of flow branch in the network
C                              I=1: index of inlet pressure node
C                                 2: index of outlet pressure node
C          H(J)--- pressure rise accross fans
C          HH(J)-- dP/dG
C
C**********************************************************************
C
          PARAMETER (IBMAX=30, NODMAX=30, ISMAX=20, IFANMAX=5)

          DIMENSION XIN(ISMAX+2*IFANMAX),OUT(27),
     &    PAR(3*IBMAX+ISMAX+IFANMAX+7),INFO(10)
          DIMENSION IA(2,IBMAX),G(IBMAX),S(IBMAX),H(IBMAX),HH(IBMAX)
      DIMENSION BB(IBMAX,IBMAX),Z(IBMAX),NB(IBMAX),P(NODMAX)
      INTEGER BRNC

      IF(INFO(7).LT.0) THEN
            INFO(6)=27
        INFO(9)=0
      ENDIF
      IF(PAR(2).EQ.1) THEN
       ROU=1.2
      ELSE
       ROU=1000.
      END IF
      BRNC=INT(PAR(4))
      NODE=INT(PAR(5))
      CRON=PAR(3)
      MS=PAR(6)
```

```
NFAN=PAR(7)

      DO 10 I=1,BRNC
      IA(1,I)=INT(PAR(7+I)/100.)
      IA(2,I)=INT(PAR(7+I))-IA(1,I)*100
10          CONTINUE
      FAULT=0.0
      DO 30 I=1,BRNC
       DO 20 J=1,NODE
       IF(IA(1,I).GT.NODE.OR.IA(2,I).GT.NODE) THEN
          FAULT=1.0
          GOTO 40
       ENDIF
20           CONTINUE
30         CONTINUE
40         IF(FAULT.EQ.1.0) THEN
           WRITE(*,*) 'NETWORT CONNECTION DESCRIBTION MISTAKE!'
           PAUSE
      END IF

      DO 70 I=1,BRNC
      NB(I)=I
      S(I)=PAR(7+BRNC+I)
      Z(I)=PAR(7+2*BRNC+I)
           H(I)=0.0
           HH(I)=0.0
70         CONTINUE
      P(1)=PAR(1)
      DO 80 I=1,MS
      J=PAR(7+3*BRNC+I)
80         S(J)=S(J)+XIN(I)
      DO 90 I=1,NFAN
      J=PAR(7+3*BRNC+MS+I)
           H(J)=XIN(MS+I)
90         HH(J)=XIN(MS+NFAN+I)

           CALL NETB(BRNC,NODE,G,H(1),S,NB,IA(1,1),CRON,NM,N1M,BB,IR)

      IF(IR.EQ.1) THEN
```

```
IF(INFO(8).LE.1.) THEN
                DO 110 I=1,8
110             OUT(I)=0.0
                DO 120 I=9,19
120             OUT(I)=P(1)
                DO 130 I=20,27
130             OUT(I)=0.0
            GOTO 160
          ELSE
            WRITE(*,*) 'ERROR:',
       &          ' UNREASINABLE RESISTANCE DISTRIBUTION!'
            WRITE(*,*) 'RESISTANCE=',(S(I),I=1,BRNC)
            STOP
          ENDIF
        ENDIF

            CALL
CCC(BRNC,NODE,S,H(1),HH(1),NM,N1M,G,IA(1,1),Z,NB,1.E-3,BB,ROU,P)

            OUT(1) = G(2)*ROU
            OUT(2) = G(4)*ROU
            OUT(3) = G(5)*ROU
            OUT(4) = G(21)*ROU
            OUT(5) = G(1)*ROU
            OUT(6) = G(24)*ROU

            OUT(7) = G(25)*ROU
            OUT(8) = G(22)*ROU
            OUT(9) = P(6)
            OUT(10)= P(7)
            OUT(11)= P(8)
            OUT(12)= P(9)
            OUT(13)= P(10)
            OUT(14)= P(11)
            OUT(15)= P(12)
            OUT(16)= P(13)
            OUT(17)= P(5)-0.6*(G(5)/0.5/1.2)**2
            OUT(18)= P(14)
            OUT(19)= P(5)
```

```
OUT(20)= G(6)*ROU
          OUT(21)= G(8)*ROU
          OUT(22)= G(10)*ROU
          OUT(23)= G(12)*ROU
          OUT(24)= G(20)*ROU
          OUT(25)= G(14)*ROU
          OUT(26)= G(18)*ROU
          OUT(27)= G(16)*ROU

160       CONTINUE
      RETURN
      END

C ***********************************************************************
C         This program is used to form the basic circuit matrix B
C         after all the broken branches are deleted.
C         Input:
C         N---branch's amount in total
C         N1---node's amount in total
C         IA(j,i)---branches relationship
C                 i--branch's name(i<=N), j=1--from node, j=2--to node
C         S(i)---resistent coefficient of ith branch(mmAq/sq.(kg/hr))
C         G(i)---flow rate initial values of ith branch(kg/hr)
C         SBRO---value of S(i) for defining breaking. When S(i)>SBRO
C                   the branch i is thought broken.
C         H(i)---pressure rise of ith branch with fan
C         NB(i)---ith branch's name(number), input/output
C
C         Output:
C         NM---branch's amount after deleting broken branchs
C         N1M---node's amount after deleting broken branchs
C         BB---basic circuit matrix B
C         IR---error sign. 1: sum of resistances of a circuit is zero
C             but pressure is not zero. 0: normal.
C
C         DD,EE---midle variables
C ********************************************************************** C
      SUBROUTINE NETB(N,N1,G,H,S,NB,IA,SBRO,NM,N1M,BB,IR)
          DIMENSION G(N),H(N),NB(N),S(N),IA(2,N)
```

```
      PARAMETER (IBMAX=30, NODMAX=30)

      DIMENSION BB(IBMAX,IBMAX),SUC(IBMAX)
      COMMON /ACOM/DD(NODMAX,IBMAX),EE(IBMAX,IBMAX)
C =======================================
C      K      ---amount of basic curcuits
C      K1      ---line of network relation matrix
C =======================================
      K=N-N1+1
      K1=N1-1
      DO 60 I=1,N
      L=NB(I)
60     SUC(I)=S(L)
C ----------------------------------
C      make order by smallest SUC(I)
C ----------------------------------
      CALL RCD(N,NB,SUC)
C ------------------------------------------------
C      to form the network relation matrix A       --DD(I,J)
C ------------------------------------------------
      DO 130 I=1,N1
      DO 130 J=1,N
130    DD(I,J)=0.0
      DO 140 I=1,N
      IA1=IA(1,NB(I))
      IA2=IA(2,NB(I))
      DD(IA1,I)=1.
140    DD(IA2,I)=     -1.
C ------------------------------------------------------------
C      to form the smallest tree and basic        curcuit matrix B--EE(i,j)
C ------------------------------------------------------------
      CALL FTFC(N,N1,NB)
C=============================================================
C
C      To delete the broken branches of which S>SBRO
C      Fo      r the broken branches: G(i) is set 0.0, order NB(i) is changed
C      M      --total amount of broken branches
C=============================================================
```

```
      M=0
      DO 150 I=N,N1,-1
      L=NB(I)
      IF(S(L).LE.SBRO) GOTO 150
      G(L)=0.0
      M=M+1
      IF((N-I+1).GT.M) THEN
      SUC(1)=NB(I)
      DO 160 J1=I,N-M
      NB(J1)=NB(J1+1)
      DO 160 J=1,K
160     EE(J,J1)=EE(J,J1+1)
      DO 165 J1=I-K1,K-M
      DO 165 J=1,N
165     EE(J1,J)=EE(J1+1,J)
      NB(N-M+1)=SUC(1)
      ENDIF
150     CONTINUE
      NM=N-M
      KM=K-M

      IF(KM.EQ.0) THEN
      NM=0
      DO 222 I=1,N
222     G(I)=0.
      GOTO 230
      ENDIF
      IF(M.EQ.0) GOTO 230
      I=0
205     I=I+1
      DO 210 J=1,KM
210     IF(EE(J,I).NE.0.) GOTO 200
      M=M+1
      G(NB(I))=0.
      SUC(1)=NB(I)
      DO 220 I1=I,N-M
      NB(I1)=NB(I1+1)
      DO 220 J1=1,KM
```

```
220       EE(J1,I1)=EE(J1,I1+1)
      NB(N-M+1)=SUC(1)
      I=I-1
200       IF(I.LT.(N-M)) GOTO 205
      NM=N-M
C -----------------------------------------------------------------
C           To check how many networks the system is divided by deleting
C           broken branches, and KN is the amount.
C           If no fan/pump branch is existing, to use one network as one
C           to be calculated. Or else the network with fan/pump is chosen
C           as one to be simulated. The flow rates of other branches are set 0.0.
C -----------------------------------------------------------------
      DO 30 I=1,KM
30        DD(I,I)=1.
      DO 70 I=1,KM
      DO 70 J=I+1,KM
      DO 80 II=1,NM
      IF(EE(J,II).NE.0..AND.EE(I,II).NE.0.) THEN
      DD(I,J)=1.
      GOTO 70
      ENDIF
80        CONTINUE
      DD(I,J)=0.
70        CONTINUE
      DO 90 I=KM,2,-1
      DO 95 J=1,I-1
      IF(DD(J,I).EQ.1.) THEN
      DO 100 II=I+1,KM
      IF(DD(I,II).EQ.1.) DD(J,II)=1.
100       CONTINUE
      DD(I,I)=0.
      ENDIF
95        CONTINUE
90        CONTINUE
      DO 170 I=1,KM
      IF(DD(I,I).EQ.0.) GOTO 170
      DO 180 J=1,KM
      IF(J.EQ.I.OR.DD(J,J).EQ.0.) GOTO 180
      DO 185 JJ=J+1,KM
```

```
185       IF(DD(I,JJ).EQ.1..AND.DD(J,JJ).EQ.1.) GOTO 190
      GOTO 180
190       DO 250 JJ=J,KM
250       IF(DD(J,JJ).EQ.1.) DD(I,JJ)=1.
      DD(J,J)=0.
180       CONTINUE
170       CONTINUE
      KN=0
      DO 105 I=1,KM
105       IF(DD(I,I).EQ.1.) KN=KN+1
      IF(KN.EQ.1) GOTO 225
      NK=0
      DO 110 I=1,NM
          IF(H(NB(I)).NE.0.) THEN
      DO 325 J=1,KM
      IF(EE(J,I).NE.0.) THEN
      NK=J
      GOTO 115
      ENDIF
325       CONTINUE
      ENDIF
110       CONTINUE
115       IF(NK.EQ.0) THEN
      DO 120 I=1,KM
120       IF(DD(I,I).NE.0.) NK=I
      ELSE
      DO 270 I=1,NK
      IF(DD(I,I).NE.0..AND.DD(I,NK).NE.0.) THEN
      NK=I
      GOTO 275
      ENDIF
270       CONTINUE
      ENDIF
275       CONTINUE
C    ------------------------------------------------------
C     To form the B matrix of the network you have chosed.
C ------------------------------------------------------
      KN=0
      DO 320 I=NK,KM
```

```
IF(DD(NK,I).EQ.0.) GOTO 320
      KN=KN+1
      IF(KN.NE.I) THEN
      DO 330 J=1,NM
330   EE(KN,J)=EE(I,J)
      ENDIF
320   CONTINUE
      KM=KN
      I=0
340   I=I+1
      DO 350 J=1,KM
350   IF(EE(J,I).NE.0.) GOTO 360
      M=M+1
      G(NB(I))=0.0
      SUC(1)=NB(I)
      DO 370 II=I,N-M
      NB(II)=NB(II+1)
      DO 370 J1=1,KM
370   EE(J1,II)=EE(J1,II+1)
      NB(N-M+1)=SUC(1)
      I=I-1
360   IF(I.LT.(N    -M)) GOTO 340
225   NM=N     -M
230   N1M=NM     -KM+1
C ---------------------
C   B matrix is formed.
C ---------------------
      DO 380 I=1,KM
      DO 380 J=1,NM
380   BB(I,J)=EE(I,J)
C     ----------------------------
C    circuit resistance checking
C     ----------------------------
      IR=0
      DO 400 I=1,KM
      SUMR=0.0
      SUMH=0.0
      DO 410 J=1,NM
      IF(BB(I,J).NE.0.0) THEN
```

```
SUMR=SUMR+S(NB(J))
              SUMH=SUMH+H(NB(J))
      ENDIF
410       CONTINUE
      IF(SUMR.EQ.0.0.AND.SUMH.NE.0.0) IR=1
400       CONTINUE
      RETURN
      END
C ***************************************************************
C           This program is used to calculated the flowrate in a hydrolic network in MKP
C           method.
C
=================================================================
C           Input:
C           S(i)---resistent coefficiencis of ith branch[mmAq/sq.(kg/hr)]C
C           Z(i)---location difference of ith branch outlet over inlet(m)C
C           N---branch's amount after deleting the broken branches
C           M---node's amount after deleting the broken branches
C           N0---original branch's amount in total
C           N1---original node's amount in total
C           IA(i,j)---node linked to jth branch. i=1 from, i=2 to
C           H(i)---pressure rise of ith branch
C           NB(i)---ith branch's order name(number)
C           EG---relative tolerance of G for iteration, dimensionless
C           B(i,j)---basic circuit matrix
C                   j--branch's number, i--circuit's number
C           RO---fluid density(kg/cu.m)
C
C           Output:
C           G(i)---flow rate of ith branch(kg/hr), but initial values are input
C           P(j)---pressure(static+flow) of jth node(mmAq)
C ***************************************************************** C
          SUBROUTINE CCC(N0,N1,S,H,HH,N,M,G,IA,Z,NB,EG,B,RO,P)
          DIMENSION NB(N),Z(N),S(N0),IA(2,N0),H(N0),HH(N0),P(N1),G(N0)
          PARAMETER (IBMAX=30)
      DIMENSION HK(IBMAX),DG(IBMAX),DP(IBMAX),SG(IBMAX),
       &   BB(IBMAX,IBMAX),B(IBMAX,IBMAX)
      IF(N.EQ.0) RETURN
      K=N-M+1
```

```
K9=K+1
      K1=M-1
      DO 300 J=1,N
      I=NB(J)
      DG(I)=0.
          IF(H(I).NE.0..AND.G(I).EQ.0.) G(I)=SQRT(ABS(H(I)))
300       SG(I)=G(I)
      DO 100 ITIME=1,50
          CALL MAXWEL(N0,N,M,S,G,BB,B,NB,HH)
C -------------------------------------------------------------
C           Calculate the pressure deviation of all circuits--HK(i)
C -------------------------------------------------------------
      DO 220 J=1,N
      I=NB(J)
          IF(H(I).NE.0.) THEN
            DP(I)=H(I)
      ELSE
       DP(I)=0.
      END IF
      DP(I)=-S(I)*G(I)*ABS(G(I))+DP(I)
      DP(I)=DP(I)-RO*Z(I)
220       CONTINUE
      DO 4 I=1,K
      HK(I)=0.
      DO 4 II=1,N
      IF(B(I,II).EQ.1.) HK(I)=HK(I)+DP(NB(II))
4         IF(B(I,II).EQ.-1.) HK(I)=HK(I)-DP(NB(II))
C -------------------------------------
C           Inversing the Maxwell matrix BB
C -------------------------------------
      CALL CHOL(BB,IBMAX,K)
C -----------------------------------------
C           Calculating the flow rate deviation
C -----------------------------------------
      DO 10 I=1,K
      L=NB(I+K1)
      DG(L)=0.
      DO 10 J=1,K
10        DG(L)=DG(L)+BB(I,J)*HK(J)
```

```
DO 230 I=M,N
      L=NB(I)
      G(L)=G(L)+DG(L)
230       CONTINUE
      DO 210 I=1,K1
      L=NB(I)
      G(L)=0.
      DO 210 J=M,N
      IF(B(J-K1,I).EQ.1.) G(L)=G(L)+G(NB(J))
210       IF(B(J-K1,I).EQ.-1.) G(L)=G(L)-G(NB(J))
      DO 5 J=M,N
      I=NB(J)
      D=ABS(DG(I))/(ABS(G(I))+1.)
      IF(D.GT.EG) GOTO 100
5         CONTINUE
      GOTO 200
100       CONTINUE
200       CONTINUE
      CALL PP(N,IA,N0,N1,NB,G,H,S,Z,P,RO)
      RETURN
      END
C ********************************************************************
C          This program is used for calculate the static pressure of all nodes.
C ********************************************************************
      SUBROUTINE PP(N,IA,N0,N1,NB,G,H,S,Z,P,RO)
          DIMENSION IA(2,N0),G(N0),S(N0),Z(N),H(N0),P(N1),NB(N)
          PARAMETER (IBMAX=30)
      DIMENSION DP(IBMAX)
C ---------------------------------------------------------
C          Calculate the pressure difference of all branches DP(i)
C ---------------------------------------------------------
      DO 10 I=2,N1
      P(I)=-1.0E+7
10        CONTINUE
      DO 60 J=1,N
      I=NB(J)
      IF(IA(1,I).EQ.1.OR.IA(2,I).EQ.1) GOTO 70
60        CONTINUE
      P(IA(1,NB(1)))=P(1)
```

```
70          CONTINUE
      DO 30 J=1,N
      I=NB(J)
           IF(H(I).NE.0.) THEN
             DP(I)=H(I)
      ELSE
        DP(I)=0.
      END IF
      DP(I)=-S(I)*G(I)*ABS(G(I))+DP(I)
      DP(I)=DP(I)-RO*Z(I)
30          CONTINUE
C -------------------------
40          DO 20 I=1,N
      J=NB(I)
      IF(P(IA(1,J)).GT.-1.E+6.AND.P(IA(2,J)).GT.-1.E+6) GOTO 20
      IF(P(IA(1,J)).GT.-1.E+6) THEN
      P(IA(2,J))=P(IA(1,J))+DP(J)
      ELSE IF(P(IA(2,J)).GT.-1.E+6) THEN
      P(IA(1,J))=P(IA(2,J))-DP(J)
      ENDIF
20          CONTINUE
      DO 50 I=1,N
      J=NB(I)
      IF(P(IA(1,J)).LT.-1E+6) GOTO 40
      IF(P(IA(2,J)).LT.-1E+6) GOTO 40
50          CONTINUE
      DO 80 I=2,N1
80          IF(P(I).LT.-1.E+6) P(I)=P(1)
      RETURN
      END
C ************************************************************C
C       RCD is used for making branches in a line according to S.
C       The branches with smaller S values are put in front of
C       the line, and that with larger S values are put in the end.
C       N---amount of branches, input
C       NB(i)---name of ith branches(number), input/output
C       S(i)---value of ith branched for making line
C ************************************************************ C
      SUBROUTINE RCD(N,NB,S)
```

```
DIMENSION NB(N),S(N)
10        DO 100 I=2,N
      K=I
20        I1=K-1
      IF(S(K).GE.S(I1)) GOTO 100
      SUB=NB(K)
      NB(K)=NB(I1)
      NB(I1)=SUB
      SUB=S(K)
      S(K)=S(I1)
      S(I1)=SUB
      IF(K.GT.2) THEN
      K=K-1
      GOTO 20
      ENDIF
100       CONTINUE
      RETURN
      END
C ************************************************************** C
C           This is a program searching for the smallist tree and
C           constructing the basic circuit matrix B.
C           NO--- branch's amount, input
C           AA----matrix of network relationship, input
C           B---- basic circuit matrix B, output
C ************************************************************** C
      SUBROUTINE FTFC(NO,N1,NB)
      DIMENSION NB(NO)
          PARAMETER (IBMAX=30, NODMAX=30)
      COMMON /ACOM/AA(NODMAX,IBMAX),B(IBMAX,IBMAX)

      K1=N1-1
      K=NO-K1
      DO 10 I=1,K1
      IF(AA(I,I).EQ.0.) THEN
      DO 40 J=I+1,K1
      IF(AA(J,I).NE.0.) THEN
      DO 50 L=1,NO
      SUB=AA(J,L)
      AA(J,L)=AA(I,L)
```

```
50        AA(I,L)=SUB
      GOTO 45
      ENDIF
40        CONTINUE
      DO 55 J=I+1,NO
      DO 55 I1=I,K1
      IF(AA(I1,J).NE.0.) THEN
      DO 65 L=1,K1
      SUB=AA(L,J)
      DO 67 M=J,I+1,-1
67        AA(L,M)=AA(L,M-1)
65        AA(L,I)=SUB
      KUB=NB(J)
      DO 110 M=J,I+1,-1
110       NB(M)=NB(M-1)
      NB(I)=KUB
      DO 120 M=1,NO
      SUB=AA(I1,M)
      AA(I1,M)=AA(I,M)
120       AA(I,M)=SUB
      GOTO 45
      ENDIF
55        CONTINUE
      WRITE(*,*) 'AI IS A STRANG MATRIX!',I
      WRITE(*,*) 'There is mistake in network connection discription!'
      STOP
      ENDIF
45        IF(AA(I,I).EQ.-1.) THEN
      DO 30 J=1,NO
30        IF(AA(I,J).NE.0.) AA(I,J)=-AA(I,J)
      ENDIF
      DO 20 J=I+1,K1
      IF(AA(J,I).NE.0.) THEN
      SUB=AA(J,I)
      DO 60 L=I,NO
60        AA(J,L)=AA(J,L)-SUB*AA(I,L)
      ENDIF
20        CONTINUE
10        CONTINUE
```

```
DO 70 I=K1-1,1,-1
      DO 70 J=K1,I+1,-1
      IF(AA(I,J).NE.0.) THEN
      SUB=AA(I,J)
      DO 80 L=J,NO
80          AA(I,L)=AA(I,L)-SUB*AA(J,L)
      ENDIF
70          CONTINUE
      DO 90 I=1,K
      J=I+K1
      DO 90 J1=1,K
      IF(I.EQ.J1) THEN
      B(J1,J)=1.
      ELSE
      B(J1,J)=0.
      ENDIF
90          CONTINUE
      DO 100 I=1,K
      DO 100 J=1,K1
      B(I,J)=-AA(J,I+K1)
100         CONTINUE
      RETURN
      END
C ************************************************************** C
C           The program is used to construct the Maxwell matrix.
C           BB---maxwell matrix, output
C           N0---amount of branches, input
C           Other variables's meaning see above.
C ************************************************************** C
            SUBROUTINE MAXWEL(N0,N,M,S,G,BB,B,NB,HH)
            DIMENSION S(N0),G(N0),HH(N0),NB(N)
            PARAMETER (IBMAX=30)
      DIMENSION BB(IBMAX,IBMAX),SG(IBMAX),X(IBMAX),AB(IBMAX,IBMAX),
       &    B(IBMAX,IBMAX)
      DO 40 I=1,N
      J=NB(I)
      IF(ABS(G(J)).LE.1.E-6) THEN
         SG(J)=1.E-6
      ELSE
```

```
SG(J)=G(J)
      ENDIF
40        CONTINUE
      K1=M-1
      K=N-K1
      DO 21 J=1,N
      I=NB(J)
          X(I)=HH(I)
      X(I)=X(I)-2.*S(I)*ABS(SG(I))
      X(I)=-X(I)
21        CONTINUE
      DO 10 I=1,K
      DO 10 J=1,K1
      AB(I,J)=0.
      IF(B(I,J).EQ.1.) AB(I,J)=X(NB(J))
10        IF(B(I,J).EQ.-1.) AB(I,J)=-X(NB(J))
      DO 23 I=1,K
      DO 24 J=I,K
      BB(I,J)=0.0
      DO 24 II=1,K1
      IF(B(J,II).EQ.1.) BB(I,J)=BB(I,J)+AB(I,II)
24        IF(B(J,II).EQ.-1.) BB(I,J)=BB(I,J)-AB(I,II)
      BB(I,I)=BB(I,I)+X(NB(I+K1))
23        CONTINUE
      DO 30 I=2,K
      DO 30 J=1,I-1
30        BB(I,J)=BB(J,I)
      RETURN
      END
C ***************************************************************************
C         This is a program used for inversing symmethic, possitively
C         definited matrix with square-root method.
C         A--matrix to be inversed
C         M--max. dimension of data group A
C         N--rank of matrix A
C ***************************************************************************
      SUBROUTINE CHOL(A,M,N)
      DIMENSION A(M,N)
      DO 10 I=2,N
```

```
DO 20 J=1,I-1
      X=0.
      DO 30 K=1,J-1
30          X=X+A(I,K)*A(J,K)
20          A(I,J)=A(I,J)-X
      DO 40 J=1,I-1
40          A(I,J)=A(I,J)/A(J,J)
      Y=0.
      DO 50 K=1,I-1
50          Y=Y+A(I,K)**2*A(K,K)
      A(I,I)=A(I,I)-Y
10          CONTINUE
      DO 60 I=1,N
      DO 70 J=1,I-1
      X=0.
      DO 80 K=J+1,I-1
80          X=X+A(I,K)*A(J,K)
70          A(J,I)=-A(I,J)-X
60          A(I,I)=1/A(I,I)
      DO 90 I=2,N
      DO 90 J=1,I-1
      X=0.
      DO 100 K=I+1,N
100         X=X+A(I,K)*A(J,K)*A(K,K)
90          A(I,J)=A(J,I)*A(I,I)+X
      DO 110 I=1,N
      X=0.
      DO 120 K=I+1,N
120         X=X+A(I,K)**2*A(K,K)
110         A(I,I)=A(I,I)+X
      DO 130 I=1,N-1
      DO 130 J=2,N
130         A(I,J)=A(J,I)
      RETURN
      END
```

APPENDIX B – MAIN PROGRAM (FddVAV.for)

```
C ************************************************************
C    THIS is the main PROGRAM of VAV FDD.
C    THIS PROGRAM READS IN BMS DATA.
C    Nvar is the number of variables in the PCA system matrix.
C    Nbox is the number of variables in the PCA box matrix.
C    Nsmp is the number of samples in the PCA training matrix.
C    NNsmp is the number of samples after filter.
C    Nts    IS THE NUMBER OF SASMPLES IN THE TESTING MATRIX.
C    ALFAQ is the confidential level of the Q-statistic threshold
C    ALFAT is the confidential level of the T2 threshold
C    FINDEX IS THE FAULT INDEX.
C ************************************************************
C
      REAL:: PST(361),Chard(31,4),Tse(61,2),Fset(61),Fcon(901,3)
      INTEGER:: FF1,FF2,FF3,FF4,FF5,FF6,FF7,FF8
      INTEGER:: FF7TS,FF7TO,FF7FS,FF7FO
     INTEGER:: NVAV,Nfault
      REAL,ALLOCATABLE,DIMENSION(:,:):: P,TST,ETST,Pb,CORTRNb,EIGVXb
      REAL,ALLOCATABLE,DIMENSION(:,:):: TRAIN,VAVTEST,CONT,TRN,NFTRN
      REAL,ALLOCATABLE,DIMENSION(:):: MTRN,STDTRN,Q,T2,EIGX,DX,HTRN
      REAL,ALLOCATABLE,DIMENSION(:):: MTRNb,STDTRNb,EIGXb,DXb,Qb,T2b,Z
      REAL,ALLOCATABLE,DIMENSION(:,:):: TSTb,TST1,ETSTb,EIGVX,CORTRN
      REAL,DIMENSION(10)::Fn
      REAL,DIMENSION(10)::TTHFn
C
      INTEGER:: FINDEX,FT2,Teig,FINDEXb,FINDEX1
      INTEGER,PARAMETER::NALA=10
      INTEGER:: MP,CS1,MF1,CS2,MF2,CS3,MF3,CS4,MF4
      INTEGER:: CS5,MF5,CS6,MF6,CS7,MF7,CS8,MF8,TF
      COMMON /ALFA/ALFAQ,ALFAT
      COMMON /CONFSYS/MP,CS1,MF1,CS2,MF2,CS3,MF3,CS4,MF4,
     &                CS5,MF5,CS6,MF6,CS7,MF7,CS8,MF8,TF
        COMMON /HOTEL05/Fn
      COMMON /TTH/TTHFn
C     ! Fn is the F-distribution level
        DATA Fn/4.16,3.32,2.93,2.71,2.57,2.47,2.40,2.36,2.32,2.30/
```

```
DATA TTHFn/4.15,3.31,2.92,2.70,2.56,2.46,2.39,2.34,2.30,2.27/
C
      INTEGER:: Rpst,Rfset,Rf
      Nfault=0
      NVAV=8
C    **********************Fault 1*******************************
       OPEN(1,FILE='F:\SOFTWARE\FDDVAV\PSTNE.TXT',STATUS='OLD')
       READ(1,*) (PST(I),I=1,360)
       CLOSE(1)
          DO 2 I=2,360
            PST(I)=0.5*PST(I-1)+0.5*PST(I)
2      CONTINUE
C         Read in new data
5         OPEN(11,FILE='F:\SOFTWARE\FDDVAV\PST.TXT',STATUS='OLD')
       READ(11,*) PST(361)
       CLOSE(11)
       DO 10 I=1,359
            PST(I)=PST(I+1)
10     CONTINUE
          PST(360)=0.5*PST(360)+0.5*PST(361)
       CALL SCHEME1(PST,361,Rpst,FF1)
C      PRINT*,Rpst
       PRINT*,'FF1=',FF1
C      PAUSE 'Scheme 1 Conducted'
C      IF (FF1.EQ.0) GO TO 5
C    **********************Fault 2*******************************
       DO 1 II=1,NVAV
       OPEN(2,FILE='F:\SOFTWARE\FDDVAV\TseNE.TXT',STATUS='OLD')
       READ(2,*) ((Tse(I,J),J=1,2),I=1,60)
       CLOSE(2)
C         Read in new data
53        OPEN(21,FILE='F:\SOFTWARE\FDDVAV\Tse.TXT',STATUS='OLD')
       READ(21,*) Tse(61,1),Tse(61,2)
       CLOSE(21)
       DO 55 I=1,60
            Tse(I,1)=Tse(I+1,1)
            Tse(I,2)=Tse(I+1,2)
55     CONTINUE
          CALL SCHEME2(Tse,61,2,FF2)
```

```
PRINT*,’Terminal’,II
      PRINT*,'FF2=',FF2
C     PAUSE 'Scheme 2 Conducted'
C     IF (FF2.EQ.0) GO TO 53
C    **********Fault 3**********
      OPEN(3,FILE='F:\SOFTWARE\FDDVAV\ChardNE.TXT',STATUS='OLD')
      READ(3,*) ((Chard(I,J),J=1,4),I=1,30)
C     WRITE(*,'(1X,4F10.2)') ((Chard(I,J),J=1,4),I=1,30)
        CLOSE(3)
C        Read in new data
80      OPEN(31,FILE='F:\SOFTWARE\FDDVAV\Chard.TXT',STATUS='OLD')
      READ(31,*) (Chard(31,J),J=1,4)
        CLOSE(31)
      DO 95 I=1,30
         DO 90 J=1,4
            Chard(I,J)=Chard(I+1,J)
90       CONTINUE
95    CONTINUE
        CALL SCHEME3(Chard,31,4,FF2,FF3)
        PRINT*,’Terminal’,II
        PRINT*,'FF3=',FF3
C     PAUSE 'Scheme 3 Conducted'
C     IF (FF3.EQ.0) GO TO 80
C    **********Fault 4/5**********
      OPEN(4,FILE='F:\SOFTWARE\FDDVAV\ChardNE.TXT',STATUS='OLD')
      READ(4,*) ((Chard(I,J),J=1,4),I=1,30)
C     WRITE(*,'(1X,4F10.2)') ((Chard(I,J),J=1,4),I=1,30)
        CLOSE(4)
C        Read in new data
120     OPEN(41,FILE='F:\SOFTWARE\FDDVAV\Chard.TXT',STATUS='OLD')
      READ(41,*) (Chard(31,J),J=1,4)
        CLOSE(41)
      DO 140 I=1,30
         DO 130 J=1,4
            Chard(I,J)=Chard(I+1,J)
130      CONTINUE
140   CONTINUE
        CALL SCHEME4(Chard,31,4,FF2,FF4)
        PRINT*,’Terminal’,II
```

```
PRINT*,'FF4=',FF4
C     PAUSE 'Scheme 4 Conducted'
C     IF (FF4.EQ.0) GO TO 120
C    **********Fault 6**********
      OPEN(6,FILE='F:\SOFTWARE\FDDVAV\FfroNE.TXT',STATUS='OLD')
      READ(6,*) (Fset(I),I=1,60)
        CLOSE(6)
C        Read in new data
170   OPEN(61,FILE='F:\SOFTWARE\FDDVAV\Ffro.TXT',STATUS='OLD')
      READ(61,*) Fset(61)
        CLOSE(61)
      DO 180 I=1,60
         Fset(I)=Fset(I+1)
180   CONTINUE
        CALL SCHEME5(Fset,61,Rfset,FF5)
C     PRINT*,Rfset
        PRINT*,'Terminal',II
        PRINT*,'FF5=',FF5
C     PAUSE 'Scheme 5 Conducted'
C     IF (FF5.EQ.0) GO TO 170
C    **********Fault 7**********
     OPEN(7,FILE='F:\SOFTWARE\FDDVAV\ChardNE.TXT',STATUS='OLD')
      READ(7,*) ((Chard(I,J),J=1,4),I=1,30)
C     WRITE(*,'(1X,4F10.2)') ((Chard(I,J),J=1,4),I=1,30)
        CLOSE(7)
C        Read in new data
253   OPEN(71,FILE='F:\SOFTWARE\FDDVAV\Chard.TXT',STATUS='OLD')
      READ(71,*) (Chard(31,J),J=1,4)
        CLOSE(71)
      DO 256 I=1,30
          DO 255 J=1,4
              Chard(I,J)=Chard(I+1,J)
255       CONTINUE
256   CONTINUE
        CALL SCHEME6(Chard,31,4,FF6)
        PRINT*,'Terminal',II
        PRINT*,'FF6=',FF6
C     PAUSE 'Scheme 6 Conducted'
C      IF (FF6.EQ.0) GO TO 253
```

```
C    ********************Fault 8/9/10*****************************
      OPEN(8,FILE='F:\SOFTWARE\FDDVAV\Fcontroller.TXT',STATUS='OLD')
      READ(8,*) ((Fcon(I,J),J=1,3),I=1,900)
      CLOSE(8)
C     Read in new data
280    OPEN(81,FILE='F:\SOFTWARE\FDDVAV\Fcontrol.TXT',STATUS='OLD')
      READ(81,*) (Fcon(901,J),J=1,3)
       CLOSE(81)
      DO 295 I=1,900
          DO 290 J=1,3
              Fcon(I,J)=Fcon(I+1,J)
290         CONTINUE
295   CONTINUE
       CALL SCHEME7(Fcon,901,3,FF1,FF2,FF3,FF4,FF5,FF6,
     &          FF7,FF7FS,FF7FO,FF7TS,FF7TO)
      PRINT*,'Terminal',II
      PRINT*,'FF7=',FF7,'    FF7FS=',FF7FS,'    FF7FO=',FF7FO,
     &          ' FF7TS=',FF7TS,'    FF7TO=',FF7TO
C     PAUSE 'Scheme 7 Conducted'
C     IF (FF7.EQ.0) GO TO 280
       PAUSE 'Scheme 1-7 Conducted'
C
        IF ((FF1.EQ.1).OR.(FF2.EQ.1).OR.(FF3.EQ.1).OR.(FF4.EQ.1)
     &      .OR.(FF5.EQ.1).OR.(FF6.EQ.1).OR.(FF7.EQ.1)) THEN
            Nfault=Nfault+1
       ENDIF
C
1      CONTINUE
C    **********************Fault 11*********************************
        IF (Nfault.GE.1) GO TO 900
C    ****************SYSTEM CONFIGURATION*****************
      OPEN(3,FILE='F:\SOFTWARE\FDDVAV\CONFSYS.TXT',STATUS='OLD')
      READ (3,*) MP,CS1,MF1,CS2,MF2,CS3,MF3,CS4,MF4,
     &                  CS5,MF5,CS6,MF6,CS7,MF7,CS8,MF8,TF
C        PRINT *,"MP=",MP,"CS1=",CS1,"MF1=",MF1,"CS2=",CS2
C        PRINT *,"MF2=",MF2,"CS3=",CS3,"MF3=",MF3,"CS4=",CS4
C        PRINT *,"MF4=",MF4,"CS5=",CS5,"MF5=",MF5,"CS6=",CS6
C        PRINT *,"MF6=",MF6,"CS7=",CS7,"MF7=",MF7,"CS8=",CS8
C        PRINT *,"MF8=",MF8,"TF=",TF
```

```
CLOSE(3)
      Nvar=MP+CS1+MF1+CS2+MF2+CS3+MF3+CS4+MF4
     &        +CS5+MF5+CS6+MF6+CS7+MF7+CS8+MF8+TF
C     PRINT*,Nvar
C
      OPEN(2, FILE='F:\software\FDDVAV\ALFA.TXT',STATUS='OLD')
       READ(2,*) ALFAQ,ALFAT
C      PRINT *,"ALFAQ=",ALFAQ,"ALFAT=",ALFAT
       CLOSE(2)
C
      OPEN(1,FILE='F:\software\FDDVAV\numsmp.txt',status='old')
           READ(1,*) Nsmp,Nts
C          PRINT *,"Nsmp=",Nsmp,"Nts=",Nts
        CLOSE(1)
C
        ALLOCATE (TRAIN(18,Nsmp),VAVTEST(18,Nts))
        OPEN(6,FILE='F:\software\FDDVAV\TRAIN.TXT',STATUS='OLD')
         READ(6,*) ((TRAIN(I,J),I=1,18),J=1,Nsmp)
        CLOSE(6)
        OPEN(6,FILE='F:\software\FDDVAV\VAVtest.TXT',STATUS='OLD')
         READ(6,*) ((VAVTEST(I,J),I=1,18),J=1,Nts)
        CLOSE(6)
C      ********************************************************
C           !     HOTELLING-T2 FILTER
       ALLOCATE(TRN(Nvar,Nsmp),HTRN(Nsmp))
      CALL PCAmatrix(TRAIN,18,Nsmp,TRN,Nvar)
      CALL HOTELLING(TRN,Nvar,Nsmp,HTRN,Teig)
C     PRINT*,Teig
      OPEN(8,FILE='F:\software\FDDVAV\HTRN.TXT',STATUS='OLD')
           WRITE(8,60) (HTRN(I),I=1,Nsmp)
60     FORMAT(1X,F10.4)
       CLOSE(8)
      CALL HT2TH(Nsmp,Teig,TTH)
      OPEN(10,FILE='F:\SOFTWARE\FDDVAV\TTH.TXT',STATUS='OLD')
      WRITE (10,*) TTH
      CLOSE(10)
        NNsmp=0    !count the number of the samples in Hotelling-T2 control
        DO 20 I=1,Nsmp
          IF (HTRN(I).LT.TTH) THEN
```

```
NNsmp=NNsmp+1
          END IF
20       CONTINUE
C         PRINT*,NNsmp
         ALLOCATE (NFTRN(18,NNsmp))
       CALL FILT(TRAIN,Nsmp,18,HTRN,TTH,NNsmp,NFTRN) !NFTRN is the new trn
matix.
       OPEN (20,FILE='F:\software\FDDVAV\nftrn.txt',status='old')
           WRITE(20,*) ((NFTRN(I,J),I=1,18),J=1,NNsmp)
       CLOSE(20)
C      ******************************************************
       ALLOCATE (MTRN(Nvar),STDTRN(Nvar), ETST(Nts,Nvar))
       ALLOCATE (Q(Nts),T2(Nts),TST(Nvar,Nts),CORTRN(Nvar,Nvar))
        CALL SCHEME8(NFTRN,VAVTEST,Nvar,NNsmp,Nts,
     &         TTHT2,Q,T2,Ieig,MTRN,STDTRN,ETST,TST,CORTRN)
       ALLOCATE (P(Nvar,Ieig),EIGX(Nvar),DX(Nvar),EIGVX(Nvar,Nvar))
         OPEN(5,FILE='F:\software\FDDVAV\EIGX.TXT',STATUS='OLD')
          READ(5,*) (EIGX(I),I=1,Ieig)
       CLOSE(5)
         OPEN(6,FILE='F:\software\FDDVAV\P.TXT',STATUS='OLD')
             READ(6,*) ((P(I,J),I=1,Nvar),J=1,Ieig)
         CLOSE(6)
C      PRINT*, ((P(I,J),I=1,Nvar),J=1,Ieig)
C        PRINT*, (Q(I),I=1,Nts)
C        PRINT*, (T2(I),I=1,Nts)
         DO 91 I=1,Ieig
          DX(I)=SQRT(EIGX(I))
91     CONTINUE
         CALL EIG1(CORTRN,Nvar,EIGX,EIGVX)
C      PRINT*,(EIGX(I),I=1,Nvar)
       CALL QTHQ(EIGX,Nvar,Ieig,QTH1)
       PRINT*,'QTH1=',QTH1
C       **********ISOLATE THE FAULT SOURCE******************
       DO 92 I=1,Nts
           IF (Q(I).LE.QTH1) THEN
               FINDEX=0
             ELSE
               FINDEX=FINDEX+1
           END IF
```

```
92      CONTINUE
        PRINT*,"FINDEX=",FINDEX
C
      DO 93 I=1,Nts
        IF (T2(I).LE.TTHT2) THEN
          FT2=0
        ELSE
          FT2=FT2+1
        END IF
93      CONTINUE
        PRINT*,"FT2=",FT2
C
        IF (FINDEX.GE.NALA) THEN
          CALL ISOLT(ETST,Nts,Nvar,NUM)
      END IF
      PRINT*,'NUM=',NUM
C
       Nbox=4
       ALLOCATE (MTRNb(Nbox),STDTRNb(Nbox))
      ALLOCATE (Qb(Nts),T2b(Nts),TST1(Nvar,Nts),Z(Nts))
      ALLOCATE (TSTb(Nbox,Nts),ETSTb(Nts,Nbox),CORTRNb(Nbox,Nbox))
     ALLOCATE (Pb(Nbox,Nbox),EIGXb(Nbox),DXb(Nbox),EIGVXb(Nbox,Nbox))
C
        Kitr=0
430   FINDEXb=0
        FINDEX1=0
      MP=1
      CS1=0
      MF1=0
       CS2=0
      MF2=0
       CS3=0
      MF3=0
      CS4=0
      MF4=0
       CS5=0
      MF5=0
       CS6=0
      MF6=0
```

```
CS7=0
      MF7=0
      CS8=0
      MF8=0
      TF=1
      IF (NUM.EQ.3) THEN
          CS1=1
          MF1=1
      ELSEIF (NUM.EQ.5) THEN
          CS2=1
          MF2=1
      ELSEIF (NUM.EQ.7) THEN
          CS3=1
          MF3=1
      ELSEIF (NUM.EQ.9) THEN
          CS4=1
          MF4=1
      ELSEIF (NUM.EQ.11) THEN
          CS5=1
          MF5=1
      ELSEIF (NUM.EQ.13) THEN
          CS6=1
          MF6=1
        ELSEIF (NUM.EQ.15) THEN
          CS7=1
          MF7=1
      ELSEIF (NUM.EQ.17) THEN
          CS8=1
          MF8=1
      ENDIF
C
        CALL SCHEME8(NFTRN,VAVTEST,Nbox,NNsmp,Nts,
     &          TTHT2b,Qb,T2b,Ieigb,MTRNb,STDTRNb,ETSTb,TSTb,CORTRNb)
        OPEN(5,FILE='F:\software\FDDVAV\EIGX.TXT',STATUS='OLD')
         READ(5,*) (EIGXb(I),I=1,Ieigb)
         CLOSE(5)
        OPEN(6,FILE='F:\software\FDDVAV\P.TXT',STATUS='OLD')
        READ(6,*) ((Pb(I,J),I=1,Nbox),J=1,Ieigb)
        CLOSE(6)
```

```
DO 910 I=1,Ieigb
        DXb(I)=SQRT(EIGXb(I))
910  CONTINUE
       CALL EIG1(CORTRNb,Nbox,EIGXb,EIGVXb)
C      PRINT*,(EIGX(I),I=1,Nvar)
       CALL QTHQ(EIGXb,Nbox,Ieigb,QTHb1)
       PRINT*,'QTHb1=',QTHb1
         DO 920 I=1,Nts
          IF (Qb(I).LE.QTHb1) THEN
              FINDEXb=0
            ELSE
              FINDEXb=FINDEXb+1
          END IF
920       CONTINUE
         PRINT*,"FINDEXb=",FINDEXb
C
         IF (FINDEXb.GE.NALA) THEN
          FF8=1
          PRINT*,"FF8=",FF8
       ELSE
          FF8=0
          PRINT*,"FF8=",FF8
          GO TO 1000
       ENDIF
       CALL RECOVER(TSTb,Nbox,Nts,Ieigb,MTRNb,STDTRNb,Pb,Z)
C
         DO 405 I=1,Nvar
            DO 406 J=1,Nts
              TST1(I,J)=TST(I,J)
406         CONTINUE
405  CONTINUE
       DO 410 I=1,Nts
        TST1(NUM,I)=Z(I)
410  CONTINUE
         CALL TEST1(TST1,Nvar,Nts,Ieig,MTRN,STDTRN,DX,P,ETST,Q,T2)
         DO 420 I=1,Nts
          IF (Q(I).LE.QTH1) THEN
              FINDEX1=0
            ELSE
```

```
FINDEX1=FINDEX1+1
          END IF
420     CONTINUE
        PRINT*,"FINDEX1=",FINDEX1
        IF (FINDEX1.GE.NALA) THEN
          Kitr=Kitr+1
          CALL ISOLT(ETST,Nts,Nvar,NUM1)
          PRINT*,'NUM1=',NUM1
          IF(NUM1.EQ.NUM) THEN
              GO TO 1000
          ELSEIF(Kitr.LT.((Nvar-1)/2)) THEN
               NUM=NUM1
                 DO 407 I=1,Nvar
                 DO 408 J=1,Nts
                  TST(I,J)=TST1(I,J)
408              CONTINUE
407              CONTINUE
             GO TO 430
          ENDIF
      END IF
C
1000 ALLOCATE(CONT(Nts,Nvar))
      IF ((FINDEX.LT.NALA).AND.(FT2.GE.NALA)) THEN
          CALL ISOLTPro(TST,Nvar,Nts,Ieig,MTRN,STDTRN,EIGX,P,CONT,NUMT)
      END IF
C     PRINT*,'NUMT=',NUMT
      DEALLOCATE(P,TST,ETST,MTRN,STDTRN,Q)
      DEALLOCATE(TRAIN,VAVTEST,T2,EIGX,DX,CONT)
      DEALLOCATE(MTRNb,STDTRNb,Pb,TSTb,ETSTb)
      DEALLOCATE(EIGXb,DXb,Qb,T2b,Z,TST1)
      DEALLOCATE(TRN,HTRN,NFTRN,EIGVX,CORTRN,CORTRNb,EIGVXb)
900    END
```

PUBLICATIONS ARISING FROM THE THESIS

Journal Papers

2005 Wang, Shengwei and Qin, Jianying. "Sensor Fault Detection and Validation of VAV Terminals in Air-conditioning Systems", Energy Conversion and Management 46, pp: 2482-2500.

2005 Qin, Jianying and Wang, Shengwei. "A Fault Detection and Diagnosis Strategy of VAV Air-Conditioning Systems for Improved Energy and Control Performances", Energy and Buildings 37, pp: 1035-1048.

2006 Qin, Jianying and Wang, Shengwei. "An Automatic Commissioning Strategy for VAV Air Distribution System", submitted to Applied Energy.

2006 Qin, Jianying and Wang, Shengwei. "An Automatic Commissioning Tool for VAV Air Distribution Systems", accepted by HKIE Transactions.

Conference Papers

2004 Qin, Jianying and Wang, Shengwei. "Automatic Commissioning of Multiple VAV Terminals" *The 4th International Conference for Enhanced Building Operation (ICEBO Oct. 2004), Paris, France*